Activation of Small Molecules via Organometallic Pincer Catalysts and Small Rhodium Clusters (pure and doped): A Density Functional Theory Approach

Thesis Submitted to AcSIR for the Award of the Degree of

DOCTOR OF PHILOSOPHY

in Chemical Sciences

By

Kamalika Ghatak

Registration Number: 10CC12A26054

Under the guidance of

Dr. Sourav Pal

Physical Chemistry Division CSIR-

National Chemical Laboratory,

Pune - 411008, India

August 2015

सीएसआयआर–राष्ट्रीय रासायनिक प्रयोगशाला
(वैज्ञानिक तथा औद्योगिक अनुसंधान परिषद)
डॉ. होमी भाभा मार्ग, पुणे – 411 008. भारत
CSIR-NATIONAL CHEMICAL LABORATORY
(Council of Scientific & Industrial Research)
Dr. Homi Bhabha Road, Pune - 411008. India

Certificate

This is to certify that the work incorporated in this Ph.D. thesis entitled ***Activation of Small Molecules via Organometallic Pincer Catalysts and Small Rhodium Clusters (pure and doped): A Density Functional Theory Approach*** submitted by ***Ms. Kamalika Ghatak*** to Academy of Scientific and Innovative Research (AcSIR) in fulfillment of the requirements for the award of the Degree of ***Doctor of Philosophy in Chemical Sciences***, embodies original research work under my supervision. I further certify that this work has not been submitted to any other University or Institution in part or full for the award of any degree or diploma. Research material obtained from other sources has been duly acknowledged in the thesis. Any text, illustration, table etc., used in the thesis from other sources, have been duly cited and acknowledged.

Kamalika Ghatak	Dr. Sourav Pal	Dr. Kumar Vanka
(Student)	(Supervisor)	(Co-supervisor)
	Former Director, CSIR-NCL, Pune	Scientist, CSIR-NCL,Pune
	Presently Professor at IITB, Powai	

Date: 10th August, 2015

Place: Pune

Communication Channels
NCL Level DID : 2590
NCL Board No. : +91-20-25902000
EPABX : +91-20-25893300
: +91-20-25893400
FAX
Director's Office : +91-20-25902601
COA's Office : +91-20-25902660
COS&P's Office : +91-20-25902664
WEBSITE
www.ncl-india.org

Dedicated to

Mr. Saktipada Ghatak

Acknowledgements

It gives me immense pleasure to take this opportunity to thank all the people who have helped and supported me throughout my Ph.D years at CSIR-National Chemical Laboratory.

I would like to express my gratitude towards my research supervisor **Dr. Sourav Pal** for giving me an opportunity to work with him as a student in his group and providing me the independence to choose my research area. I would especially like to mention Sir's Quantum Chemistry classes, without which this work would not have been possible. Sir's lectures are unique and they have given me the real essence of Quantum Chemistry and extended my horizon about the subject. On a personal front, Sir is an amazing human being with a bag full of positivity and a good sense of humour. Thanks Sir for making my stay comfortable in the lab. Thank you for guiding me through this great journey of learning and making it an enjoyable experience overall. I am forever indebted for teaching me to think critically and making me into a scientist.

I would also like to convey my special regards to my co-supervisor **Dr. Kumar Vanka** for his constant support, encouragement and guidance to overcome all the difficulties during my research tenure. His advises as well as constructive suggestions have assisted me to upgrade my research knowledge

I would like to pay special thanks to my research collaborator **Dr. Sailaja Krishanmurty** for her sincere and continuous support during the last couple of years of my doctoral studies. Her useful contributions and suggestions about my research and paper writing are much appreciated. I am also grateful to **Dr. Nayana Vaval** for her unconditional help and support throughout my PhD years.

I would like to thank all my current and previous lab mates for providing a vibrant and conducive atmosphere in the group. My thanks to all my colleagues Sumantra, Himadri De, Subrata, Lalita, Deepti, Sapna, Debarati, Jitendra, Mudit, Achintya, Aryya, Susanta, Sayali, Anagha, Himadri Pathak, Manzoor, Turbasu, Sudip, Deepak, Kaushik, Amrita, Shantanu, Manoj, Nisha, Jaya, Jugal, Yuvraj and Mritunjay for making the lab a wonderful and enjoyable place. In this regard, I want to convey my special thanks to Sumantra Da, Deepti Di, Debarati Di, Susanta, Manzoor, Sayali, Turbasu, Amrita, Manoj and Shantanu. I also thank the post doctoral candidates Madhulita, Vidhika, Saba of our group and wish them luck. My special thanks to the scientists and students of the

Electronic Structure and Theory Group at NCL. I would also like to thank all my friends outside NCL particularly Nivedita, Swagata, Veena and Sutapa Di.

I would also like to thank my DAC members; Dr. Anil Kumar, Dr. Nayana Vaval, Dr. Debashree Ghosh for their time and valuable suggestions throughout my PhD career.

I would also like to thank **Dr. Vijayamohanan Pillai**, Acting Director CSIR-NCL and **Dr. Anil Kumar**, Head and Chairman of Physical and Materials Chemistry Division for providing all the necessary infrastructural facilities. I am grateful to CSIR, New Delhi, for the financial support and to Academy of Scientific & Innovative Research (AcSIR) for giving me an opportunity for pursuing a doctoral degree. I would like to thank Students Academic Office CSIR-National Chemical Laboratory for their helpful services.

Last but not the least; I would like to extend my gratitude and thanks to all my family members for their love, support and encouragement throughout my life. I am really very much grateful to my parents (Mr. Dibyendu Ghatak and Mrs. Debomaya Ghatak) and to my uncle (Mr. Saktipada Ghatak) for their unconditional love and support and for shaping me into who I am today. I specially acknowledge my mother's rock solid support throughout the entire Ph. D. tenure. Thank you all for teaching me to be fearless and letting me pursue my dreams.

Finally I would like to thank my best friend cum my husband, Arkaprabha for being there in all the ups and downs throughout my journey. I will not be able to pursue my dreams without his continuous encouragement and support. Thanks Arka for keeping faith in me.

Kamalika Ghatak

TABLE OF CONTENTS

Abstract

Activation of small molecules is one of the key steps in a large number of chemical reactions. Their activation plays a major role a) in fuel cells,[1-5] b) in dehydrogenation of metal hydrides, ammonia borane (NH_3BH_3), methanol, formic acid etc.[6-10] c) in many organic syntheses,[11-14] d) in biological reactions,[15-17] e) in H_2 production and storage[18-21] and f) in conversion of toxic molecules to less toxic or useful products.[22, 23] My thesis research involves dehydrogenation of ammonia borane via Iridium pincer catalyst, Ir(POCOP)(H_2) ([POCOP = η^3-1,3(OP^tBu_2)$_2C_6H_3$],[9] which is one of the most efficient catalysts and on the activation of methanol molecule via ruthenium–doped and pure Rh_6 clusters.

Ammonia borane and the corresponding amine borane complexes have attracted attention as potential candidates for solid state hydrogen storage materials due to their high hydrogen content. It needs a catalytic support to dehydrogenate the same. I have considered the mechanistic pathways for dehydrogenating ammonia borane via a modified catalyst as well as other concurrent reactions enabled by the original catalyst.

Methyl alcohol is one of the most versatile compounds having several applications in areas such as a) organic synthesis; b) wastewater denitrification; c) in steam reforming and most importantly d) in fuel cell. A necessary step in almost every applications regarding methanol requires the activation of its strong O–H and C–H bonds. In this respect, I have considered the corresponding bond scission by Rh_6 (octahedral) and Rh_4Ru_2 (octahedral) catalyst from both thermodynamics and as well as kinetics approaches.

Chapter 1

First chapter of this thesis discusses about activation of small molecules, specially ammonia borane and methanol. It also gives a brief introduction about the catalysis activity of transition metal based pincer complexes and small transition metal clusters.

Chapter 2

I have used density functional theory (DFT) for all my calculations reported in chapters 3, 4 and 5. The second chapter presents a brief overview regarding the basics of DFT.

Chapter 3

It is necessary to regenerate ammonia borane (NH_3BH_3) in an effortless manner following its dehydrogenation to make its application economically viable. Most frequently detected side product of the above mentioned dehydrogenation reaction is the polyborazylene (PB) complex. It is important to note that PB is soluble in nature and regeneration of AB from the same posed a big challenge. However, some of the recent studies (both experimental and computational) proposed the idea of solving the regeneration problem.[24-26] An interesting point to be noted is that Ir(POCOP)(H_2) catalysed (one of the fastest catalyst to dehydrogenate ammonia borane) dehydrogenation of ammonia borane produces an insoluble cyclic pentamer ($[NH_2BH_2]_5$)[9, 27] as the side product instead of PB and thus Ir(POCOP)(H_2) is very unique in its own way. The third chapter demonstrates the complete mechanistic pathways involving Iridium centre towards the formation of $[NH_2BH_2]_5$ and eventually suggests some definite modifications to produce PB over insoluble pentamer.

Chapter 4

The first successful description of dehydrogenation mechanism of the ammonia borane via Ir(POCOP)(H_2) catalyst was proposed by Paul and co–workers[28]. Paul−Musgrave dehydrogenation mechanism proceeds through the coordination of ammonia borane to the catalyst, followed by removal of NH_2BH_2. The formed (POCOP)–IrH_4 intermediate is then converted to the Ir(POCOP)(H_2) catalyst along with H_2. In this respect, the likelihood of the dehydrogenation of ammonia borane from the metal−*sp*2 carbon activation pathway is the sole focus of this fourth chapter. It would proceed with the loss of two hydrogen atoms, with

the protic hydrogen being taken up by the ipso carbon of the phenyl ring and the hydridic hydrogen forming a bond with the metal center. Oxidative metalation step would complete the reaction cycle by evolving H_2 and reforming the original catalyst. I have studied both the possible pathways and found the Paul−Musgrave pathway to be more efficient for the (POCOP)IrH_2 catalyst. I have also identified the probable reason to be steric hindrance, imposed by the tridentate nature of the bonding of the ligand at the metal center for the motion of the phenyl ring out of the POCOP plane during dehydrogenation. This would be possible if the catalyst employed were to have an aromatic bidentate ligand coordination (to reduce steric restriction) instead of the tridentate ligand. This point has been taken into consideration by calculations using model (POC)IrH_2 catalyst. I have also considered the efficiency of the (POC)IrH_2 catalyst towards other important reactions such as: dehydrogenation of formic acid[6] and aromatic N−H bond activation[29, 30]. I have also considered the efficiency of some other catalysts (already synthesized Ta-bidentate catalyst, non–metal catalyst and tridenate catalyst with aromatic ring at the terminal end) towards AB dehydrogenation and compared the results with the model (POC)IrH_2 catalyst.

Chapter 5

Several theoretical studies have focused on identifying the potential of metal oxide (TiO_2), metal surfaces(Pt, Ir, Cu, Pd etc.) and as well as small metal clusters(Co_4, Cu_4, Pd_4, V_3^+,Ni_n^+ Au_n and $Cu_nAu_m^+$ etc.) towards the activation of either O–H bond or C–H bond of methanol molecule.[31-41] Rh–Pt bimetallic clusters are one of the efficient and well studied catalysts for the oxidation of alcohols in direct alcohol fuel cell.[42-47] Incorporation of Rh doping in Pt clusters is due to the capability of Rh atom to decrease the CO poisoning effect in the Pt clusters.[43, 46, 48-50] On the other hand, Ru is well known to enhance the rate of methanol oxidation reactions while doped with platinum.[51-54] In this chapter, I have considered the unique combination of Rh–Ru binary clusters to unfold its potential over its

parent cluster towards the activation of O–H and C–H bond of the methanol molecule.

References

[1] S. Park, J. M. Vohs, R. J. Gorte *Nature*. **2000**, 404, 265-267.
[2] X. Cheng, Z. Shi, N. Glass, L. Zhang, J. Zhang, D. Song, Z.-S. Liu, H. Wang, J. Shen *Journal of Power Sources*. **2007**, 165, 739-756.
[3] A. Hamnett *Catalysis Today*. **1997**, 38, 445-457.
[4] N. A. Choudhury, R. K. Raman, S. Sampath, A. K. Shukla *Journal of Power Sources*. **2005**, 143, 1-8.
[5] V. Kiran, T. Ravikumar, N. T. Kalyanasundaram, S. Krishnamurty, A. K. Shukla, S. Sampath *Journal of The Electrochemical Society*. **2010**, 157, B1201-B1208.
[6] J. F. Hull, Y. Himeda, W.-H. Wang, B. Hashiguchi, R. Periana, D. J. Szalda, J. T. Muckerman, E. Fujita *Nat Chem*. **2012**, 4, 383-388.
[7] B. Sakintuna, F. Lamari-Darkrim, M. Hirscher *International Journal of Hydrogen Energy*. **2007**, 32, 1121-1140.
[8] R. J. Keaton, J. M. Blacquiere, R. T. Baker *Journal of the American Chemical Society*. **2007**, 129, 1844-1845.
[9] M. C. Denney, V. Pons, T. J. Hebden, D. M. Heinekey, K. I. Goldberg *Journal of the American Chemical Society*. **2006**, 128, 12048-12049.
[10] N. Takezawa, N. Iwasa *Catalysis Today*. **1997**, 36, 45-56.
[11] K. Godula, D. Sames *Science*. **2006**, 312, 67-72.
[12] B. Blank, S. Michlik, R. Kempe *Advanced Synthesis & Catalysis*. **2009**, 351, 2903-2911.
[13] R. Grigg, T. R. B. Mitchell, S. Sutthivaiyakit, N. Tongpenyai *Tetrahedron Letters*. **1981**, 22, 4107-4110.
[14] J. Moran, A. Preetz, R. A. Mesch, M. J. Krische *Nat Chem*. **2011**, 3, 287-290.
[15] M. D. Fryzuk, S. A. Johnson *Coordination Chemistry Reviews*. **2000**, 200–202, 379-409.
[16] M. P. Shaver, M. D. Fryzuk *Advanced Synthesis & Catalysis*. **2003**, 345, 1061-1076.
[17] B. A. MacKay, M. D. Fryzuk *Chemical Reviews*. **2004**, 104, 385-402.
[18] K. Otsuka, C. Yamada, T. Kaburagi, S. Takenaka *International Journal of Hydrogen Energy*. **2003**, 28, 335-342.
[19] W. Grochala, P. P. Edwards *Chemical Reviews*. **2004**, 104, 1283-1316.
[20] B. K. Boggs, G. G. Botte *Journal of Power Sources*. **2009**, 192, 573-581.
[21] K. Damen, M. v. Troost, A. Faaij, W. Turkenburg *Progress in Energy and Combustion Science*. **2006**, 32, 215-246.
[22] P. G. Jessop, T. Ikariya, R. Noyori *Chemical Reviews*. **1995**, 95, 259-272.
[23] W. Wang, S. Wang, X. Ma, J. Gong *Chemical Society Reviews*. **2011**, 40, 3703-3727.
[24] P. M. Zimmerman, A. Paul, Z. Zhang, C. B. Musgrave *Inorganic Chemistry*. **2009**, 48, 1069-1081.
[25] B. L. Davis, D. A. Dixon, E. B. Garner, J. C. Gordon, M. H. Matus, B. Scott, F. H. Stephens *Angewandte Chemie International Edition*. **2009**, 48, 6812-6816.
[26] A. D. Sutton, A. K. Burrell, D. A. Dixon, E. B. Garner, J. C. Gordon, T. Nakagawa, K. C. Ott, J. P. Robinson, M. Vasiliu *Science*. **2011**, 331, 1426-1429.
[27] K. W. Böddeker, S. G. Shore, R. K. Bunting *Journal of the American Chemical Society*. **1966**, 88, 4396-4401.
[28] A. Paul, C. B. Musgrave *Angewandte Chemie*. **2007**, 119, 8301-8304.
[29] M. Feller, Y. Diskin-Posner, L. J. W. Shimon, E. Ben-Ari, D. Milstein *Organometallics*. **2012**, 31, 4083-4101.
[30] E. Khaskin, M. A. Iron, L. J. W. Shimon, J. Zhang, D. Milstein *Journal of the American Chemical Society*. **2010**, 132, 8542-8543.

[31] X. Sun, X. Sun, C. Geng, H. Zhao, J. Li *The Journal of Physical Chemistry A*. **2014**, 118, 7146-7158.
[32] W. A. Donald, C. J. McKenzie, R. A. J. O'Hair *Angewandte Chemie International Edition*. **2011**, 50, 8379-8383.
[33] C. J. Zhang, P. Hu *The Journal of Chemical Physics*. **2001**, 115, 7182-7186.
[34] W. T. Lee, F. Thomas, R. I. Masel *Surface Science*. **1998**, 418, 479-483.
[35] D. Wang, E. R. Farquhar, A. Stubna, E. Münck, L. Que *Nat Chem*. **2009**, 1, 145-150.
[36] V. M. Sánchez, J. A. Cojulun, D. A. Scherlis *The Journal of Physical Chemistry C*. **2010**, 114, 11522-11526.
[37] S. K. Desai, M. Neurock, K. Kourtakis *The Journal of Physical Chemistry B*. **2002**, 106, 2559-2568.
[38] X.-K. Gu, W.-X. Li *The Journal of Physical Chemistry C*. **2010**, 114, 21539-21547.
[39] H. Wang, C.-z. He, L.-y. Huai, J.-y. Liu *The Journal of Physical Chemistry C*. **2013**, 117, 4574-4584.
[40] F. Mehmood, J. Greeley, L. A. Curtiss *The Journal of Physical Chemistry C*. **2009**, 113, 21789-21796.
[41] F. Mehmood, J. Greeley, P. Zapol, L. A. Curtiss *The Journal of Physical Chemistry B*. **2010**, 114, 14458-14466.
[42] K. Bergamaski, E. R. Gonzalez, F. C. Nart *Electrochimica Acta*. **2008**, 53, 4396-4406.
[43] J. P. I. de Souza, S. L. Queiroz, K. Bergamaski, E. R. Gonzalez, F. C. Nart *The Journal of Physical Chemistry B*. **2002**, 106, 9825-9830.
[44] T. E. Shubina, M. T. M. Koper *Electrochimica Acta*. **2002**, 47, 3621-3628.
[45] B. D. McNicol, D. A. J. Rand, K. R. Williams *Journal of Power Sources*. **1999**, 83, 15-31.
[46] S. Sen Gupta, J. Datta *Journal of Electroanalytical Chemistry*. **2006**, 594, 65-72.
[47] F. Tao, M. E. Grass, Y. Zhang, D. R. Butcher, F. Aksoy, S. Aloni, V. Altoe, S. Alayoglu, J. R. Renzas, C.-K. Tsung, Z. Zhu, Z. Liu, M. Salmeron, G. A. Somorjai *Journal of the American Chemical Society*. **2010**, 132, 8697-8703.
[48] Z.-Y. K. Tzi-Yi Wu, Jiin-Jiang Jow,Chung-Wen Kuo,Cheng-Jang Tsai,Pin-Rong Chen,Ho-Rei Chen *International Journal of Electrochemical Science*. **2012**, 7, 8076-8090.
[49] M. Li, W. P. Zhou, N. S. Marinkovic, K. Sasaki, R. R. Adzic *Electrochimica Acta*. **2013**, 104, 454-461.
[50] F. Hahn, B. Beden, C. Lamy *Journal of Electroanalytical Chemistry and Interfacial Electrochemistry*. **1986**, 204, 315-327.
[51] M. Watanabe, S. Motoo *Journal of Electroanalytical Chemistry and Interfacial Electrochemistry*. **1975**, 60, 267-273.
[52] J. W. Guo, T. S. Zhao, J. Prabhuram, R. Chen, C. W. Wong *Electrochimica Acta*. **2005**, 51, 754-763.
[53] M. S. Löffler, H. Natter, R. Hempelmann, K. Wippermann *Electrochimica Acta*. **2003**, 48, 3047-3051.
[54] K. A. Friedrich, K. P. Geyzers, U. Linke, U. Stimming, J. Stumper *Journal of Electroanalytical Chemistry*. **1996**, 402, 123-128.

Abbreviations

DFT	Density Functional Theory
AB	Ammonia Borane
MP2	Second Order Møller-Plesset Perturbation Theory
RI	Resolution of Identity
MARIJ	Multipole Accelerated Resolution of Identity –J
QM	Quantum Mechanical
CI	Configuration Interaction
CC	Coupled Cluster
KS	Kohn–Sham
LDA	Local Density Approximation
GGA	Generalised Gradient Approximation
TS	Transition State
IRC	Intrinsic Reaction Coordinate
ECP	Effective Core Potential
RECP	Relativistic Effective Core Potential
COSMO	Conductor-Like Screening Model
MO	Molecular Orbital
HOMO	Highest Occupied Molecular Orbital
LUMO	Lowest Unoccupied Molecular Orbital
NBO	Natural Bond Orbital
BP-86	Becke-Perdew' 86
PBE	Perdew, Burke and Ernzerhof
B3-LYP	Becke 3 parameter exchange + Lee, Yang and Parr correlation
LANL2DZ	Los Alamos National Laboratory ECP (Duble Zeta) basis set
TZVP	Triple Zeta Valence Polarized
BOMD	Born-Oppenheimer Molecular Dynamics

List of Publications

1. **K. Ghatak,** K. Vanka, "A computational investigation of the role of the iridium dihydrogen pincer complex in the formation of the cyclic pentamer $(NH_2BH_2)_5$" ***Computational and Theoretical Chemistry***, **992**, 18 (2012).

2. **K. Ghatak,** M. Mane, K. Vanka, "Metal or Nonmetal Cooperation with a Phenyl Group: Route to Catalysis? A Computational Investigation", ***ACS Catalysis***, **3 (5)**, 920 (2013).

3. **K. Ghatak**, T. Sengupta, S. Krishnamurty, and S. Pal, "Computational Investigation on the Catalytic Activity of Rh6 and Rh4Ru2 Clusters Towards Methanol Activation", ***Theoretical Chemistry Accounts***,134: 1597, (2014).

Publications not included in the thesis

1. M. Mane, A. Venkatnathan, **K. Ghatak**, K. Vanka, "Exploring the Potential of Doped Zero-Dimensional Cages for Proton Transfer in Fuel Cells: A Computational Study", ***The Journal of Physical Chemistry B***, **116 (32)**, 9803 (2012).

2. M. Dixit, T. Adit Maark, **K. Ghatak**, R. Ahuja, S. Pal, "Scandium-Decorated MOF-5 as Potential Candidates for Room-Temperature Hydrogen Storage: A Solution for the Clustering Problem in MOFs", ***The Journal of Physical Chemistry C***, **116 (33)**, 17336 (2012).

Chapter 1: Introduction

Objective

The primary objective of my thesis research is to widen up and contribute to the existing scientific knowledge about catalysis and small molecule activation via various organometallic complexes and metal clusters. I approached the problems of catalysis and small molecule activation by investigating: a) the role of Ir–pincer catalysts on ammonia borane dehydrogenation and b) the effect of Ruthenium doping in the Rh_6 cluster towards methanol activation. The fundamental theme of my thesis is to try and minimize the activation barriers and discern the molecular mechanistic pathways for the above mentioned processes along the reaction coordinate through various strategies. This chapter presents a brief introduction to the various important concepts required in order to fully understand and substantiate the significance of this work.

1.1 Catalysis

A substance possessing the capability of significantly altering the rate of a chemical reaction along with the ability to recycle itself at the end of the concerned reaction is called a catalyst and the entire process is known as catalysis. Two variants of catalysts are known to us: a) positive catalysts or catalysts that increase the reaction rate; and b) negative catalysts; also known as inhibitors which slows down the reaction rate. It is important to note that a catalyst may undergo several chemical transformations during the entire chemical process, however regains its original form upon completion of the reaction. Catalysis activity of a particular reaction is subjected to change under the influence of inhibitor molecules and promoter molecules. In an extremely generalized form, a reaction is a process where reactants react among themselves and lead to the formation of product or products via a transition state. The

transition state of a chemical reaction is the highest point of the potential energy curve across a reaction coordinate and the energy difference between the reactants and the corresponding transition state is known as activation energy (E_a). According to the Arrhenius equation (equation no. 1.1), the term activation energy (E_a) is related to the rate constant (k) and is the dominant factor controlling the rate of an equation. The form of the Arrhenius equation is as follows;

$$k = Ae^{-E_a/RT} \qquad (1.1)$$

where k is the rate constant, A is the pre-exponential factor (also known as frequency factor), R is the universal gas constant and **T** is the temperature at which the reaction takes place. Transition state theory deals with another equation, formulated by Wigner et al.[1], relating the rate constant of the reaction with the Gibbs free energy of activation ($\Delta G^{\#}$). It has almost similar form as the Arrhenius equation, the only difference being that it deals with Gibbs free energy of activation ($\Delta G^{\#}$) instead of activation energy (E_a). The new equation is as follows;

$$k = \frac{k_B T}{h} e^{-\Delta G^{\#}/RT} \qquad (1.2)$$

where k_B is the Boltzmann's and h is the Planck's constant and the rest of the terms have the same meaning as mentioned previously. From the above two equations, it is clear that lower the value of E_a and $\Delta G^{\#}$, higher is the rate of the concerned reaction. A catalyst's work is to reorient the transition state structure in order to get a lower energy structure which eventually results in lowering of the free energy of activation. It is pertinent to mention here that catalysts don't affect the free energies of the original reactants or products (see **Fig. 1.1**).

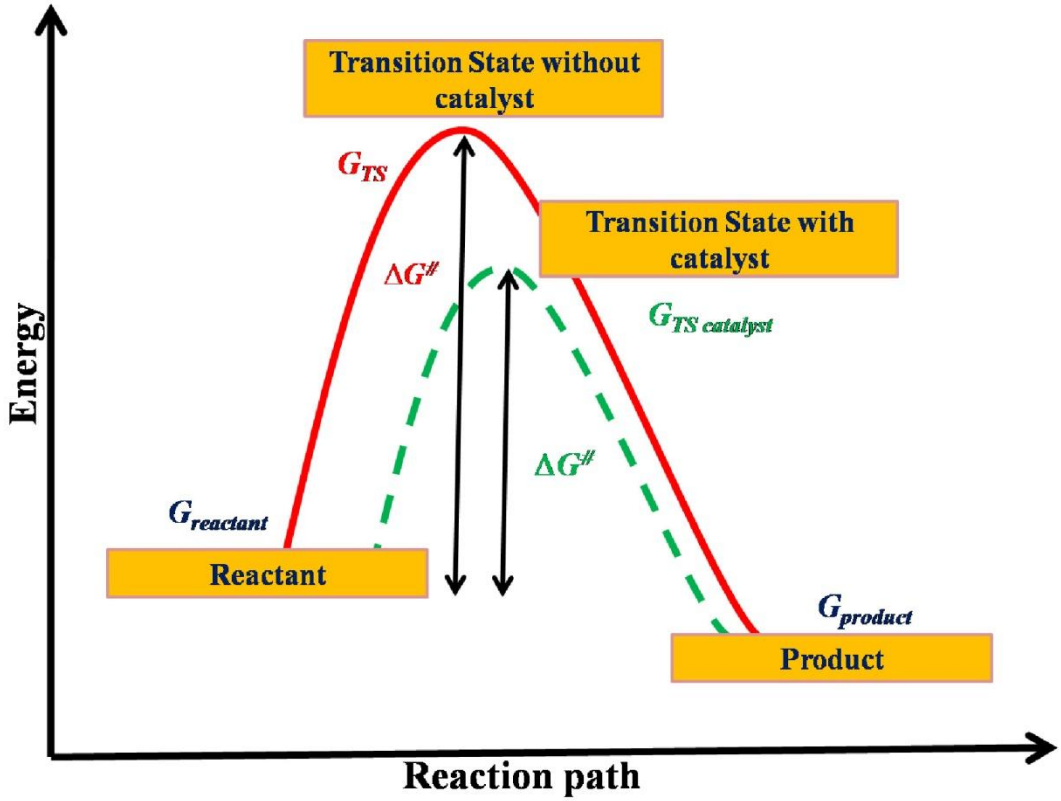

Figure 1.1 Pictorial description of the reduction of transition state barrier in presence of catalyst.

1.1.1 Types of Catalysts

Catalysts are generally categorized as: a) homogeneous catalysts, where catalysts are in the same phase as the reactants (for example; soluble in solvent of the liquid phase reaction mixture), and b) heterogeneous catalysts, where catalysts and reactants are in different phases (for example; insoluble solid phase catalysts in liquid phase reaction mixture of solvent and reactants).

During homogenous catalysis, reaction between the catalyst and reactants (one or multiple) takes place, which eventually leads to the formation of an intermediate. The formed intermediate then reacts further to form the final product and it also reproduces the catalyst back. A representative reaction scheme is shown below:

$$C \xrightarrow{R_1} C + R_1 \rightarrow I \xrightarrow{R_2} I + R_2 \rightarrow P + C \qquad (1.3)$$

where *C*, R_1 ,*I*, R_2 and *P* represent the catalyst, reactant (1), intermediate, reactant (2) and the product respectively. These types of processes generally require the use of a solvent to dissolve the catalyst and it actually limits the temperature range (low temperature; lower than the boiling point of the solvent used) for the concerned reaction. The low temperature requirement is also in the favour of fairly limited stability of the homogeneous catalyst. Homogeneous catalysts are known to have important qualities, such as: a) high selectivity, b) high diffusivity, c) well defined active sites and d) availability of easy techniques to figure out the reaction mechanisms etc. Soluble organometallic complexes, which are one of the important classes of homogenous catalysts, are very easy to modify (by tuning the electronic and steric attributes) to achieve essential changes in the reaction medium. Not only organometallic catalysts, acid–base catalysts, Lewis acid catalyst, metal ion catalysts and various enzymes also belong to this category. However, expensive separation technique of the products and the catalyst from the reaction media limits the industrial application of these types of catalysis. On the other hand, most of the industrial applications (mainly chemical and energy) are based on heterogeneous catalysis.

As mentioned earlier, a physical phase difference between catalyst and reactant/s exists in case of heterogeneous catalysis. Generally, the catalyst is in solid phase, whereas the reactants are in gas or liquid phase[2]. Almost the entire phenomenon of heterogeneous catalysis involves the adsorption of the reactant/s on the catalyst surface and formation of chemical bonds as the crucial first step. After the completion of the reaction, the formed products get desorbed from the surface and are separated out. Mainly three mechanisms exist for these types of surface reactions:

a) *Rideal–Eley mechanism*: Here the first molecule (A) gets adsorbed on the catalyst surface and then the next molecule (B) reacts with the first molecule and forms the

new molecule A–B. It is important to note here that the second molecule (B) never gets adsorbed (chemisorbed) to the surface (see **Fig. 1.2**).

b) *Langmuir–Hinshelwood mechanism*: Here both the molecules (A and B) gets adsorbed to the catalyst bed and then they react to form the new molecule A–B (see **Fig. 1.2**).

While adsorbed to the surface, the A and B "meet," bond, and then form the new molecule AB

c) *Precursor mechanism*: Here one of the two molecules (A) collides to the catalyst and converts itself into a mobile precursor form. Then this precursor reacts with the other molecule (B; which is already adsorbed on the surface of the catalyst) to form the new molecule A–B.

Heterogeneous catalysts are widely used due to their inexpensive separation techniques by utilising the phase differences between the products and catalyst. Few more advantages are present in case of heterogeneous catalysis; such as: a) easier and efficient recycling methods, b) lower cost, c) reduction of metal leaching, d) improved handling and process control, and e) higher selectivity etc. Although, selectivity of heterogeneous catalysis is generally low as a result of difficulties related to the modifications of the steric and electronic properties of the catalyst. Only few methods are present to control the size of the particle and to determine the active site of the concerned catalyst. Reaction mechanisms of heterogeneous catalysis are very difficult to determine and generally indirect methods (by checking the products) are employed to find out. It is important to note here that computational methods are more accurate in determining the reaction mechanisms for the homogeneous process rather than the heterogeneous cases. Theoretical models for Homogeneous catalysis deal with the authentic molecular orbital theory. On the other hand, heterogeneous catalysis

methods use less accurate band–theory. Some of the very important examples of both types of catalysts are described in the next section.

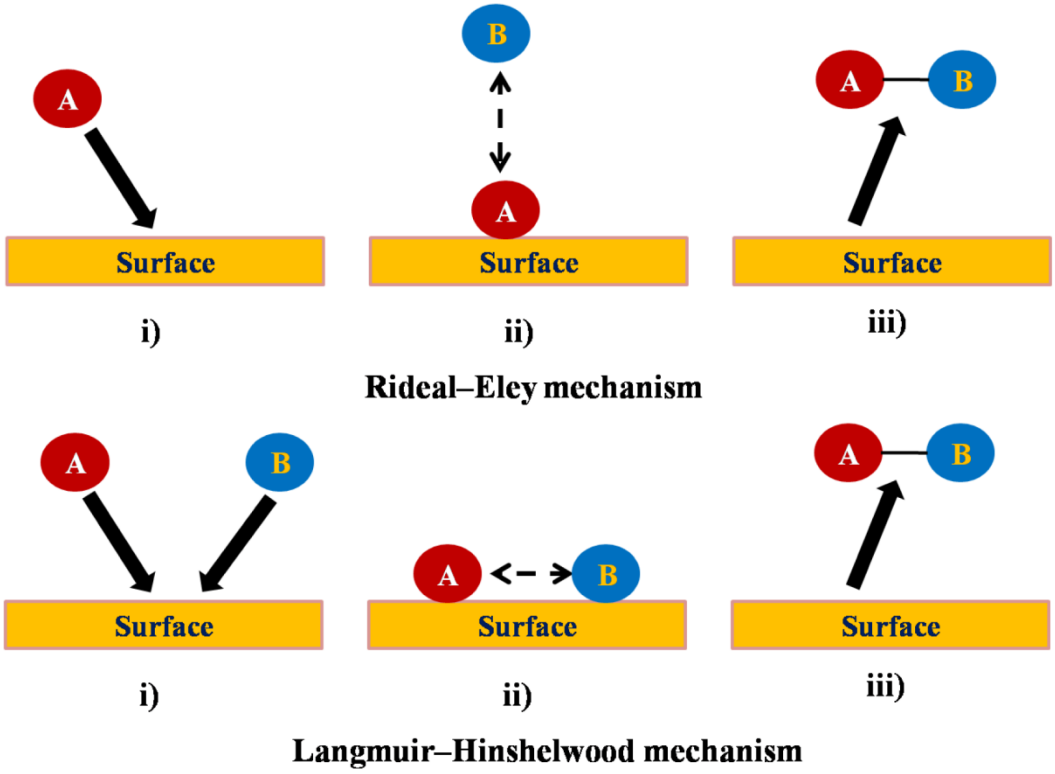

Figure 1.2 Illustration of the Rideal-Eley (top) and Langmuir-Hinshelwood (bottom) mechanisms.

1.1.2 Examples of Catalysts

Various examples of homogeneous catalyst systems are available in the literature[3, 4] and some of the very important examples are: a) catalysis by acids or bases, b) metal ions mediated catalysis, c) catalysis by organometallic complexes, d) Lewis acids catalysis, and e) enzymatic catalysis. Dehydration of ethyl alcohol to ethylene, synthesis of ethyl acetate ester from ethanol and acetic acid, condensation of phenol and acetone to *bis*–phenol are some of the very important examples of acid catalyzed homogeneous reactions. Hydrolysis of esters and halogenations of ketones are the examples of base catalyzed homogeneous reactions. Generally, metal ions act as redox catalysis and hydrolysis of α–amino esters and phosphate esters by Cu_2^+ ion and Mg_2^+ ions respectively are homogeneous in nature. Reactions catalyzed by

organometallic catalysts are also homogeneous catalysts and are capable of catalysing a variety of reactions including hydrogenation, dehydrogenation, hydroformylation, partial oxidation, hydrocarbon rearrangement etc. Diels alder reactions, epoxidation of alkenes are also examples of homogeneous catalysis. Reaction involving the catalytic activity of carbonic anhydrase (a bodily enzyme) towards the acceleration of CO_2 release from the blood stem into the lungs, is one of the important homogeneous biological phenomenon.[5]

Most of the large scale industrial synthetic methods[6] are based on heterogeneous catalysis: a) ammonia synthesis on Fe/Al_2O_3 (known as Haber–Bosch process), b) H_2SO_4 synthesis catalysed by vanadium oxide, c) HNO_3 synthesis by Pt/Rh based catalyst (known as Ostwald process), d) Hydrogen production (known as steam reforming), and e) HCN synthesis (known as Andrussow process) etc. Moreover, some of the other important reactions like petroleum cracking, Ziegler–Natta polymerization and desulfurization of petroleum etc. also belong to this category.

1.2 Activation of Small Molecules

Small molecules are extremely abundant in nature and it is a representative name for almost all of naturally stable, inexpensive and easily accessible molecules. The air constituents such as H_2, N_2, O_2, CO_2, CO, H_2O etc. belong to this category and not only that these molecules are often found to take part in many of the natural elementary reactions including our metabolic processes. Hydrocarbons, organic alcohols, carboxylic acids, aldehydes, ketones, N_xO_y, H_xO_y, CO_x, N_xH_y, B_xH_y, P_xH_y etc. are either naturally abundant or can be easily formed from the natural feedstock and thus fall under this category. Generally, small molecules show extreme stability and as a result their activation demands higher energy. Therefore, catalysts (mainly

transition metal based catalysts) are used in the activation of small molecules. Such phenomenon has grabbed the attention of the researchers due its multitude of practical applications. Some of the important chemical problems incorporating activation of small molecules are biological processes catalyzed by enzymes,[7-9] hydrogen production and their storage, water splitting[10, 11] and transformation of poisonous elements such as CO and CO_2 to less toxic or useful feed stock such as methanol, formic acid, formaldehydes[12, 13] etc. My work is focused on the dehydrogenation of ammonia borane and methanol and thus a brief introduction to these two compounds is presented in the following subsections.

1.2.1 Ammonia Borane

Ammonia borane (NH_3BH_3) is a chemical compound which is isoelectronic with ethane. It is a colourless solid at ambient pressure and temperature, and thus displays comparable gravimetric densities with the corresponding hydrocarbon. Large scale synthesis of ammonia borane is generally done at low temperature via the direct reaction of ammonia with diborane by passing diborane into liquid ammonia.[14-16] Eventually, the reaction generates an ionic salt, diammoniate of diborane ($BH_2[(NH_3)_2]^+[BH_4]^-$) due to the asymmetric cleavage of the diborane but symmetric cleavage of the diborane gives a mixture of ammonia borane plus the diammoniate of diborane salt (equation 1.4).[16] On the other hand, if borane–tetrahydrofuran ($BH_3(THF)$) or borane –dimethyl sulphide ($BH_3(SMe_2)$) is used, pure ammonia borane is obtained (equation 1.5).[17]

$$2NH_3 + B_2H_6 \rightarrow [BH_2(NH_3)]^+[BH_4]^- \qquad (1.4)$$

$$BH_3(THF) + NH_3 \rightarrow NH_3BH_3 + THF \qquad (1.5)$$

The molecular structure of ammonia borane is same as ethane but unlike ethane it is a donor–acceptor molecule with a dative bond formed between the Lewis acid (BH_3)

and the Lewis base (NH_3). Therefore, ammonia borane contains both types of hydrogen atoms such as: a) hydridic hydrogen atoms attached to the boron atom and b) protic hydrogen atoms attached to the nitrogen atom. The B–N bond distance is ~1.582 Å and this bond is very strong due to delocalization of nitrogen's electron to the empty *p* orbital of boron. It is important to mention here that due to the strong nature of the B–N bond, dissociation of hydrogen is a more favourable process compared to the disruption of the B–N bond. It is very interesting that ammonia borane is solid at room temperature and pressure while ethane is a gas at similar conditions. Dihydrogen bonding between the $H_{\boldsymbol{N}}$ and the $H_{\boldsymbol{B}}$ centres and strong dipole–dipole interactions are the two main reason behind the solid structure of ammonia borane.[18]

Given that the world is running out of its fossil fuel resources fast and facing severe environmental issues based on the usage of the same, it is high time to look forward to an alternative environment friendly and economically viable fuel source. The use of dihydrogen as a fuel has garnered severe attention from the researchers due to its low cost, high energy content and for being environmentally friendly. However, there exists substantial problem related to the storage of dihydrogen in order to use it as a transportation fuel.[19-24] In this regard, solid state storage of hydrogen has gained much attention of late due to its safe and efficient nature compared to the liquid gas and gaseous phase. Specifically, researchers showed much interests towards the use of ammonia borane as a solid state hydrogen storage material due to its stability at ambient temperatures and its high hydrogen content (19.6 wt %).[25] In order to release the hydrogen from the ammonia borane at a reasonable rate and at an ambient temperature, systematic dehydrogenation methods are much required. Generally, five such methods are reported in literature such as: a) solid state

thermal decomposition,[26-31] b) catalysis by ionic liquid,[32] c) thermal dehydrogenation in solution phase,[33] d) catalysis by transition metal complexes,[34-37] and e) thermal dehydrogenation of nanophase ammonia borane encapsulated in mesoporous silica SBA-15.[38] In this thesis, I have specifically studied transition metal (Ir–POCOP pincer complex[36]) catalyzed ammonia borane dehydrogenation and related problems. The details of the same are the contents of the third and fourth chapter of this thesis.

1.2.2 Methanol

Methyl alcohol (methanol in common language), with the formula CH_3OH, is the simplest among all the aliphatic alcohols. It is colourless, volatile, flammable and poisonous liquid at room temperature with characteristic smells. It is important to note that methanol has higher hydrogen content than the H_2 cylinders or the metal hydrides. History of methanol synthesis begins from the ancient Egyptian era and it was obtained in a mixture along with other elements through the pyrolysis of wood. Later on Robert Boyle successfully isolated it through the distillation of boxwood and thus methanol is also known *wood alcohol*.[39] Nowadays industrial methanol productions are done from several sources: a) from syngas (a mixture of fuel gas containing hydrogen, carbon monoxide, and a small portion of carbon dioxide) by using mainly copper, zinc oxide, and alumina catalysts,[40] b) from methane[41, 42] and c) from carbon dioxide.[43] Some amount of methanol is also available in nature and some of the bacterial metabolism also generates methanol.[44] Methanol has several versatile applications such as: a) in organic synthesis,[45-47] b) in wastewater denitrification,[48-53] c) in pure hydrogen production, known as steam reforming,[54-57] d) as a transportation fuel,[58] e) to generate electricity,[59] f) as a chemical feedstock towards the production of formaldehyde, acetic acid and olefins,[60-62] g) as a

precursor in the plastic industry,[63] h) as an automobile coolant antifreeze material[64] and most importantly i) in fuel cell.[65] An interesting observation is that in almost each application, O–H and C–H bond activation is detected as one of the essential step.[66-69] Moreover, the first step of the methanol dissociation has high energy requirements due to the strong C–H (~96.1 kcal/mol) and O–H(~104.6 kcal/mol) bonds of methanol. Therefore it requires the help of various catalysts[70-74] and detailed discussion of the same is described in the fifth chapter.

1.3 Pincer Catalysts

Literal meaning of the term *pincer* is "a front claw of a lobster or a crab". Accordingly, pincer ligands belong to the group of chelating agents with three adjacent coplanar sites which usually bind to the transition metal centre in a meridional manner.[75] Pincer ligand and metal cooperativity generate a class of organometallic complexes which eventually turn out to be very effective catalysts for many reactions. These pincer catalysts are thermally very stable and have very high melting points as a result of their rigid structure. It is interesting to mention here that most pincer ligands contain phosphines.[76] The very first pincer complex was synthesized in the year 1976 by Shaw and co–worker .[77] At that time, this ligand was not given much importance; rather it was considered just a novel derivative of phosphine. Then again in the late 80's methodical observations revealed the extraordinary potency of these complexes in order to be used as homogeneous catalysts. Presently, these pincer complexes are not only bound into the region of homogeneous catalysis, but have extended their horizon in the fields of nanosciences towards the usage in chemical sensors, switches and supramolecular chemistry.[78-80]

Pincer complexes are the combination of the pincer framework and metal centre. In the pincer framework, the tridentate ligand is attached to the metal via at

least one metal–carbon σ bond. Commonly, an aryl anion is directly bonded to the metal centre through the metal–carbon σ bond. The ortho substituents to this σ bond are not directly connected to the metal but are attached to the metal site via coordinated donor atoms; such as: O, S, N or P etc (see **Fig. 1.3**). Examples of some of the well known pincer ligands are PCP, POCOP, NCN, SCS, CNC, PCN and PNP frameworks.[78, 80] The term PCP represents that the three atoms (phosphorous, carbon and phosphorous) are directly coordinated to the metal centre.

It is important to mention that POCOP ligand [$C_6H_3(R')(P(R)_3O)_2$–1,2,6] is a special variety of the PCP ligand [$C_6H_3(R')(P(R)_3CH_2)_2$–1,2,6], where the ortho substituents to the metal–carbon σ bond are oxygen instead of an alkyl group. Interestingly, the CNC ligand is generally coordinated to the metal atom via two metal–carbon σ bonds. These pincer ligands in union with transition metals such as iridium, platinum, rhodium, osmium and ruthenium have manifested to be very versatile catalysts to ease the activation of many small molecules.

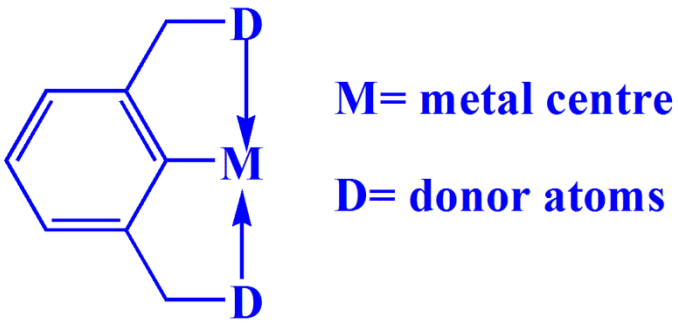

Figure 1.3 Pictorial dscription of a trivial pincer complex.

The reason behind the unique stability of this type of complexes is its strong metal–carbon σ bond which avoids the dissociation of the ligand from the metal centre. Fine tuning of the donor atoms and their substituents decides the structural and electronic properties of the corresponding complexes. The scope of modification to these complexes make them very attractive towards different domains of chemistry,

especially in the field of catalysis.[80]

1.3.1 Catalytic Applications of Pincer Complexes

Several important reactions are catalyzed by pincer complexes and examples of some of the very important reactions will be discussed in this section. Many organic syntheses involves the presence of pincer catalysts to accelerate the process. Palladium catalysed vinylation of aryl halides, known as Heck reaction is one of the important organic reaction since its discovery in 1960s.[81] Conventionally, Heck reaction combines a terminal alkene and an aryl iodide or bromide and the process demands the involvement of the derivatives of Pd(II) or Pd(0) in excess PPh_3.[82, 83] The main problem with this reaction is that the intermediates are found to be very sensitive to oxygen and are thermally unstable, and thus cause difficulties in this coupling. Since several years, many fold research works have been conducted and new advancement has been implemented to design an ideal catalyst with the bona fide features of reactivity and stability to fulfill this process. After many years of works on this field, researchers finally suggested the use of ortho metallated complexes, such as: the pincer ligands. The first reported case of using tridentate Pd(II)–PCP pincer complexes (see **Fig. 1.4 (i)** and **(ii)**) in the Heck coupling reaction was by Milstein and co–workers.[84] These type of pincer complexes are highly stable in solution (140^{o} C and up to 300 hours) and are found to be less-sensitive in presence of oxygen and moisture. Suzuki–Miyaura coupling[85] is another similar type of reaction where aryl halides couple with arylboronic acid and therefore many of the Heck catalysts are proved very efficient for this reaction. Employment of Pd–POCOP and Pd–SCS pincer complexes[86, 87] (see **Fig. 1.4 (iii)** and **(iv)**) for the coupling of aryl halides and phenyl boronic acid have been proved to be a very successful attempt. Hydrogen transfer reaction is another important reaction where the reaction starts with a ketone

and an alcohol and eventually it proceeds via the reduction of the ketone to their corresponding alcohol. Both Ru–NCN and Ru–PCP complexes (see **Fig. 1.4 (v)** and **(vi)**) are known to be effective catalysts for this particular reaction but the best yield is reported in case of the PCP derivative.[88-90] Standard synthesis of pure enantiomeric oxazolines are produced from the enantioselective aldol condensation reactions between a ketone and an aldehyde, catalyzed by the gold complexes.[91] Venanzi et *al*.[92, 93] introduced enantiomerically pure Pt–PCP pincer complex (see **Fig. 1.5 (i)**) as catalyst in the asymmetric aldol condensation of methyl-α-isocyanoacetate with aldehydes but it was reported to show moderate enantiomeric yield for *cis* (32% ee) and *trans* (65% ee) variety of oxazolines. Difficulties in the synthetic process of these enantiomeric pincer complexes limit their application in the practical field. Later on, a simple synthetic method for similar kind of Pd–PCP (see **Fig. 1.5 (ii)**) was proposed by Zhang and co-workers[94] and was implemented by Venanzi et al. in enantiomeric aldol condensation reactions. It was reported that the Pd derivative was found to exhibit higher yield with higher enantioselectivity towards the production of the *cis*-oxazolines. Moreover, some of the Pd–NCN[95] and Pd–SCS[96] complexes have also been employed as catalysts in aldol condensation reactions. Use of Pd–NCN complex (see **Fig. 1.6 (i)**) as catalyst was proposed to be very successful in case Michael reaction.[95] A series of chiral Rh–NCN complexes (see **Fig. 1.6 (ii)**) with different R groups were employed to examine the enantioselectivity for the Asymmetric allylation of carbonyl compounds.[95, 97] Moreover, pincer complexes are also used in some of the other reactions such as in cyclopropanation reactions,[97] in asymmetric allylic alkylation[98] and most importantly in the dehydrogenation of alkanes and ammonia–borane and their relative compounds. The next section will briefly discuss about the various dehydrogenation reactions catalyzed by pincer complexes.

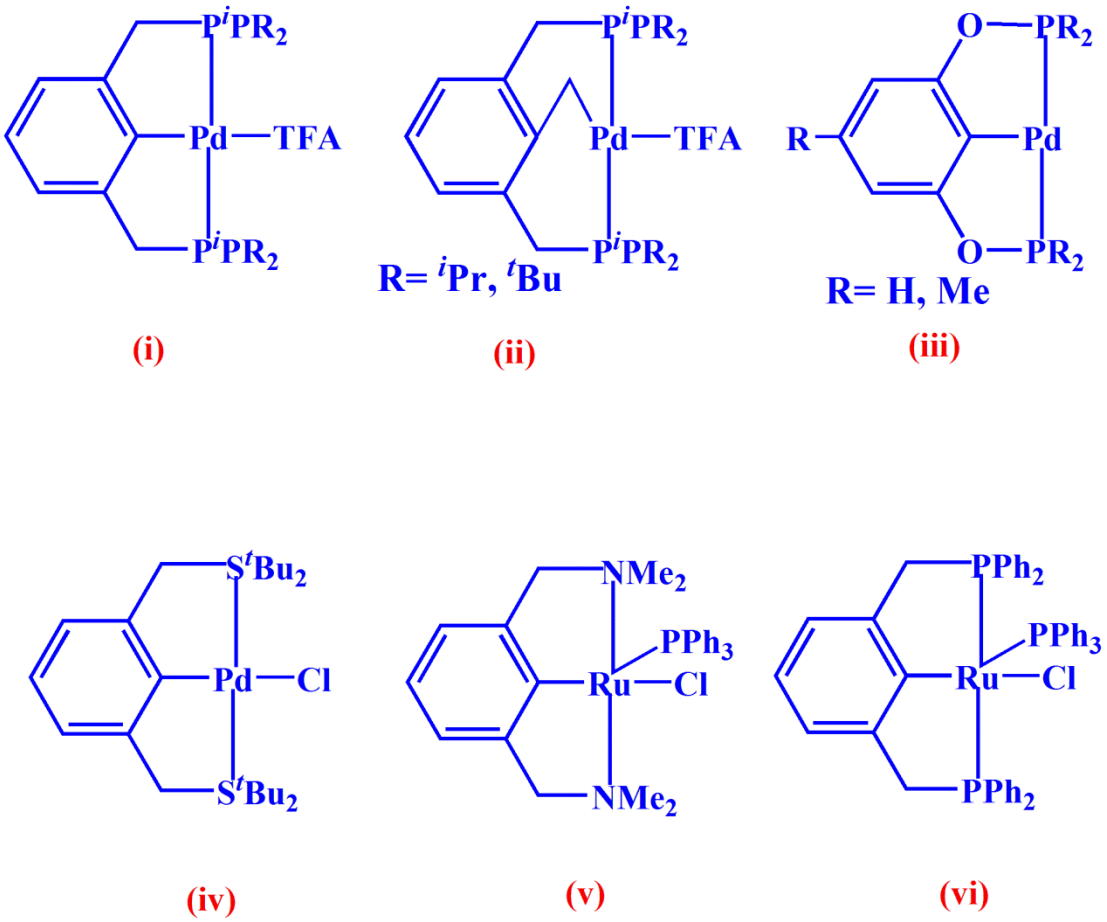

Figure 1.4 Illustration of some of the important pincer catalysts used in Heck, Suzuki–Miyaura coupling and Hydrogen–T transfer reactions.

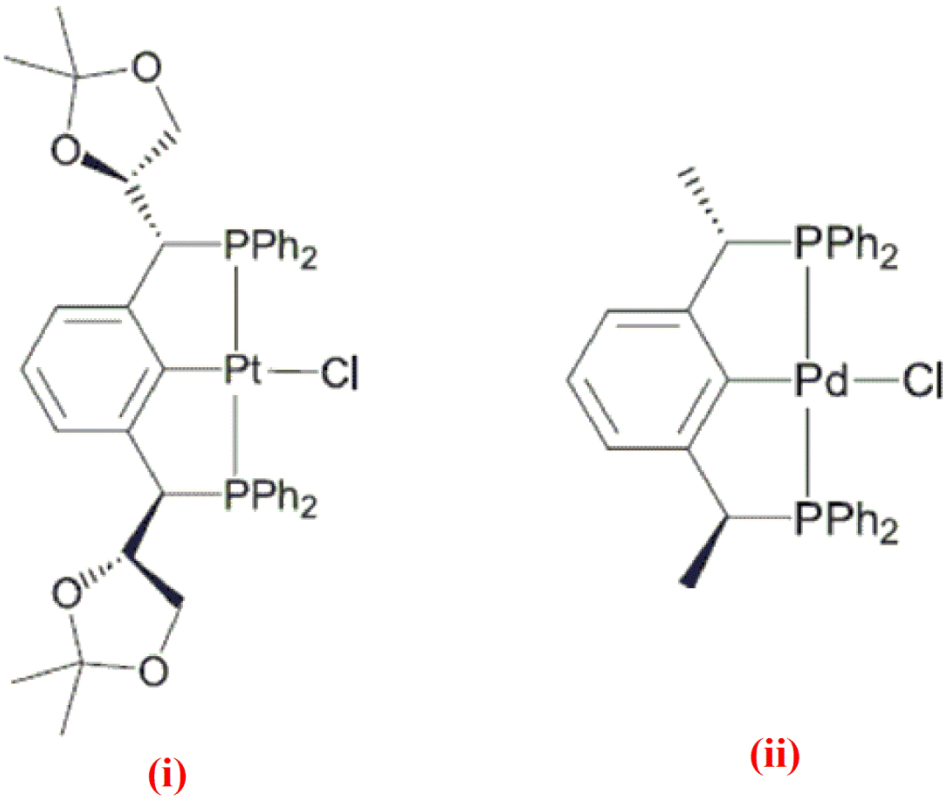

Figure 1.5 Illustration of some of the important chiral pincer catalysts: Pt–PCP and Pd–PCP .[99, 100]

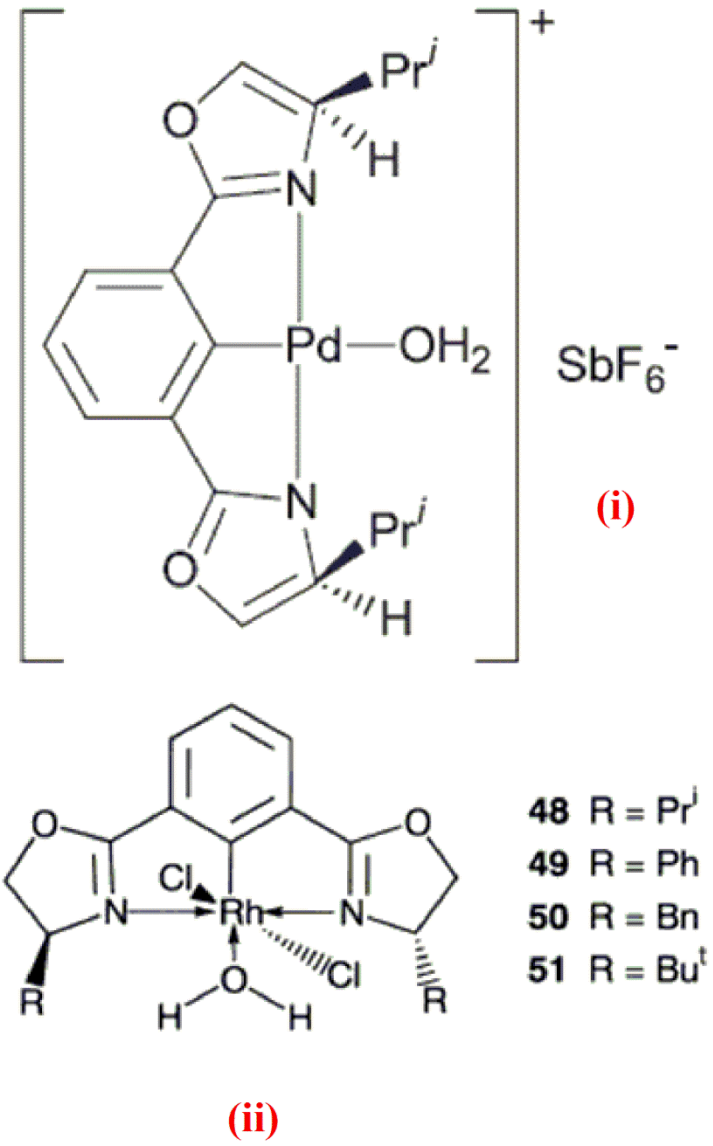

Figure 1.6 Illustration of some of the important chiral pincer catalysts: Pd–NCN and Rh–NCN.[99, 100]

Pincer Catalysts on Dehydrogenation Reactions:

Alkanes are the most naturally abundant and obtainable materials in the earth[101] but their inherent dormant nature restricts their use. On the other hand, reactive alkenes with unsaturated bonds are very attractive and has multiple usage in the industries. An elegant way out to deal with this situation is to activate the strong C–H bonds of the alkanes towards the production of alkenes. The dehydrogenation of

alkanes is endothermic in nature, symmetrically forbidden and generally happens under UV irradiation. Although many transition metal complexes are examined and are reported to have the ability to dehydrogenate alkanes under mild conditions but their quite low reaction rates, the small turnover numbers and instability of some of the catalysts under employed reaction conditions limit their practical use.[102-104] Jensen et *al*. employed the iridium pincer complexes for the very first time to dehydrogenate alkanes.[105] Iridium–PCP pincer complexes[76, 79, 80, 105-109] (see **Fig. 1.7 (i)** and **(ii)**) are the most efficient catalysts for the dehydrogenation reactions of alkanes towards the formation of alkenes and dihydrogen. Dehydrogenation of cycloalkanes, tetrahydrofuran and ethylbezene are also reported for the above mentioned pincer catalysts.[80] The most remarkable modifications of the Ir–PCP complexes are reported by Brookhart et. al and Jensen et.al by introducing Ir–POCOP (see **Fig. 1.7 (iii)**) complexes in place of Ir–PCP complexes.[110-112] These catalysts exhibited higher catalytic activity compared to the Ir–PCP complexes towards the benchmarked dehydrogenation reaction of cyclooctane in presence of *tertiary*–butylethylene. As already mentioned, ammonia borane is iso–electronic with the ethane and the dehydrogenation of ammonia borane and amine boranes are also very important phenomenon from the view of solid state hydrogen storage. Therefore, many Ru and Rh based transition metal complexes have been employed to dehydrogenate the ammonia borane and relative compounds.[19, 113] In this regard, one of the fastest reported rate of dehydrogenation of ammonia borane in presence of Ir–POCOP catalyst with the tertiary butyl group in the ancillary phosphorous atoms was proposed by Goldberg and co–workers.[36] Later on, Musgrave et. al demonstrated the dehydrogenation mechanism of the same from the view point of DFT and they proposed that the dehydrogenation mechanism of ammonia–borane differs from that

of ethane dehydrogenation.[114]

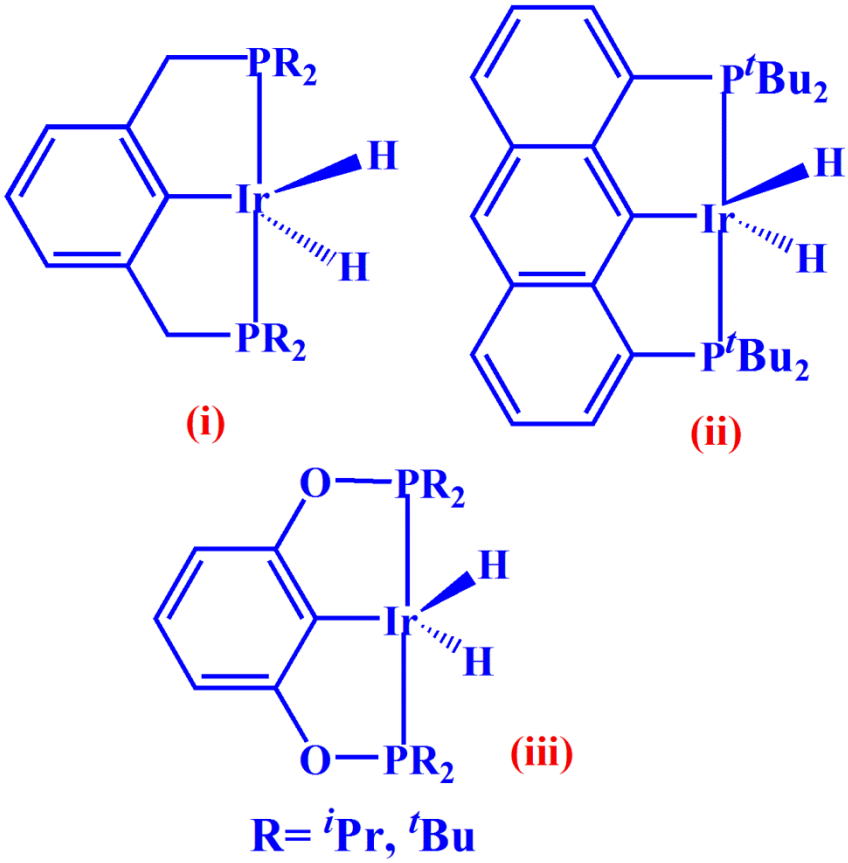

Figure 1.7 Illustration of some of the important Ir–pincer catalysts used in dehydrogenation reactions.

1.4 Atomic Clusters

An aggregate (finite number) of atoms or molecules are generally termed as "*clusters*" among physicists and chemists. Formation of clusters takes place via the cooling and eventually condensation of the hot gaseous stream of atoms or molecules. It is important to note here that molecules and nanoparticles are also aggregate of atoms like clusters, but there exists minor differences between these species. Both clusters and molecules may contain any number of atoms (up to thousands), starting from merely two atoms. Typically, clusters are prepared inside laboratory under special conditions (vacuum or cold flow conditions).On the other hand, molecules are prevalent in nature due to their ability to sustain under ambient pressures and

temperatures. Moreover, interactions of atoms inside the clusters are known to be much stronger than in the molecule and small clusters are also found to fuse together to generate bigger clusters. Atomic compositions in molecules are generally chosen by nature, whereas size and as well atomic compositions in clusters can easily be reorganized by varying the preparation conditions. Atoms in the molecules are generally attached to each other through covalent bonds, whereas clusters are known to form varieties of bonds starting from weak van der Waals to metallic and strong covalent or ionic bonds.

There exists a fine line between clusters (fewer atoms) and nanoparticle (more number of atoms than clusters) and clusters are basically sub–group of the nanoparticle family. It is to be noted here that the size and composition of the nanoparticle cannot be regulated with the same precision as clusters. Furthermore, property evaluation of clusters (one atom at a time) is different from the nanoparticle. As clusters are composed of fewer atoms, the properties (mainly electronic, magnetic and optical) often changes drastically on addition or subtraction of a single atom and thus properties of clusters have size dependency. With the increasing number of atoms, properties of the clusters approach towards the bulk. Clusters and nanoparticles are two parallel fields of research and the distinction between these two fields have narrowed down either with the increasing size of the clusters or with the decreasing size of the nanoparticles. Nowadays, clusters are often referred to as nanoclusters and are critically studied to gain some insight about the properties of the corresponding nanoparticles and of the bulk.

1.4.1 Types of Atomic Clusters

Clusters are categorized based on the nature of chemical bonding in the aggregate. Some of the most abundant types will be discussed in this section.

van der Waals clusters

Atoms in this type of clusters are bound together by weak induced-dipole dispersion force resulting in lower binding energy/atom (≤ 0.3 eV per atom) for them. They have low melting and boiling points due to the weak binding nature and as a result, experimentalists are very much interested to study these types of clusters. Moreover, lots of theoretical studies are also available which mainly focus to the solid–liquid phase transition problems in small clusters. Molecular clusters which are formed as aggregates of closed shell molecules, like $(N_2)_n$, $(CO_2)_n$, $(I_2)_n$ and $(SF_6)_n$ etc. also belong to this family.

Metal clusters

Metals are classified into various groups; such as: a) simple metals, like Na or Al, where valence electrons show *sp* character, b) transition metals, like Fe, Co, Ni etc.; where important role was played by the localized *d* electrons, and c) polyvalent non–transition metals like Pb forming a group in between. Likewise, metal clusters display the similar features of the corresponding metal atoms. The forces inside the metal clusters are complicated (partially directional) because of the existence of the non close–packed structures for several metals. The values of binding energy per atom for metal clusters vary from medium to high range, typically in between 0.5 to 3.0 eV. Electronic shell effects[115] play the key role on determining the characteristics of the *sp* clusters and extensive research works[116-118] are available based on its electronic and structural properties. Electronic shell effects also have a great impact on the induced fragmentation of these clusters.[119] These clusters are specifically known for the low energy electronic excitation due to their electronic states delocalization.[120] It is important to note here that for small clusters (at the primary stage of the growth), the electronic and structural features are correlated to each other

and properties of the system change significantly with the addition of each new atom for these *sp* clusters.

The transition metal clusters are more difficult to deal with due to the presence of valence *d* electrons in the corresponding transition metals. These clusters are widely studied over the last fifty years. Experimentalists and theoreticians are mainly attracted to the transition metal clusters due to their wide applicability in catalysis.[121-123] These types of clusters are also well known for their huge demand in the field of nanoelectronics.[124, 125] Unique magnetic properties and variation of the same according to the cluster size is another great topic of interest among the researchers.[126-128] Theoreticians are much more interested in the electronic, structural and physicochemical properties of these clusters.[129-131]Recently, scientists have broadened their research area towards the bimetallic nanoclusters or doped nanoclusters to gain insight about the mechanism of formation of them at nanoscale.[132, 133] The scope to endeavour a range of combinations of any two metal atoms towards the formation of bimetallic clusters have created a huge area of research.[134, 135] In this regard, bimetallic clusters with the combinations of transition metals and noble metals[134, 136] are well studied due to the drastic changes in their properties as compared to their monometallic analogues.[137-139] Generally, the technique of doping is known to increase the binding energy of these bimetallic clusters and it also enhances the catalytic activity of the bimetallic clusters.[117, 140-147] Moreover, magnetic properties of the doped clusters also differ from the parent clusters.[148-150] Synergistic effect, caused by the correlative effects of different adjacent metal atoms, is the reason behind the different physical as well as chemical properties in the doped clusters.[151] In this thesis, I have studied the effect of Ru doping on Rh_6 cluster and compared the catalytic activities of both doped and pure

clusters by considering methanol activation as the representative case. The details of the same are described in the fifth chapter of this thesis.

Clusters of ionic materials

Closely packed cations (for example; Na^+) and anions (for example; Cl^-) combine themselves to generate ionic materials (for example; NaCl salt). Generally, electropositive metals and electronegative elements are known to form these type of ionic salts and aggregate of these salts via the cohesive forces lead to the formation of clusters of ionic materials (for example; $(NaCl)_n$).[152-154] Attractive forces among these clusters are mainly due to the electrostatic monopoles and repulsive part is the result of overlap of the electronic clouds of ions. Binding energies of these clusters are very high and can go up to 24 eV/atom.

Network clusters

Materials like Si, Ge and C are capable of forming network clusters due to their ability of forming extensive covalent bonding network.[155] Solid crystals and the amorphous forms of those elements are also capable of forming this type of networks. In small clusters, most of the elements are exposed (on the cluster surface) and thus contain dangling bonds. This results in the reconstruction of the covalent network between small clusters leading to the formation of bigger network clusters. Binding energies of these clusters typically vary within 1–4 eV/atom. C_{60} fullerene is the most accurate representative example of this type of cluster.[156]

1.4.2 Metal Clusters on Methanol Adsorption

Size dependent quantum confinement effects, such as, magnetic arrangements, optical properties, various geometrical structures as well as catalytic properties make the small transition metal clusters attractive to the current researchers.[157, 158] Rousseau et *al*. investigated the structural, electronic and dynamical properties of the

single methanol adsorbed neutral and cationic clusters of Au_n (n = 1 –10).[159] Their observations disclosed much higher binding energy for the cationic gold clusters compared to their neutral analogues. Another theoretical work[160] by Li et *al*. demonstrated the structural, energetic and electronic properties of methanol (mono and poly) adsorbed cationic gold clusters such as: $[Au^{3+}–(CH_3OH)_m]$ (m = 1 – 3) and $[Au^{5+} –(CH_3OH)_m]$ (m = 1 – 5). According to their study, the positive charge on the clusters and their coordination numbers were indicated to be the commanding factors towards the strengthening of the chemical bonds between the adsorbate and adsorbent molecules. Recently, Tenney et *al*.[161] reported the enhanced activity of TiO_2 supported Au clusters towards the formation of formaldehyde from the adsorbed methanol molecules. Another recent study by the same group[162] explained the potential of Au–Pt/TiO_2 towards methanol dehydrogenation and observed CO and H_2 to be the final dehydrogenated products. Moreover, higher CO resistance of these bimetallic clusters compared to Pt was also reported. An ab–initio molecular dyanamics simulation on Cu_n (n= 2 – 9) clusters unleashed that these clusters are known to experience systematic dimensional (one-dimension to two-dimension and then to three-dimension) changes, but remain unaffected on the adsorption of methanol molecule.[163] Charge transfer between the methanol molecule and the corresponding neutral Cu clusters was identified as the main reason behind the strong methanol adsorption on these small clusters. A study by Mehmood et *al*.[164] revealed the potential of Cu_4 and Co_4 clusters for complete dissociation of methanol leading to the formation of CO and H_2 as the end products. Their study demonstrated that the pathway for methanol dissociation was initiated by C–H bond breaking in case of Cu_4, whereas O–H bond breaking was identified as the first step for the case of Co_4. Moreover, reaction pathway for the Co_4 case was found to be more favourable from

both the thermodynamics and kinetics point of view but it was reported to have strong CO poisoning effect. The CO poisoning effect was known to get minimised in case of Cu_4 cluster. Another study by the same group[165] represented the methanol dehydrogenation pathway for Pd_4 cluster and their DFT study referred the C–H bond breaking as the initial step towards the complete dehydrogenation to form CO and H_2. Furthermore, a comparative study on the extended Pd surface was also performed and it was comprehended that all reaction intermediates (fragmented intermediates of methanol molecule) were bound to the cluster more strongly than to the surface. A detailed study[166] of gas phase interactions of cationic vanadium clusters V_n^+ (n = 1 – 7) with methanol molecule were performed and a relation between the reactivity with the size of the clusters were explored. The complete dehydrogenation of methanol to form $[V_n^+(CO)]$ intermediate was detected only for those clusters where $n \geq 3$. In 2014, Zhao et *al*.[167] investigated the electronic and geometric properties of methanol (mono and bi molecular) adsorbed cationic $Cu_nAu_m^+$ clusters ($n + m \leq 5$). In the case of $[Cu_nAu_m^+\text{-}(CH_3OH)]$ complexes, all the Cu–binding structures were found to be more stable than the Au–binding structures but energy differences were noted to decrease with increase in the Au composition. For the clusters where $n + m \leq 4$; binding energies of Cu–binding structures was found to increase with the increase in number of Au atoms and binding energies of Au–binding was found to decrease with increase in the Cu atom numbers. The structures of the $[Cu_nAu_m^+\text{–}(CH_3OH)_2]$ complexes were also reported and the next methanol molecule was also found to prefer Cu site for binding and binding energies of the second methanol molecule were lower in most cases.

Various advancements have already been achieved to identify an efficient catalyst which are capable of showing moderate rate on methanol dehydrogenation kinetics

and are reasonably resistant to CO poisoning. Many theoretical works have already been explored to predict a good cost effective catalyst but practical trial of these clusters are yet to be done. Moreover, most of the kinetically favourable catalysts are expensive (Au, Pt etc.), so there still remains scope to develop new efficient, cost effective metal cluster catalysts in the near future.

1.5 References

[1] E. Wigner *Transactions of the Faraday Society*. **1938**, 34, 29-41.
[2] H. Bönnemann *Applied Organometallic Chemistry*. **2008**, 22, 412-412.
[3] P. W. Van Leeuwen, Homogeneous catalysis: understanding the art, Springer Science & Business Media, **2006**.
[4] J. C. Chadwick, R. Duchateau, Z. Freixa, P. W. van Leeuwen, Homogeneous Catalysts: Activity-Stability-Deactivation, John Wiley & Sons, **2011**.
[5] H. Steiner, B.-H. Jonsson, S. Lindskog *European Journal of Biochemistry*. **1975**, 59, 253-259.
[6] N. Chen, Shape selective catalysis in industrial applications, CRC press, **1996**.
[7] M. P. Shaver, M. D. Fryzuk *Advanced Synthesis & Catalysis*. **2003**, 345, 1061-1076.
[8] M. D. Fryzuk, S. A. Johnson *Coordination Chemistry Reviews*. **2000**, 200–202, 379-409.
[9] B. A. MacKay, M. D. Fryzuk *Chemical Reviews*. **2004**, 104, 385-402.
[10] J. L. Fillol, Z. Codolà, I. Garcia-Bosch, L. Gómez, J. J. Pla, M. Costas *Nat Chem*. **2011**, 3, 807-813.
[11] D. J. Wasylenko, R. D. Palmer, C. P. Berlinguette *Chemical Communications*. **2013**, 49, 218-227.
[12] P. G. Jessop, T. Ikariya, R. Noyori *Chemical Reviews*. **1995**, 95, 259-272.
[13] W. Wang, S. Wang, X. Ma, J. Gong *Chemical Society Reviews*. **2011**, 40, 3703-3727.
[14] R. W. Parry, L. J. Edwards *Journal of the American Chemical Society*. **1959**, 81, 3554-3560.
[15] G. W. Schaeffer, M. D. Adams, F. J. Koenig, S. J. Koenig *Journal of the American Chemical Society*. **1956**, 78, 725-728.
[16] S. G. Shore, K. W. Boddeker *Inorganic Chemistry*. **1964**, 3, 914-915.
[17] R. M. Adams, J. Beres, A. Dodds, A. J. Morabito *Inorganic Chemistry*. **1971**, 10, 2072-2074.
[18] J. R. Weaver, S. G. Shore, R. W. Parry *The Journal of Chemical Physics*. **1958**, 29, 1-2.
[19] N. C. Smythe, J. C. Gordon *European Journal of Inorganic Chemistry*. **2010**, 2010, 509-521.
[20] R. F. Service *Science*. **2004**, 305, 958-961.
[21] F. H. Stephens, V. Pons, R. Tom Baker *Dalton Transactions*. **2007**, 2613-2626.
[22] L. J. Murray, M. Dinca, J. R. Long *Chemical Society Reviews*. **2009**, 38, 1294-1314.
[23] U. Eberle, M. Felderhoff, F. Schüth *Angewandte Chemie International Edition*. **2009**, 48, 6608-6630.

[24] R. Snurr *Nat Chem*. **2009**, 1, 426-427.
[25] T. B. Marder *Angewandte Chemie International Edition*. **2007**, 46, 8116-8118.
[26] F. Baitalow, J. Baumann, G. Wolf, K. Jaenicke-Rößler, G. Leitner *Thermochimica Acta*. **2002**, 391, 159-168.
[27] G. Wolf, J. Baumann, F. Baitalow, F. P. Hoffmann *Thermochimica Acta*. **2000**, 343, 19-25.
[28] G. Wolf, J. C. van Miltenburg, U. Wolf *Thermochimica Acta*. **1998**, 317, 111-116.
[29] V. Sit, R. A. Geanangel, W. W. Wendlandt *Thermochimica Acta*. **1987**, 113, 379-382.
[30] M. G. Hu, R. A. Geanangel, W. W. Wendlandt *Thermochimica Acta*. **1978**, 23, 249-255.
[31] R. Komm, R. A. Geanangel, R. Liepins *Inorganic Chemistry*. **1983**, 22, 1684-1686.
[32] M. E. Bluhm, M. G. Bradley, R. Butterick, U. Kusari, L. G. Sneddon *Journal of the American Chemical Society*. **2006**, 128, 7748-7749.
[33] J. S. Wang, R. A. Geanangel *Inorganica Chimica Acta*. **1988**, 148, 185-190.
[34] Q. Xu, M. Chandra *Journal of Power Sources*. **2006**, 163, 364-370.
[35] M. Chandra, Q. Xu *Journal of Power Sources*. **2006**, 156, 190-194.
[36] M. C. Denney, V. Pons, T. J. Hebden, D. M. Heinekey, K. I. Goldberg *Journal of the American Chemical Society*. **2006**, 128, 12048-12049.
[37] Y. Chen, J. L. Fulton, J. C. Linehan, T. Autrey *Journal of the American Chemical Society*. **2005**, 127, 3254-3255.
[38] A. Gutowska, L. Li, Y. Shin, C. M. Wang, X. S. Li, J. C. Linehan, R. S. Smith, B. D. Kay, B. Schmid, W. Shaw, M. Gutowski, T. Autrey *Angewandte Chemie International Edition*. **2005**, 44, 3578-3582.
[39] R. Boyle, The Sceptical Chymist: The Classic 1661 Text, Courier Corporation, **1911**.
[40] T. Chang, R. W. Rousseau, P. K. Kilpatrick *Industrial & Engineering Chemistry Process Design and Development*. **1986**, 25, 477-481.
[41] E. M. C. Alayon, M. Nachtegaal, M. Ranocchiari, J. A. van Bokhoven *CHIMIA International Journal for Chemistry*. **2012**, 66, 668-674.
[42] C. Hammond, R. L. Jenkins, N. Dimitratos, J. A. Lopez-Sanchez, M. H. ab Rahim, M. M. Forde, A. Thetford, D. M. Murphy, H. Hagen, E. E. Stangland *Chemistry-a European Journal*. **2012**, 18, 15735-15745.
[43] G. A. Olah, A. Goeppert, G. K. S. Prakash *The Journal of Organic Chemistry*. **2009**, 74, 487-498.
[44] B. Schink, J. G. Zeikus *Current microbiology*. **1980**, 4, 387-389.
[45] B. Blank, S. Michlik, R. Kempe *Advanced Synthesis & Catalysis*. **2009**, 351, 2903-2911.
[46] R. Grigg, T. R. B. Mitchell, S. Sutthivaiyakit, N. Tongpenyai *Tetrahedron Letters*. **1981**, 22, 4107-4110.
[47] J. Moran, A. Preetz, R. A. Mesch, M. J. Krische *Nat Chem*. **2011**, 3, 287-290.
[48] Y. Pan, L. Ye, B.-J. Ni, Z. Yuan *Water Research*. **2012**, 46, 4832-4840.
[49] Y. Pan, B.-J. Ni, P. L. Bond, L. Ye, Z. Yuan *Water Research*. **2013**, 47, 3273-3281.
[50] P. Timmermans, A. Van Haute *Water Research*. **1983**, 17, 1249-1255.
[51] G. Lettinga *Antonie van Leeuwenhoek*. **1995**, 67, 3-28.
[52] G. Claus, H. Kutzner *Appl Microbiol Biotechnol*. **1985**, 22, 378-381.
[53] L. Foglar, F. Briški *Process Biochemistry*. **2003**, 39, 95-103.

[54] M. Li, K. Duraiswamy, M. Knobbe *Chemical Engineering Science*. **2012**, 67, 26-33.
[55] R. Pérez-Hernández, A. Gutiérrez-Martínez, M. E. Espinosa-Pesqueira, M. L. Estanislao, J. Palacios *Catalysis Today*.
[56] N. Yi, R. Si, H. Saltsburg, M. Flytzani-Stephanopoulos *Applied Catalysis B: Environmental*. **2010**, 95, 87-92.
[57] G. L. Chiarello, M. H. Aguirre, E. Selli *Journal of Catalysis*. **2010**, 273, 182-190.
[58] J. Vancoillie, J. Demuynck, L. Sileghem, M. Van De Ginste, S. Verhelst *International Journal of Hydrogen Energy*. **2012**, 37, 9914-9924.
[59] G. A. Olah *Angewandte Chemie International Edition*. **2005**, 44, 2636-2639.
[60] C. D. Chang *Catalysis Reviews*. **1983**, 25, 1-118.
[61] R. N. Hader, R. D. Wallace, R. W. McKinney *Industrial & Engineering Chemistry*. **1952**, 44, 1508-1518.
[62] F. E. Paulik, J. F. Roth *Chemical Communications (London)*. **1968**, 1578a-1578a.
[63] G.-Q. Chen, M. K. Patel *Chemical Reviews*. **2012**, 112, 2082-2099.
[64] W. P. Yant, H. H. Schrenk, R. R. Sayers *Industrial & Engineering Chemistry*. **1931**, 23, 551-555.
[65] S. Sharma, B. G. Pollet *Journal of Power Sources*. **2012**, 208, 96-119.
[66] O. Blum, D. Stöckigt, D. Schröder, H. Schwarz *Angewandte Chemie International Edition in English*. **1992**, 31, 603-604.
[67] J. S. Owen, J. A. Labinger, J. E. Bercaw *Journal of the American Chemical Society*. **2006**, 128, 2005-2016.
[68] G. Deo, I. E. Wachs *Journal of Catalysis*. **1994**, 146, 323-334.
[69] F. Schager, K. Seevogel, K.-R. Pörschke, M. Kessler, C. Krüger *Journal of the American Chemical Society*. **1996**, 118, 13075-13076.
[70] X. Sun, X. Sun, C. Geng, H. Zhao, J. Li *The Journal of Physical Chemistry A*. **2014**, 118, 7146-7158.
[71] W. A. Donald, C. J. McKenzie, R. A. J. O'Hair *Angewandte Chemie International Edition*. **2011**, 50, 8379-8383.
[72] C. J. Zhang, P. Hu *The Journal of Chemical Physics*. **2001**, 115, 7182-7186.
[73] W. T. Lee, F. Thomas, R. I. Masel *Surface Science*. **1998**, 418, 479-483.
[74] D. Wang, E. R. Farquhar, A. Stubna, E. Münck, L. Que *Nat Chem*. **2009**, 1, 145-150.
[75] M. Panzner, C. Tessier, W. Youngs in The Chemistry of Pincer Compounds. 1. Morales-Morales, D.; Jensen, CM., editors, Vol. (Ed.^Eds.: Editor), Elsevier Amsterdam:, City, **2007**.
[76] C. M. Jensen *Chemical Communications*. **1999**, 2443-2449.
[77] C. J. Moulton, B. L. Shaw *Journal of the Chemical Society, Dalton Transactions*. **1976**, 1020-1024.
[78] M. Albrecht, G. van Koten *Angewandte Chemie International Edition*. **2001**, 40, 3750-3781.
[79] D. Morales-Morales, C. G. Jensen, The chemistry of pincer compounds, Elsevier, **2011**.
[80] M. E. van der Boom, D. Milstein *Chemical Reviews*. **2003**, 103, 1759-1792.
[81] R. F. Heck *Journal of the American Chemical Society*. **1968**, 90, 5518-5526.
[82] R. F. Heck in *Palladium-Catalyzed Vinylation of Organic Halides, Vol.*, John Wiley & Sons, Inc., **2004**.
[83] W. Cabri, I. Candiani *Accounts of Chemical Research*. **1995**, 28, 2-7.
[84] M. Ohff, A. Ohff, M. E. van der Boom, D. Milstein *Journal of the American Chemical Society*. **1997**, 119, 11687-11688.

[85] A. Suzuki *Journal of Organometallic Chemistry*. **1999**, 576, 147-168.
[86] R. B. Bedford, S. M. Draper, P. Noelle Scully, S. L. Welch *New Journal of Chemistry*. **2000**, 24, 745-747.
[87] D. Zim, A. S. Gruber, G. Ebeling, J. Dupont, A. L. Monteiro *Organic Letters*. **2000**, 2, 2881-2884.
[88] P. Dani, T. Karlen, R. A. Gossage, S. Gladiali, G. van Koten *Angewandte Chemie International Edition*. **2000**, 39, 743-745.
[89] T. Naota, H. Takaya, S.-I. Murahashi *Chemical Reviews*. **1998**, 98, 2599-2660.
[90] P. Dani, M. Albrecht, G. P. M. van Klink, G. van Koten *Organometallics*. **2000**, 19, 4468-4476.
[91] Y. Ito, M. Sawamura, T. Hayashi *Journal of the American Chemical Society*. **1986**, 108, 6405-6406.
[92] F. Gorla, L. M. Venanzi, A. Albinati *Organometallics*. **1994**, 13, 43-54.
[93] F. Gorla, A. Togni, L. M. Venanzi, A. Albinati, F. Lianza *Organometallics*. **1994**, 13, 1607-1616.
[94] J. M. Longmire, X. Zhang, M. Shang *Organometallics*. **1998**, 17, 4374-4379.
[95] M. A. Stark, C. J. Richards *Tetrahedron Letters*. **1997**, 38, 5881-5884.
[96] R. Giménez, T. M. Swager *Journal of Molecular Catalysis A: Chemical*. **2001**, 166, 265-273.
[97] S. E. Denmark, R. A. Stavenger, A.-M. Faucher, J. P. Edwards *The Journal of Organic Chemistry*. **1997**, 62, 3375-3389.
[98] J. M. Longmire, X. Zhang *Tetrahedron Letters*. **1997**, 38, 1725-1728.
[99] J. T. Singleton *Tetrahedron*. **2003**, 59, 1837-1857.
[100] D. Morales-Morales *Rev. Soc. Quim. Mex*. **2004**, 48, 338-346.
[101] W. D. Jones *Science*. **2000**, 287, 1942-1943.
[102] R. H. Crabtree, J. M. Mihelcic, J. M. Quirk *Journal of the American Chemical Society*. **1979**, 101, 7738-7740.
[103] D. Baudry, M. Ephritikhine, H. Felkin, R. Holmes-Smith *Journal of the Chemical Society, Chemical Communications*. **1983**, 788-789.
[104] H. Felkin, T. Fillebeen-khan, R. Holmes-Smith, L. Yingrui *Tetrahedron Letters*. **1985**, 26, 1999-2000.
[105] M. Gupta, C. Hagen, R. J. Flesher, W. C. Kaska, C. M. Jensen *Chemical Communications*. **1996**, 2083-2084.
[106] M. Gupta, C. Hagen, W. C. Kaska, R. E. Cramer, C. M. Jensen *Journal of the American Chemical Society*. **1997**, 119, 840-841.
[107] D. Morales-Morales, D. W. Lee, Z. Wang, C. M. Jensen *Organometallics*. **2001**, 20, 1144-1147.
[108] Z. Huang, M. Brookhart, A. S. Goldman, S. Kundu, A. Ray, S. L. Scott, B. C. Vicente *Advanced Synthesis & Catalysis*. **2009**, 351, 188-206.
[109] J. Choi, A. H. R. MacArthur, M. Brookhart, A. S. Goldman *Chemical Reviews*. **2011**, 111, 1761-1779.
[110] I. Göttker-Schnetmann, P. White, M. Brookhart *Journal of the American Chemical Society*. **2004**, 126, 1804-1811.
[111] I. Göttker-Schnetmann, M. Brookhart *Journal of the American Chemical Society*. **2004**, 126, 9330-9338.
[112] D. Morales-Morales, R. o. Redón, C. Yung, C. M. Jensen *Inorganica Chimica Acta*. **2004**, 357, 2953-2956.
[113] C. A. Jaska, K. Temple, A. J. Lough, I. Manners *Journal of the American Chemical Society*. **2003**, 125, 9424-9434.
[114] A. Paul, C. B. Musgrave *Angewandte Chemie*. **2007**, 119, 8301-8304.

[115] W.-D. Knight, K. Clemenger, W. A. de Heer, W. A. Saunders, M. Chou, M. L. Cohen *Physical review letters*. **1984**, 52, 2141.
[116] F. Baletto, R. Ferrando *Reviews of modern physics*. **2005**, 77, 371.
[117] H. Häkkinen, S. Abbet, A. Sanchez, U. Heiz, U. Landman *Angewandte Chemie International Edition*. **2003**, 42, 1297-1300.
[118] M. L. Steigerwald, L. E. Brus *Annual Review of Materials Science*. **1989**, 19, 471-495.
[119] B. Rao, P. Jena, M. Manninen, R. Nieminen *Physical review letters*. **1987**, 58, 1188.
[120] G. Onida, L. Reining, R. W. Godby, R. Del Sole, W. Andreoni *Physical review letters*. **1995**, 75, 818-821.
[121] C. R. Henry *Applied Surface Science*. **2000**, 164, 252-259.
[122] S. Bhaduri *CURRENT SCIENCE-BANGALORE*-. **2000**, 78, 1318-1324.
[123] J. D. Aiken Iii, R. G. Finke *Journal of Molecular Catalysis A: Chemical*. **1999**, 145, 1-44.
[124] G. Schmid *Chemical Reviews*. **1992**, 92, 1709-1727.
[125] Y. Volokitin, J. Sinzig, L. J. de Jongh, G. Schmid, M. N. Vargaftik, I. I. Moiseevi *Nature*. **1996**, 384, 621-623.
[126] A. Enders, R. Skomski, D. J. Sellmyer in *Designed Magnetic Nanostructures, Vol.* (Eds.: J. P. Liu, E. Fullerton, O. Gutfleisch, D. J. Sellmyer), Springer US, **2009**, pp.67-103.
[127] G. M. Pastor, J. Dorantes-Dávila, K. H. Bennemann *Physical Review B*. **1989**, 40, 7642-7654.
[128] G. M. Pastor, J. Dorantes-Dávila, S. Pick, H. Dreyssé *Physical review letters*. **1995**, 75, 326-329.
[129] J. Wang, G. Wang, J. Zhao *Physical Review B*. **2002**, 66, 035418.
[130] L. S. Wang, H. S. Cheng, J. Fan *The Journal of Chemical Physics*. **1995**, 102, 9480-9493.
[131] E. M. Fernández, J. M. Soler, I. L. Garzón, L. C. Balbás *Physical Review B*. **2004**, 70, 165403.
[132] J. H. Sinfelt *Accounts of Chemical Research*. **1987**, 20, 134-139.
[133] T. Momin, A. Bhowmick *Journal of Alloys and Compounds*. **2013**, 559, 24-33.
[134] R. Ferrando, J. Jellinek, R. L. Johnston *Chemical Reviews*. **2008**, 108, 845-910.
[135] F. Delogu *The Journal of Physical Chemistry C*. **2010**, 114, 19946-19951.
[136] M. Gaudry, E. Cottancin, M. Pellarin, J. Lermé, L. Arnaud, J. Huntzinger, J. Vialle, M. Broyer, J. Rousset, M. Treilleux *Physical Review B*. **2003**, 67, 155409.
[137] T. Shibata, B. A. Bunker, Z. Zhang, D. Meisel, C. F. Vardeman, J. D. Gezelter *Journal of the American Chemical Society*. **2002**, 124, 11989-11996.
[138] S. Darby, T. V. Mortimer-Jones, R. L. Johnston, C. Roberts *The Journal of Chemical Physics*. **2002**, 116, 1536-1550.
[139] G. Rossi, A. Rapallo, C. Mottet, A. Fortunelli, F. Baletto, R. Ferrando *Physical review letters*. **2004**, 93, 105503.
[140] K. Bergamaski, E. R. Gonzalez, F. C. Nart *Electrochimica Acta*. **2008**, 53, 4396-4406.
[141] J. P. I. de Souza, S. L. Queiroz, K. Bergamaski, E. R. Gonzalez, F. C. Nart *The Journal of Physical Chemistry B*. **2002**, 106, 9825-9830.
[142] T. E. Shubina, M. T. M. Koper *Electrochimica Acta*. **2002**, 47, 3621-3628.
[143] S. Sen Gupta, J. Datta *Journal of Electroanalytical Chemistry*. **2006**, 594, 65-72.
[144] F. Tao, M. E. Grass, Y. Zhang, D. R. Butcher, F. Aksoy, S. Aloni, V. Altoe, S.

Alayoglu, J. R. Renzas, C.-K. Tsung, Z. Zhu, Z. Liu, M. Salmeron, G. A. Somorjai *Journal of the American Chemical Society*. **2010**, 132, 8697-8703.
[145] N. K. Jena, K. Chandrakumar, S. K. Ghosh *The Journal of Physical Chemistry Letters*. **2011**, 2, 1476-1480.
[146] M. B. Torres, E. M. Fernández, L. C. Balbas *The Journal of Physical Chemistry A*. **2008**, 112, 6678-6689.
[147] D. Manzoor, S. Krishnamurty, S. Pal *The Journal of Physical Chemistry C*. **2014**, 118, 7501-7507.
[148] J. M. Matxain, M. Piris, E. Formoso, J. M. Mercero, X. Lopez, J. M. Ugalde *ChemPhysChem*. **2007**, 8, 2096-2099.
[149] P. I. Archer, S. A. Santangelo, D. R. Gamelin *Journal of the American Chemical Society*. **2007**, 129, 9808-9818.
[150] H. Liu, S. Wang, G. Zhou, J. Wu, W. Duan *The Journal of Chemical Physics*. **2006**, 124, 174705-174705.
[151] F. Massicot, R. Schneider, Y. Fort, S. Illy-Cherrey, O. Tillement *Tetrahedron*. **2000**, 56, 4765-4768.
[152] I. V. Yudanov, V. A. Nasluzov, K. M. Neyman, N. Rösch *International Journal of Quantum Chemistry*. **1997**, 65, 975-986.
[153] A. Ayuela, J. M. López, J. A. Alonso, V. Luaña *Z Phys D - Atoms, Molecules and Clusters*. **1993**, 26, 213-215.
[154] M. Riedler, A. R. B. de Castro, A. Kolmakov, J. O. Löfken, C. Nowak, A. V. Soldatov, A. Wark, G. Yalovega, T. Möller *Physical Review B*. **2001**, 64, 245419.
[155] J. C. Phillips *The Journal of Chemical Physics*. **1987**, 87, 1712-1716.
[156] W. Krätschmer, L. D. Lamb, K. Fostiropoulos, D. R. Huffman *Nature*. **1990**, 347, 354-358.
[157] M. B. Knickelbein *Annual review of physical chemistry*. **1999**, 50, 79-115.
[158] J. A. Alonso *Chemical Reviews*. **2000**, 100, 637-678.
[159] R. Rousseau, D. Marx *The Journal of Chemical Physics*. **2000**, 112, 761-769.
[160] Y.-C. Li, C.-L. Yang, M.-Y. Sun, X.-X. Li, Y.-P. An, M.-S. Wang, X.-G. Ma, D.-H. Wang *The Journal of Physical Chemistry A*. **2009**, 113, 1353-1359.
[161] S. A. Tenney, B. A. Cagg, M. S. Levine, W. He, K. Manandhar, D. A. Chen *Surface Science*. **2012**, 606, 1233-1243.
[162] S. A. Tenney, S. I. Shah, H. Yan, B. A. Cagg, M. S. Levine, T. S. Rahman, D. A. Chen *The Journal of Physical Chemistry C*. **2013**, 117, 26998-27006.
[163] W.-D. Hsu, M. Ichihashi, T. Kondow, S. B. Sinnott *The Journal of Physical Chemistry A*. **2007**, 111, 441-449.
[164] F. Mehmood, J. Greeley, P. Zapol, L. A. Curtiss *The Journal of Physical Chemistry B*. **2010**, 114, 14458-14466.
[165] F. Mehmood, J. Greeley, L. A. Curtiss *The Journal of Physical Chemistry C*. **2009**, 113, 21789-21796.
[166] S. Feyel, D. Schröder, H. Schwarz *The Journal of Physical Chemistry A*. **2009**, 113, 5625-5632.
[167] S. Zhao, H. Tang, Y. Ren, A. Xu, J. Wang *Computational and Theoretical Chemistry*. **2014**, 1037, 14-21.

Chapter 2: Methodology

Abstract

This thesis focuses on the catalytic activity of organometallic pincer complexes and small metal clusters towards the dissociation of small molecules (such as: NH_3BH_3, HCOOH, CH_3OH etc.) and involves the structural (ground state as well as transition state structures), electronic, thermodynamic and kinetic investigation of the various complexes. The present chapter provides an overview of the theoretical techniques used to study the same. Determining the ground state and transition state geometries and the associated electrostatics of the complex molecules is the prime goal of this thesis. The methodology employed is based on Density Functional Theory.

2.1 The many-electron problem

2.1.1 Schrödinger Equation

The time independent non–relativistic Schrödinger equation[1] is the fundamental equation of quantum mechanics which is used to solve problems in chemistry by extracting the energy of the concerned systems. It has the form

$$H\Psi = E\Psi \tag{2.1}$$

where Ψ is the many–electron wave function, H is the Hamiltonian operator and E is the energy of the corresponding system. Solutions of this equation provides set of wave functions Ψ_i , (i = 1, 2,...) which correspond to the set quantum states of the system for the i^{th} state. **H,** the Hamiltonian operator, is the sum of the kinetic energy ***T*** and potential energy *V* operators. The expression of *H* is expanded as follows

$$\begin{aligned} H &= T + V \\ T &= -\sum_{i=1}^{N} \frac{1}{2m} \Delta_i^2 - \sum_{A=1}^{M} \frac{1}{2M_A} \Delta_A^2 \\ V &= -\sum_{i=1}^{N} \sum_{A=1}^{M} \frac{Z_A}{r_{iA}} + \sum_{i=1}^{N} \sum_{j>i}^{N} \frac{1}{r_{ij}} - \sum_{A=1}^{M} \sum_{B>A}^{M} \frac{Z_A Z_b}{R_{AB}} \end{aligned} \tag{2.2}$$

The kinetic energy operator (*T*) is the sum of electronic and nuclear parts

respectively, wherein m and M_A represent the masses of electrons and nuclei respectively. The potential energy operator is the combination of three terms, a) Coulomb potential between electrons and nuclei which are apart from each other by distance $\boldsymbol{r_{iA}}$, b) self interaction between electrons, where the $\boldsymbol{i}^{th}$ and the $\boldsymbol{j}^{th}$ electrons are separated by a distance $\boldsymbol{r_{ij}}$ and c) repulsion between nuclei R_{AB} is the distance between the A^{th} and the B^{th} nuclei.

2.1.2 Born-Oppenheimer Approximation

Nuclei are much heavier as compared to electrons; hence their movement is much slower when compared to the electronic motion. Hence, to a very good approximation, it is considered that electrons inside a molecule are moving in the field of fixed nuclei – known as Born-Oppenheimer approximation.[2] According to this approximation, the kinetic energy of the nuclei is omitted and the nuclear repulsion term is considered to be constant. Electronic operator Hamiltonian (which has parametric dependence on nuclear coordinate) for a system consisting of N electrons and M nuclei, is described as

$$H_{elec} = -\sum_{i=1}^{N} \frac{1}{2}\Delta_i^2 - \sum_{i=1}^{N}\sum_{A=1}^{M} \frac{Z_A}{r_{iA}} + \sum_{i=1}^{N}\sum_{j>i}^{N} \frac{1}{r_{ij}} \qquad (2.3)$$

The above eigenvalue equation 2.3 is solved and the total energy is obtained by summing up the electronic energy and the constant nuclear repulsion energy term. The most challenging part of the multi electronic problem is to solve the electron–electron repulsion term (third term of equation 2.3). Many theoretical approximation methods such as Hartree–Fock (HF), Configuration Interaction (CI), Coupled Cluster (CC) etc have been employed to solve the multi–electronic problem.[3] Density functional theory (DFT)[4] is one of the important and well known methods where the concept of electron density is introduced as a basic variable instead of the wave

function. DFT provides the ground state properties of a multi–electron system and it is also computationally inexpensive compared to other *ab initio* theories. It is important to note that DFT handles the electron–electron correlation differently than other methods such as, HF.

2.2 Density Functional Theory

DFT is an extremely convenient and practical tool for the calculations of electronic structures and the ground state properties of atoms, molecules, metals, semiconductors, etc. It begins via replacing the complicated N-electron wave function and the associated Schrödinger wave equation by a much easier electron density. In 1920s, two famous scientists, Thomas and Fermi initiated the practice of DFT based on some specific approximations. Thomas–Fermi[5-7] model estimates the distribution of electrons in an atom through statistical considerations. Their ideal model assumes that the system is comprised of non–interacting electrons moving in a homogeneous gas with a density similar to the local density at the given point. Therefore, the kinetic energy can be treated as an explicit functional of density and this model completely neglects the exchange and correlation parts.

According to the Thomas-Fermi (TF) model, the total energy of an atom with a nuclear charge *Z* is expressed as

$$E_{TF}[\rho(\mathrm{r})] = C_F \int \rho^{5/3}(r)dr - z\int \frac{\rho(r)}{r}dr + \frac{1}{2}\iint \frac{\rho(r)\rho(r')}{|r-r'|}drdr' \qquad (2.4)$$

where C_F represents the Fermi coefficient possessing the value of 2.871. It proceeds via constrained minimization of the energy functional (E_{TF}) with the variation of electron density, representing the ground state of an atom. The mentioned constraint is as follows:

$$N = N[\rho(r)] = \int \rho(r)dr \qquad (2.5)$$

The Thomas–Fermi model formulates the explicit total energy for an atom but its accuracy is very low. Total energy calculation of the molecules leads to erroneous results and even questions the stability of the concerned molecule.

2.2.1 Hohenberg-Kohn Theorem

Threads of many such theoretical models (post Thomas –Fermi) are present in the literature which until 1964 was just a prototype. Two famous fundamental theorems of Hohenberg and Kohn (1964)[8] led theoreticians to develop modern density functional theory. Implementation of these two theorems shows that Thomas–Fermi model is an approximation to the ground state of the original theory. It actually manifests the existence of an exact energy functional and presence of an exact variational principle. Hohenberg and Kohn proved that the ground state properties are functionals of the electron density, $\rho(r)$, which actually lead to the foundation of the basic framework for the modern DFT.[4]

First Hohenberg –Kohn theorem[8] states that:

The external potential v(r) is determined, within a trivial additive constant, by the electron density $\rho(r)$.

In general, $\upsilon(r)$ and *N* are used as basic variables, where as this theorem endorses the application of electron density, $\rho(r)$, as basic variable.

The theory is explained as follows:

trivially, $\upsilon(r), N \xrightarrow{determines} H \xrightarrow{determines} E$

where, *N*, *H* and *E* signify total number of electrons, Hamiltonian operator and energy of the system respectively.

Since,

$\rho(r) \xrightarrow{determines} N$ and $\rho(r) \xrightarrow{determines} \Psi_i$ (ground state wave function)

and, according to the theory, $\rho(r) \xrightarrow{determines} \upsilon(r)$.

It is to be noted here that $\upsilon(r)$ is not only limited to the electron–nucleus Coulomb potential, rather it is generalized as any kind of external potential (for example, potential due to electrical and magnetic field etc.). Hence, the ground state expectation value of any observable (including the total energy) is an unique functional of the ground-state electron density $\rho(r)$

$$\rho(r) \xrightarrow{determines} \text{all properties including energy.}$$

According to this theory, the energy functional can be formulated as,

$$E_\upsilon[\rho] = T[\rho] + V_{ne}[\rho] + V_{ee}[\rho] = \int \rho(r)\upsilon(r)dr + F_{HK}[\rho] \qquad (2.6)$$

where, $$F_{HK}[\rho] = T[\rho] + V_{ee}[\rho]$$

The electron –electron repulsion term $V_{ee}[\rho]$ is the sum of the classical Coulomb repulsion term, $J[\rho]$ and the non –classical repulsion (mainly exchange-correlation energy).

The second Hohenberg –Kohn theorem[8] states that:

For a trial density $\tilde{\rho}(r)$, *such that* $\tilde{\rho}(r) \geq 0$ *and* $\int \tilde{\rho}(r)dr = N$,

$$E_0 \leq E_\upsilon[\tilde{\rho}]$$

E_0 represents the energy corresponding to the ground state electron density. The above equation starts with a trial density $\tilde{\rho}(r)$, and seeks the closest approximated possible ground state electron density (closest to the exact) and corresponding ground state energy through the minimization of the energy functional $E[\tilde{\rho}]$. However, one of the necessary condition needs to be implemented for the trial densities such that the trial density should be associated with an anti–symmetric ground state wavefunction and such densities are known as *N*–representable densities. More accurately, the

density should also correspond to some external potential to satisfy the υ–representability condition. It is necessary to mention that υ–representability condition is more strict, covering the *N*–representability condition. Densities which are not co–associated to any external potential[4] (i.e; not υ–representable) can not correspond to any ground state.

2.2.2 Kohn-Sham Equations

Thomas and Fermi approximated the term $V_{ee}[\rho]$ as the classical Coulomb potential; $J[\rho]$ by completely neglecting the non-classical part and the kinetic energy term; $T[\rho]$ was calculated by adaptation of non-interacting uniform electron gas approximation. Their direct method provides unsatisfactory results in case of kinetic energy as well as total energy calculations. Kinetic energy, which is the major part of the total energy of the system, needs to be calculated correctly to get a good approximation (closer to the exact) of the total energy of the system. In this regard, Kohn and Sham[9] brought back the orbital concept (wave function method) in order to calculate the kinetic energy part separately and these eventually promote DFT into a pragmatic method. KS introduced a method based on the theorems provide by Hohenberg and Kohn, Kohn and Sham developed a method which actually proceeds via minimization of $E[\rho]$ with respect to $\rho(r)$ over all *N* electrons.[4] Foundation of Kohn-Sham (KS) functional is established on the assumption that the ground state density of a non–interacting system is similar to the exact ground state density.

Literally, kinetic energy for an *N* non–interacting electronic system can be expressed as,

$$T_s[\rho] = \sum_{i=1}^{N} \left\langle \psi_i \left| -\tfrac{1}{2}\Delta^2 \right| \psi_i \right\rangle \qquad (2.7)$$

and the corresponding electron density is formulated as,

$$\rho(r) = \sum_{i=1}^{N} \sum_{s} |\psi_i(r,s)|^2 \tag{2.8}$$

Kohn–Sham[4, 9] substituted the many–body (interacting) problem by a non–interacting model possessing the same density within an appropriate effective potential. The energy functional is written in the following form:

$$E[\rho] = T_s[\rho] + J[\rho] + E_{xc}[\rho] + \int \upsilon(r)\rho(r)dr \tag{2.9}$$

where, $T_s[\rho]$ is expressed according to the equation 2.7. In the equation 2.9, $T_s[\rho]$ describes the kinetic energy of electrons through the employment of a model non–interacting system, sharing the same electron density with the real system and $J[\rho]$ is the classical electronic Coulomb potential. E_{xc} represents the non–classical exchange–correlation potential including the small residual correction ($T[\rho] - T_s[\rho]$; $T[\rho]$ = difference between the exact kinetic energy functional and the kinetic energy functional of the non–interacting system). Fourth term the Coulomb potential due to the electron-nucleus attraction. Now, Kohn-Sham (KS) energy functional varies with respect to electron density and this eventually provides *N* number of KS equations

$$[-\tfrac{1}{2}\Delta^2 + \upsilon_{eff}]\psi_i = \varepsilon_i\psi_i \tag{2.10}$$

where, ψ_i, ε_i and υ_{eff} represents the KS orbitals, eigenvalues and KS effective potential respectively.

υ_{eff} can be expressed as follows:

$$\upsilon_{eff}(r) = \upsilon(r) + \frac{\delta J[\rho]}{\delta\rho(r)} + \frac{\delta E_{xc}[\rho]}{\delta\rho(r)} \tag{2.11}$$

where, $\dfrac{\delta J[\rho]}{\delta\rho(r)} = \int \dfrac{\rho(r')}{|r-r'|}dr'$ and $\dfrac{\delta E_{xc}[\rho]}{\delta\rho(r)} = \upsilon_{xc}(r)$

(exchange–correlation potential) .

The expression of the total energy can be formulated as:

$$E = \sum_{i=1}^{N} \varepsilon_i - \frac{1}{2}\int \frac{\rho(r)\rho(r')}{|r-r'|} dr dr' + E_{xc}[\rho] - \int \upsilon_{xc}(r)\rho(r) dr \qquad (2.12)$$

In the above equation 2.10, dependence of $\upsilon_{eff}(r)$ upon the electron density $\rho(r)$ makes the KS equation non–linear and thus the equation needs to be solved self–consistently. As the KS kinetic energy is calculated correctly (closer to the exact), the main challenge focuses upon a good approximation to the exchange-correlation functional E_{xc}.

2.2.3 Exchange-Correlation Functional

Many more schemes have been practiced to formulate the exchange-correlation functional correctly. Among these, the local density approximation (LDA)[9] is one of the notable works which is expressed as

$$E_{xc}^{LDA} = \int \rho(r)\varepsilon_{xc}[\rho(r)] dr \qquad (2.13)$$

where ε_{xc} represents the exchange and correlation energy per particle within the approximation of uniform electron gas density $\rho(r)$. The expression of exchange–correlation potential is

$$\upsilon_{xc}^{LDA}(r) = \frac{\delta E_{xc}^{LDA}}{\delta\rho(r)} = \varepsilon_{xc}(\rho(r)) + \rho(r)\frac{\delta\varepsilon_{xc}(\rho)}{\delta\rho} \qquad (2.14)$$

and the corresponding Kohn–Sham equation takes the following form:

$$\left[-\frac{1}{2}\Delta^2 + \upsilon(r) + \int \frac{\rho(r')}{|r-r'|} dr' + \upsilon_{xc}^{LDA}(r) \right] \psi_i = \varepsilon_i \psi_i \qquad (2.15)$$

Equation 2.15 is solved self–consistently and this method is known as Kohn–Sham local density approximation method (KS–LDA method). This method is well suited for the system with slowly varying densities and failed drastically for inhomogeneous systems. The major reason behind the erroneous results is the homogeneous exchange part. A much more sophisticated way to bring improvements is the implementation of

generalized gradient approximation (GGA).[10-13] The whole purpose of this approximation is to include some heterogeneity in the exchange–correlation functional by making it a functional of both the density $(\rho(r))$ and its gradient $\left(\delta\rho(r)/\delta r\right)$.

The GGA functional has the following form:

$$E_{xc}^{GGA}[\rho(r)] = \int \rho(r) F[\rho(r), \Delta\rho(r)] dr \qquad (2.16)$$

Some of the well recognized GGA functionals are the PBE,[13] the BLYP[12, 14] and the PW91[15].

2.3 Free Volume Correction for Translational Entropy

Theoretical methods that estimate the changes in the entropy term for rigid particles are evaluated by individual calculation of four components of the total entropy i.e., the translational, rotational, vibrational, and conformational terms. Generally, translational entropy is demonstrated by the Sackur-Tetrode[16] equation :

$$S_{trans} = R \ln\left[\left(\frac{10^{-15/2}}{N_A^4[X]}\right)\left(\frac{2\pi MRTe^{5/3}}{h^2}\right)^{3/2}\right] \qquad (2.17)$$

where T (K), M (g/mol), X (mol/L), h (J s) and N_A (unitless)represent temperature, the mass of the particle, the concentration of the particles, Plank's constant, and Avogadro's number respectively. This equation accurately speculates the translational entropy for monoatomic gases but underestimates the same for the molecules in the solution phase (molecules dissolved in solution at 1.0 mol/L).The reason being that the molecular volume (V_{molec}) in a liquid, is ignored in the Sackur-Tetrode equation, which is generally the major part of the total volume acquired by van der Waals surface of the molecule. As, uncertainties in rotational and vibrational components are negligible in comparison to its translational part, and according to the definition the

fourth component S_{conf} is set to zero in case of rigid particles, therefore, considerable refinement of the translational entropy term is desirable.

In the year 1998, Whitesides and co–workers[17] gave an insight to correct the values of S_{trans} (translational entropy) of molecules in solution based on the Sackur-Tetrode equation. Their proposed theoretical model of the free volume theory presumes the liquid as a regular array of hard cubes (or maybe spheres, or other shapes). Each cube's volume defines molecular volume, V_{molec}. This model is only valid in case of infinitely dilute solutions and the modification to the translational entropy in the condensed phase can only be made by the following equation:

$$S_{trans} = R\ln\left[\left(\frac{10^{-15/2}V_{free}^{solvent}}{N_0^4[analyte]}\right)\left(\frac{2\pi MRTe^{5/3}}{h^2}\right)^{3/2}\right] \qquad (2.18)$$

where $V_{free}^{solvent}$ is expressed as,

$$V_{free}^{solvent} = C_{free}\left(\sqrt[3]{\left(\frac{10^{27}}{[X]N_0}\right)} - \sqrt[3]{V_{molec}}\right)^3 \qquad (2.19)$$

where C_{free} = 8 for hard cubes.

The terms [analyte] (mol/L) and $V_{free}^{solvent}$ (L) in the equation 2.18 describe experimental concentration of analyte and the free volume of the solvent respectively.

2.4 RI-J and MARI-J Approximations

RI–J (resolution of identity)[18-22] and MARI–J (multipole accelerated resolution of identity)[23] approximations are employed to minimize the computational time to determine the electronic Coulomb integral for both molecular and periodic systems by employing atom centred basis functions into the concerned equation. MARI–J method is known to split up the Coulomb term into two sections, such as; a) far field part: which covers all major interactions including long range

interactions and b) near field part: which involves near field interactions through direct integration of the four-center electron repulsion integrals. The equation is as follows:

$$\iint \frac{\mu(r)\nu(r)\kappa(r')\lambda(r')}{|r-r'|} dr dr' = (\mu\nu|\kappa\lambda) \tag{2.20}$$

where $\mu, \nu, \kappa, \lambda$ are the basis functions. Implementation of the RI–J approximation converts the four–center two electron repulsion integrals to a three center integral two electron integrals and, therefore, combination of both RI–J and MARI–J approximations lead to significant lowering of computational cost.

2.5 Møller–Plesset perturbation theory

The Møller–Plesset perturbation (MP2) theory is a post Hartree–Fock method introduced to incorporate correlation effects in the calculation and eventually turned out to be predicting results with higher accuracy than Hartree–Fock (HF) method. It was proposed in the year 1934 by two famous scientists Christian Møller and Milton S. Plesset.[24] It is a not a variational method and is solved perturbatively. The Hamiltonian operator can be written by the following equation:

$$H = H_0 + V \tag{2.21}$$

where *H*, H_0 and *V* represent exact Hamiltonian, HF Hamiltonian and the perturbation operator respectively. *V* has the following form

$$V = \sum_{i<j} r_{ij}^{-1} - V^{HF} = \sum_{i<j} r_{ij}^{-1} - \sum_{i} \upsilon^{HF}(i) \tag{2.22}$$

where r_{ij} stands for the exact electron–electron repulsion term and $\upsilon_{HF}(i)$ represents the average electronic HF potential.[3] It is necessary to mention here that addition of zeroth and first order corrections to the energy gives us the HF energy. Therefore, first order energy correction for HF is actually happens in the second order

perturbation theory –known as MP2 correction. Detailed derivation provides the MP2 energy as the following equation 2.23.

$$E_{MP2} = \frac{1}{4}\sum_{abrs} \frac{\left|\langle ab||rs\rangle\right|^2}{\varepsilon_a + \varepsilon_b - \varepsilon_r - \varepsilon_s} \tag{2.23}$$

Here *a, b* are the occupied and *r, s* are the virtual orbitals. $\varepsilon_{a/b/r/s}$ represent the corresponding orbital energies. In regular notation, $\langle ab||rs\rangle$ are the *four–center–two – electron* integrals. I have reported single-point MP2 energies on the BP-86 optimized structures for all my calculations presented in the third chapter.

2.6 Solvent Correction

Our calculations included the solvent effects by implementing an implicit continuum solvent model known as, the Conductor–like Screening Model (COSMO).[25, 26] In COSMO, the solute molecule is considered to form a cavity within the dielectric continuum of solvent having permittivity ε. Due to this arrangement, polarization of the dielectric medium occurs as a result of the charge distribution in the solute molecule. This eventually originates screening charges between the solute–cavity and the solvent–dielectric interface and it is called as the 'solvent accessible surface' (SAS). Screening charges can be obtained by setting the boundary condition. Cosmo uses boundary condition in a simpler way by taking zero electrostatic potential for a conductor (equivalent to the electrostatically ideal solvent with $\varepsilon = \infty$). Screening charges are scaled by a scaling factor in case of solvents having a finite dielectric constant,

$$q^* = f(\varepsilon)q \tag{2.24}$$

where scaling factor is given as, $f(\varepsilon) = \frac{\varepsilon - 1}{e + \frac{1}{2}}$

The solvation process results in the gaining of free electrostatic energy,

namely dielectric energy E_{diel}, which is half of the solute-solvent interaction energy. Therefore, the summation of the energy of the isolated system calculated with the solvated wave function $(E(\psi^{solv}))$ and the dielectric energy (E_{diel}) results in the total free energy(E) of the solvated molecule, $E = E(\psi^{solv}) + E_{diel}$

2.7 Dispersion Correction

I have incorporated the dispersion correction to some of our calculation. Generally DFT fails to properly address the intermolecular interactions, especially van der Waals interactions and this eventually questions the accuracy of the DFT results. The error is greater in the cases where dispersion effect plays an important role; such as, calculation of transition states, bio–molecules etc. Modern DFT handles all these errors by altering the functional and by including some additional additive terms. According to the recent modification,[27] the total dispersion–corrected energy is given by the following formula:

$$E_{DFT-D} = E_{KS-DFT} + E_{disp} \tag{2.25}$$

where E_{KS-DFT} and E_{disp} represents the self–consistent KS energy and empirical dispersion correction respectively. E_{disp} has the following form:

$$E_{disp} = -s_6 \sum_{i=1}^{N_{at}-1} \sum_{j=i+1}^{N_{at}} \frac{C_6^{ij}}{R_{ij}^6} f_{dmp}(R_{ij}) \tag{2.26}$$

Here, N_{at}, C_6^{ij}, s_6 and R_{ij} denotes total number of atoms, the dispersion coefficient for atom, global scaling factor and interatomic distance respectively. C_6^{ij} is a geometric mean and it is as follows:

$$C_6^{ij} = \sqrt{C_6^i C_6^j}$$

The damping function is given by the following formula:

$$f_{dmp}(R_{ij}) = \frac{1}{1+e^{-d(R_{ij}/R_r-1)}} \tag{2.27}$$

where R_r is the summation of atomic van der Waals radii. The scaling factor was set to different values for different functionals (for e.g. for BP-86 and B3-LYP s_6 is 1.05 and for PBE it is 0.75).[27]

2.8 Born Oppenheimer Molecular Dynamics

Classical Molecular Dynamics (MD) treats the motion of the nuclei (interacting via a potential in a molecular system) by employing the classical equations of motion. Forces on the atoms are determined via the use of potential fields such as, Lennard–Jones, Buckingham, etc. Classical MD is computationally cheaper because it does not consider electronic motion. MD reads the consecutive configurations of the system via the integration of the Newtons equation of motion. It generates trajectory (by solving the differential equations involved in the Newtons second law) which contains the information regarding the variations of positions and velocities of the atoms in the system with respect to time. This makes MD a deterministic method, where the future state of any system at any future time can be easily speculated from its present state.[28] Force on the atom I (F_I), derived from a given set of atoms of masses M_I at position R_I is formulated as $F_I = M_I \ddot{R}_I$.

Further, we know that the potential and the force is related to each other according to the following equation:

$$F_I = \frac{\delta E(R_I)}{\delta R_I} \tag{2.28}$$

Various algorithms have been employed to solve the above equations but one of the most efficient method is the Verlet algorithm.[28] Implementation of this method gives the following equation:

$$R_I(t+\Delta t) = 2R_I(t) - R_I(t-\Delta t) + \frac{\Delta t^2}{M_I} F_I \qquad (2.29)$$

where $R_I(t), R_I(t+\Delta t), R_I(t-\Delta t)$ represent atomic positions of the present, future and previous steps with a time interval of Δt. MD simulations store every information of the system with varying time interval of Δt, such as, velocities, forces and the instantaneous values of all the calculated properties. Classical MD fails to determine the local atomic properties such as, chemical bonding, including the path of the chemical reactions (forming and breaking bonds quantum mechanically). However, quantum dynamics simulation (large molecular system) requires high computational time. Such difficulties can be surpassed by using *ab initio* molecular dynamics (AIMD).

In AIMD, forces are derived from quantum mechanical treatments and then eventually motion of individual atoms are calculated accordingly.[29, 30] The main scheme of AIMD is that, due its much heavier weight, the nuclei moves classically according to the Newton's equation of motion under the influence of quantum mechanically derived electronic potential. Car–Parrinello molecular dynamics (CPMD) is the initial and one of the most well studied AIMD methods, where conventional MD technique was combined with the DFT methods.[31] Born-Oppenheimer molecular dynamics (BOMD) simulation is another well known technique, which deals with the optimization of the ground state electronic orbitals at each time step.

BOMD solves the static electronic structure problem (under fixed nuclear positions at the particular instance of time) in each consecutive MD step.[32] Thus, it reduces the calculation of the entire electronic structure part into solving the time independent Schrödinger equation corresponding to the each static nuclear position.

Thus, the equations of motion under BOMD simulation is formulated as

$$M_I \ddot{R}_I = -\Delta_I [\min_{\{\psi_i\}} E[\{\psi_i\};\{R_I\}]] \quad (2.30)$$

It is clear from the above equation that BOMD propagates through the minimization of the electronic energy at each consecutive MD step.

2.9 References

[1] E. Schrödinger *Physical Review*. **1926**, 28, 1049-1070.
[2] M. Born, R. Oppenheimer *Annalen der Physik*. **1927**, 389, 457-484.
[3] A. Szabo, N. S. Ostlund, Modern quantum chemistry: introduction to advanced electronic structure theory, Courier Corporation, **2012**.
[4] R. G. Parr, W. Yang, Density-functional theory of atoms and molecules, Oxford university press, **1989**.
[5] L. H. Thomas in The calculation of atomic fields, Vol. 23 (Ed.^Eds.: Editor), Cambridge Univ Press, City, **1927**, pp.542-548.
[6] E. Fermi *Zeitschrift für Physik*. **1926**, 36, 902-912.
[7] E. Fermi *Rend. Accad. Naz. Lincei*. **1927**, 6, 602-607.
[8] P. Hohenberg, W. Kohn *Physical Review*. **1964**, 136, B864-B871.
[9] W. Kohn, L. J. Sham *Physical Review*. **1965**, 140, A1133-A1138.
[10] J. P. Perdew, W. Yue *Physical Review B*. **1986**, 33, 8800-8802.
[11] J. P. Perdew *Physical Review B*. **1986**, 33, 8822-8824.
[12] A. D. Becke *Physical Review A*. **1988**, 38, 3098-3100.
[13] J. P. Perdew, K. Burke, M. Ernzerhof *Physical review letters*. **1996**, 77, 3865-3868.
[14] C. Lee, W. Yang, R. G. Parr *Physical Review B*. **1988**, 37, 785-789.
[15] J. P. Perdew, Y. Wang *Physical Review B*. **1992**, 45, 13244-13249.
[16] T. L. Hill, An introduction to statistical thermodynamics, Courier Corporation, **2012**.
[17] M. Mammen, E. I. Shakhnovich, J. M. Deutch, G. M. Whitesides *The Journal of Organic Chemistry*. **1998**, 63, 3821-3830.
[18] K. Eichkorn, O. Treutler, H. Öhm, M. Häser, R. Ahlrichs *Chemical Physics Letters*. **1995**, 240, 283-290.
[19] A. M. Burow, M. Sierka, F. Mohamed *The Journal of Chemical Physics*. **2009**, 131, 214101.
[20] J. L. Whitten *The Journal of Chemical Physics*. **1973**, 58, 4496-4501.
[21] O. Vahtras, J. Almlöf, M. W. Feyereisen *Chemical Physics Letters*. **1993**, 213, 514-518.
[22] B. I. Dunlap, J. W. D. Connolly, J. R. Sabin *The Journal of Chemical Physics*. **1979**, 71, 3396-3402.
[23] M. Sierka, A. Hogekamp, R. Ahlrichs *The Journal of Chemical Physics*. **2003**, 118, 9136-9148.
[24] C. Møller, M. S. Plesset *Physical Review*. **1934**, 46, 618-622.
[25] *User's Manual, Turbomole Version 6.4* **2012**.
[26] A. Klamt, G. Schuurmann *Journal of the Chemical Society, Perkin Transactions 2*. **1993**, 799-805.
[27] S. Grimme *Journal of Computational Chemistry*. **2006**, 27, 1787-1799.

[28] M. P. Allen, D. J. Tildesley, Computer simulation of liquids, Oxford university press, **1989**.
[29] M. C. Payne, M. P. Teter, D. C. Allan, T. A. Arias, J. D. Joannopoulos *Reviews of modern physics*. **1992**, 64, 1045-1097.
[30] M. E. Tuckerman, P. J. Ungar, T. von Rosenvinge, M. L. Klein *The Journal of Physical Chemistry*. **1996**, 100, 12878-12887.
[31] R. Car, M. Parrinello *Physical review letters*. **1985**, 55, 2471-2474.
[32] D. Marx, J. Hutter *Modern methods and algorithms of quantum chemistry*. **2000**, 1, 301-449.

Chapter 3: Role of the Iridium Dihydrogen Pincer Complex towards the Formation of $(NH_2BH_2)_5$

Abstract

Computational studies with density functional theory (DFT) and MP2 have been done to investigate the interaction between the iridium dihydrogen pincer complex: (POCOP)IrH_2 (where POCOP =η^3-1,3(OP^tBu_2)$_2C_6H_3$) and NH_2BH_2 (amino borane), the immediate side product of ammonia borane (NH_3BH_3) dehydrogenation. A mechanism has been proposed for an oligomerization process at the metal centre that involves competition between (i) insertion of an NH_2BH_2 molecule into the $(NH_2BH_2)_n$ chain and (ii) termination of the chain leading to the formation of the cyclic $(NH_2BH_2)_n$ oligomer. The calculated ΔG values show that the competition favours insertion over termination for the cases $n = 1$ to $n = 4$ but favours termination for $n = 5$. The computational studies therefore indicate that the cyclic pentamer $(NH_2BH_2)_5$ would be formed during NH_3BH_3 dehydrogenation by the (POCOP)IrH_2 catalyst, agreeing with experimental findings. The mechanistic understanding gained has implications for the facile regeneration of ammonia borane.

3.1 Introduction

The possibility of using hydrogen (H_2) as a transportation fuel has been receiving considerable attention of late because of its high energy content per unit mass (120.0 $MJkg^{-1}$) versus that of petroleum (44.0 $MJkg^{-1}$), and the potential environmental benefits of using hydrogen as a fuel. However, a key roadblock to its use is the current lack of a safe and practical method for the on-board storage of hydrogen. Several different methods[1] for hydrogen storage have been explored, including physico-chemical methods such as high-pressure and cryogenic-liquid storage,[2] adsorptive storage on high-surface-area adsorbents,[3-5] as well as chemical storage in metal hydrides[6] and complex hydrides.[7]

One strategy that holds promise involves storing hydrogen in a chemical

compound via a reversible chemical reaction. In this regard, ammonia borane (NH_3BH_3, AB) and related amine boranes have emerged as attractive candidates for hydrogen storage materials because of their high percentage by weight (wt. %) of available hydrogen.[8-11] Several transition metal based catalysts have emerged that can dehydrogenate AB and amine boranes.[12, 13] Manners *et al.* have reported the dehydrogenation of a number of amine boranes[14] and of AB[15] using the Rh(1,5-COD)(μ-Cl)]$_2$ (COD = cyclooctadiene) catalyst. Titanocenes[16] and zirconocenes[17] have been found to be effective in dehydrogenating amine boranes while Forster *et al.* have reported the use of zirconocenes in dehydrogenating AB.[18] Baker *et al.*[19] have found that the Ni(NHC)$_2$ catalyst (where NHC: N-heterocyclic carbene) is effective in producing more than two equivalents of H_2 from AB. The dehydrogenation of AB by rhodium and iridium analogues[20] of Wilkinson's catalyst has been investigated. Schneider and co-workers[21] have introduced a PNP-supported ruthenium complex for the dehydrogenation of AB. Fagnou *et al.*[22] ,Williams *et al.*[23, 24] have also employed ruthenium based systems for the highly efficient dehydrogenation catalysis of AB. Schneider *et al.* [21], Fagnou *et al.*[22] and Baker *et al.*[25] reported rapid and nearly exclusive formation of the insoluble aminoborane product using their ruthenium based catalyst. Fagnou *et al.*[22] have found that several ruthenium-amido complexes can generate up to one equivalent of H_2 from AB and up to two equivalents of H_2 from amine boranes. Peruzzini's group has studied AB dehydrogenation with [Ir(dppm)$_2$]OTf [dppm = bis(diphenylphosphanyl) methane, OTf = $(CF_3O_3S)^-$].[26] One of the most efficient AB dehydrogenation catalysts has been reported by Goldberg's group, using the iridium dihydrogen pincer ligand catalyst (POCOP)IrH_2 (where POCOP = η^3-1,3(OP^{t}Bu$_2$)$_2$C$_6$H$_3$).[27] In addition to the homogeneous systems, heterogeneous catalysts have also been investigated for AB

dehydrogenation: Burell and co-workers have recently reported on the dehydrogenation of AB using platinum, palladium, and ruthenium supported on alumina, activated carbon, and alumina respectively.[28]

Several computational studies[29-34] have also been conducted in order to understand the mechanism of the dehydrogenation process. Hall and Yang[29, 30] have reported DFT calculations elucidating the mechanism for the removal of the first[29] and second[30] equivalents of H_2 from AB for the case of the $Ni(NHC)_2$ catalyst.[19] Further light has been shed on the mechanism for the same catalytic system by Zimmerman *et al.*[31], who have shown through DFT calculations that there is a possibility of multiple active species because of the ability of AB to displace one NHC ligand from the nickel coordination sphere. DFT studies have also helped understand the dehydrogenation mechanism for the case of the $(POCOP)IrH_2$ catalyst: DFT studies by Paul *et al.*[33] indicate that the dehydrogenation mechanism for this catalyst proceeds through the concerted removal of hydrogen from AB.

The experimental and computational work investigating the dehydrogenation of AB using transition metal based catalysts has therefore produced interesting results and has led to a better understanding of the mechanism of dehydrogenation. It is, however, important to note that in order for hydrogen storage by AB to be economically viable, it is also necessary to regenerate AB in a facile manner after its dehydrogenation. This poses a problem because the most commonly observed by-product of AB dehydrogenation is a soluble B-N linked oligomer of borazine $[(BHNH)_3]$ (see **Fig. 3.1** below): the polyborazylene (PB) complex, regenerating AB from which is a challenge.

The issue of regenerating AB from PB has been tackled by both computational and experimental groups. The mechanism for PB formation has been studied by

Zimmerman *et al.*[34], who have highlighted the role of amino borane: NH_2BH_2 - the immediate product of the AB dehydrogenation – in the eventual formation of PB. Using *ab initio* CCSD(T) calculations, they have shown that free NH_2BH_2 in homogeneous catalytic systems can participate in different oligomerizing reactions and can autocatalyze the formation of different cyclic and linear oligomeric species, leading ultimately to the formation of PB. The problem of regeneration of AB from PB was experimentally studied by Davis *et al.*[35], who exploited the solubility of PB in common organic solvents to propose (with the aid of DFT calculations) the digestion of PB with 1,2-benzenedithiol in refluxing THF followed by reduction with Bu_3SnH to generate AB. The most significant development in this regard has been the work of Sutton *et al.*[36], who have recently shown that AB can be regenerated in a facile fashion from PB by its treatment with hydrazine (N_2H_4) in liquid ammonia at 40 ˚C in a sealed pressure vessel.

An interesting point to note in the work of Sutton *et al.*[36] is that they did not use the iridium dihydrogen pincer ligand catalyst (POCOP)IrH_2 in their dehydrogenation catalysis studies, even though, as mentioned earlier, it is a very efficient AB dehydrogenation catalyst[27]. The reason for this is that the (POCOP)IrH_2 catalyst system, despite its efficiency, only releases one equivalent of hydrogen from AB, as opposed to other catalysts such as the $Ni(NHC)_2$ complexes[19] that release more than two equivalents. The reason such complexes release more equivalents of H_2 is because of the fact that the NH_2BH_2 formed after the release of one H_2 equivalent from AB releases further equivalents of H_2 in the process of oligomerizing to form PB.[37] The (POCOP)IrH_2 catalyst is unique in this respect in that the NH_2BH_2 species *does not oligomerize to give PB in this case*, but instead yields an insoluble white precipitate that has been proposed[27] from solid-state ^{11}B NMR studies, as well

as IR spectrum and X-Ray powder diffraction pattern comparisons to previously reported data[38], to be the cyclic amino borane pentamer $(NH_2BH_2)_5$ (see **Fig. 3.1**).

The reason why $(NH_2BH_2)_5$, and not PB, is formed for the (POCOP)IrH_2 catalyst case has been explained through an interesting study conducted by Pons *et al.*[37] Using *in situ* ^{11}B NMR monitoring, they have demonstrated that, at room temperature, NH_2BH_2 is released into the solution after formation at the metal centre for all of the dehydrogenation catalysts studied, *except for* (POCOP)IrH_2, where it appears to remain bound to the catalyst. This indicates that the formation of the insoluble white cyclic pentamer is occurring as a result of the coordination of NH_2BH_2 to the iridium centre (see **Fig. 3.1**), although no experimental or computational studies have been reported to date to explain how the cyclic pentamer is formed, and why no other cyclic oligomeric products, such as the cyclic trimer or tetramer, are produced during the dehydrogenation catalysis using the (POCOP)IrH_2 complex.

It is important to understand how this metal mediated cyclisation reaction at the metal centre of the (POCOP)IrH_2 complex takes place. Such information would help us understand how one could reduce or eliminate the formation of $(NH_2BH_2)_5$ in favour of PB. This would be far more desirable from the viewpoint of AB regeneration.[36] Moreover, this would automatically ensure the production of a second equivalent of H_2 from AB by the (POCOP)IrH_2 catalyst. In short, mechanistic insight into $(NH_2BH_2)_5$ formation can help unlock the true potential of this very efficient AB dehydrogenation catalyst.

This is the focus of the current computational investigation. The principal objective has been to understand how NH_2BH_2 molecules can interact with the (POCOP)IrH_2 catalyst (henceforth refered to as [Ir]), and how this interaction can lead

to the formation of the observed $(NH_2BH_2)_5$ pentamer. A mechanism has been proposed to explain the oligomeization process and investigated with full quantum mechanical (QM) methods, using density functional theory and MP2. The understanding gained from the mechanistic studies has been used to suggest possible modifications to the substrate, catalyst and the reaction conditions in order to reduce the interaction between NH_2BH_2 and the [Ir] catalyst, and thus reduce or eliminate the formation of the cyclic oligomers in favour of the much more desirable soluble PB species. Moreover, the understanding gained from the current studies has provided insight into why the change of the substrate from ammonia borane, AB, NH_3BH_3, to *amine* boranes, $RR'NHBH_3$, (where R, R′ are alkyl groups) leads to the preferential formation of polyborazylene, PB,[24] instead of the insoluble pentamer, for the iridium pincer ligand as well as for other catalysts.

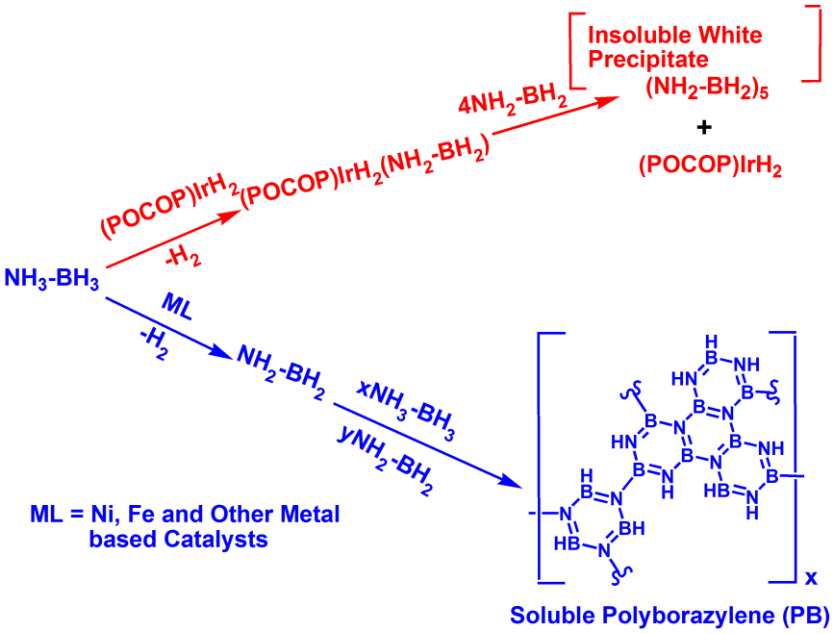

Figure 3.1 The different by-products of Ammonia Borane dehydrogenation by different catalyst systems.

3.2 Computational details

The computational procedure adopted is as follows: all the structures reported in this chapter have been optimized using density functional theory (DFT) with the

Turbomole suite of programs, using Turbomole Version 6.0.[39] The geometry optimizations were performed using the BP-86 functional[40, 41]. The electronic configuration of the atoms was described by a triple-zeta basis set augmented by a polarization function (TURBOMOLE basis set TZVP).[42-45] Since it is possible that the geometry optimization procedure with DFT may be sensitive to the nature of the functional, a further test has been done to ensure the reliability of the obtained geometry optimized structures: all the structures were also optimized with the Perdew, Burke, and Erzenhof density functional (PBE)[46] and the TZVP basis set. The resolution of identity (RI),[47] along with the multipole accelerated resolution of identity (MARIJ)[48] approximations were employed for an accurate and efficient treatment of the electronic Coulomb term for both of the sets of the density functional calculations.

A comparison was then done between the corresponding structures obtained with the BP-86 and the PBE functionals. The comparison showed very little difference in bond lengths, angles and dihedral values between the corresponding structures for all the cases. A further corroboration of the smallness of the difference between the structures obtained from the two functionals came from the comparison of the potential energy surfaces for the different reactions discussed in this chapter. The dispersion corrected ΔE values for the insertion and termination barriers for the oligomerizatiom mechanism, obtained from the two separate set of calculations, were compared and the results, shown in **Table 3.1** below, indicate that there is very little difference between the corresponding values for all the cases. In most cases, the ΔE values obtained from the two separate set of DFT calculations agreed to within 0.5 kcal/mol, thus providing further proof of the reliability of the BP-86 functional in obtaining the optimized geometries for the different species. With regard to the

transition states obtained from the two sets of calculations, care was taken to ensure that the obtained transition state structures possessed only one imaginary frequency corresponding to the correct normal mode.

Furthermore, in order to improve the calculation of the energy values, a further correction was made through single point MP2[49] calculations with the RI approximation (RIMP2), with the DFT (BP-86) optimized structures. Solvent effects were incorporated using the COSMO model,[50] with tetrahydrofuran (ε=7.52) as the solvent. The contributions of internal energy and entropy were further obtained from frequency calculations done on the DFT structures at 298.15 K: thus, the energies reported in the figures of this chapter are the ΔG values. In order to account for the fact that all the species are in solution, the translational entropy term in all the calculated structures was corrected through a free volume correction introduced by Mammen *et al*.[51]

Table 3.1 The comparison of the energy values obtained for the DFT calculations done with the BP-86 and the PBE functionals; the values shown in the columns a, b, c, and d pertain to the dispersion corrected ΔE values obtained from BP-86 calculations; while the values in the columns a´, b´, c´and d´ pertain to the dispersion corrected ΔE values obtained from the calculation done with the PBE functional; all values are in kcal/mol.

[Ir] $(NH_2BH_2)_n$	a	a'	b	b'	c	c'	d	d'
n=1	25.6	25.3	-	-	39.9	39.5	-	-
n=2	17.4	17.0	-	-	28.8	28.2	-	-
n=3	12.1	11.8	36.0	36.4	32.7	33.0	37.3	39.8
n=4	19.0	18.6	26.5	27.1	43.1	43.1	29.2	31.4
n=5	29.0	28.3	15.7	16.8	39.4	40.1	23.9	26.0

A point we note about the calculations is with regard to the competition between insertion and termination for the complex $[Ir](NH_2BH_2)_5$. The transition state for the insertion of NH_2BH_2 to yield $[Ir](NH_2BH_2)_6$ was found to lead to a structure whose size was too large for the single point rimp2 calculation. Hence for the case of $[Ir](NH_2BH_2)_5$, an SV(P) basis set[44] was employed for the iridium metal centre all the other atoms were treated with TZVP as before and all the structures for insertion and termination for this case were re-optimized, followed by single point RI-MP2 calculations on the re-optimized DFT structures. The fact that this slight change in basis set would not lead to a big change in the nature of the obtained energetics for the reactions is revealed from the comparison of the dispersion corrected ΔE values obtained for both the insertion and termination barriers at the dispersion corrected DFT level. As shown in **Table 3.2**, the ΔE values are very close for both the insertion and termination cases when comparing the two basis sets: TZVP and SV(P) used for only the iridium metal centre.

A point we note about the calculations is with regard to the competition between insertion and termination for the complex $[Ir](NH_2BH_2)_5$. The transition state

for the insertion of NH_2BH_2 to yield $[Ir](NH_2BH_2)_6$ was found to lead to a structure whose size was too large for the single point rimp2 calculation. Hence for the case of $[Ir](NH_2BH_2)_5$, an SV(P) basis set[44] was employed for the iridium metal centre all the other atoms were treated with TZVP as before and all the structures for insertion and termination for this case were re-optimized, followed by single point rimp2 calculations on the re-optimized DFT structures. The fact that this slight change in basis set would not lead to a big change in the nature of the obtained energetics for the reactions is revealed from the comparison of the dispersion corrected ΔE values obtained for both the insertion and termination barriers at the dispersion corrected DFT level. As shown in **Table 3.2**, the ΔE values are very close for both the insertion and termination cases when comparing the two basis sets: TZVP and SV(P) used for only the iridium metal centre.

Table 3.2. The comparison of the energy values (ΔG) obtained for the DFT calculations done with the BP-86 functional for the ; the values shown in the columns a, b, c, and d pertain to the dispersion corrected ΔE values.

Transition states	Ir : SV(P) (kcal/mol)	Ir : TZVP (kcal/mol)
Insertion barrier (ΔG) for the complexes : [Ir] $(NH_2BH_2)_n$, where n=5	**29.1**	**29.1**
Termination barrier (ΔG) for the complexes : $[Ir](NH_2BH_2)_n$, where n=5	**16.1**	**15.7**

3.3 Results and Discussion

3.3.1 Formation of the $[Ir](NH_2BH_2)$ Species

Paul *et al.*[33] have shown that the immediate product of the dehydrogenation of ammonia borane (AB), NH_3BH_3, by the [Ir] catalyst is the amino borane species, NH_2BH_2. As mentioned in the Introduction, Pons *et al.*[37] showed that the NH_2BH_2

formed is likely to bind to the iridium centre. The structure complex that can be formed from such an interaction: the [Ir](NH_2BH_2) complex, has been optimized and found to be octahedral in nature, with the nitrogen of NH_2BH_2 equatorially coordinated to the metal centre and the boron of NH_2BH_2 attached to one of the axial hydrides of the iridium catalyst. (It is to be noted that the other possible conformer of [Ir](NH_2BH_2), in which the nitrogen of NH_2BH_2 lies in the axial position and the hyride binding to the boron of NH_2BH_2 is at the equatorial site of the Ir catalyst, has been found to be 3.1 kcal/mol higher in energy, and therefore the less likely conformer to exist in solution). [Ir](NH_2BH_2) therefore differs from the amino borane coordinated catalyst complex that has been experimentally obtained from amine borane dehydrogenation at the ruthenium metal centre,[52] which was found to have a bis (σ-B-H) bonding, and from the bis σ-amine borane complexes found by Weller's group using rhodium based catalysts.[53, 54]. [Ir](NH_2BH_2) is also known to show resemblance with some M-NH_2BH_3 (where M=Zr[18], Mg[55], Ca[56]) complexes.

The experiments performend by Pons *et al.*[37] indicate that this [Ir](NH_2BH_2) complex is likely to be stable at room temperature. A computational comparison of two structures: (i) NH_2BH_2 coordinated to iridium with NH_3BH_3 in the vicinity and (ii) NH_3BH_3 coordinated to the iridium centre with an uncoordinated, neighbouring NH_2BH_2 (see **Fig. 3.2**) was done. The results indicate that the iridium prefers to coordinate to the NH_2BH_2 complex over NH_3BH_3: the iridium complex with NH_2BH_2 is 9.9 kcal/mol more stable (see **Fig. 3.2**). This suggests an explanation as to why the NH_2BH_2 is experimentally found to remain bound to the iridium centre at room temperature: even if NH_3BH_3 were to displace the NH_2BH_2 moiety from the iridium centre, the displaced NH_2BH_2 could return to coordinate to the metal centre due to the thermodynamic favourability of the reaction. However, at higher temperatures (60˚C),

Pons *et al*.[37] have found that the NH_2BH_2 is released from the catalyst, though they have observed that even at 60˚C, a significant amount of the product identified as $(NH_2BH_2)_5$ is still formed. This suggests that a mechanism exists by which the iridium catalyst can recapture the freed NH_2BH_2 species at higher temperatures. A mechanism by which this can occur is discussed here.

Several investigations[34, 37] have been done regarding the interactions of AB (NH_3BH_3) and NH_2BH_2 and give rise to almost similar products. Zimmerman *et al*.[34] have shown that NH_2BH_2, once free, can react with ammonia borane, NH_3BH_3, to give an $NH_3BH_2NH_2BH_3$ species, a complex that they have termed the "sp3-linear dimer". The reaction of NH_2BH_2 with NH_3BH_3 to give this product has been calculated and found to have a high barrier: ΔG = 40.4 kcal/mol (case (i), see **Fig. 3.3** below), with the ΔE value being 28.3 kcal/mol. This compares well with the barrier obtained by Zimmerman *et al.* [34] of 29.5 kcal/mol (ΔE value), the energy obtained in their case from an MP2/CCSD(T) approach. However, an alternate reaction between NH_2BH_2 and NH_3BH_3 has also been considered (case (ii) in **Fig. 3.3**), a reaction that would give rise to the cyclic complex $BH_2NH_2BH_3$ and release NH_3. The reason for considering this alternative pathway was the fact that significant amounts of NH_3 is known to be formed during AB dehydrogenation by different catalysts[57]. As indicated in **Fig. 3.3** below, the free energy surface for case (ii) indicates that it would be a more facile reaction than case (i): the barrier was found to be 33.9 kcal/mol after incorporating single point MP2 corrections as compared to 40.4 kcal/mol for the sp3-linear dimer forming reaction (see **Fig. 3.3**). The reason the barrier is lower for case (ii) is because of the fact that the transition state for this reaction involves a closer approach of the NH_2BH_2 species towards NH_3BH_3 in comparison to case (i). The N_{NH2}-B_{NH3} distance is 2.21 Å in case (ii) compared to 2.71 Å in case (i). Moreover,

the bond between the nitrogen and boron atoms of NH_3BH_3 is broken to a greater extent in case (i) in comparison to case (ii). The N_{NH3}-B_{NH3} distance is 3.01 Å for the transition state in case (i) in comparison to it being 2.20 Å for the case (ii) transition state.

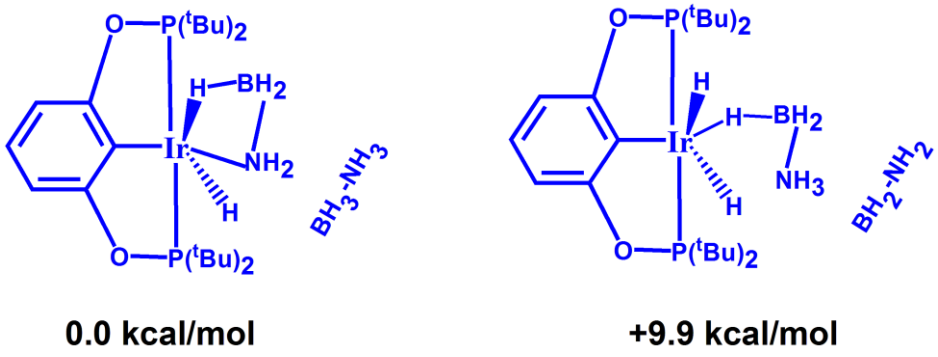

Figure 3.2 The relative stabilities of two complexes: NH_2BH_2 coordinated to iridium with NH_3BH_3 in the vicinity and NH_3BH_3 coordinated to the iridium centre with NH_2BH_2 in the vicinity.

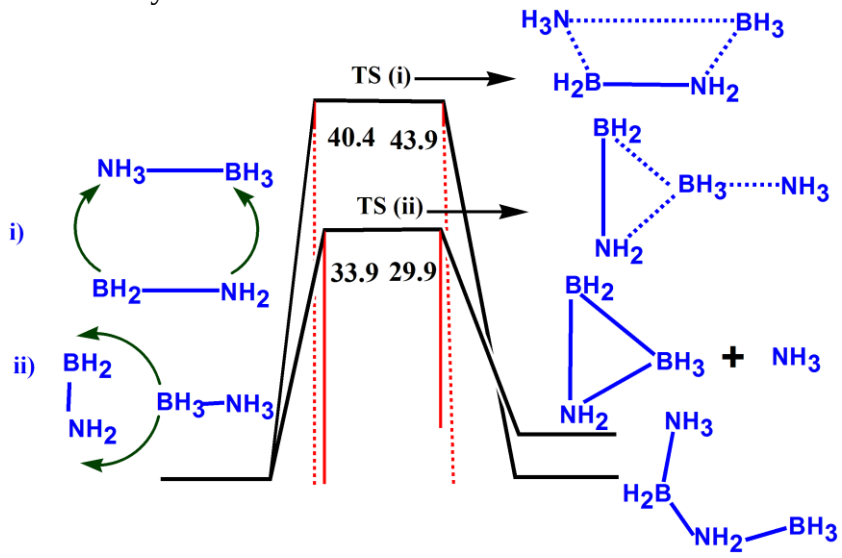

Figure 3.3 The energy (ΔG) comparison of the barriers for the formation of the products $NH_2BH_2BH_3$ and $NH_3BH_2NH_2BH_3$ from the interaction between NH_3BH_3 and NH_2BH_2; all values are in kcal/mol.

These results suggest that the cyclic $BH_2NH_2BH_3$ species is more likely to be formed than the sp3-linear-dimer when free NH_2BH_2 and NH_3BH_3 react. What is proposed is that the iridium catalyst can react with this formed cyclic $BH_2NH_2BH_3$ species to yield [Ir]($BH_2NH_2BH_3$) [see **Fig. 3.4 (i)**], which, upon further reaction with a free NH_2BH_2 molecule, will produce [Ir](NH_2BH_2) and the cyclic $BH_2NH_2BH_3$

species as the products [see **Fig. 3.4 (i)**]. The barriers for the two reactions were found to be 32.7 kcal/mol and 40.7 kcal/mol, which indicates that the reactions would be quite feasible at 60˚C: previous work [34, 58, 59] indicates that barriers calculated to be greater than 40.0 kcal/mol are achievable in the AB dehydrogenation systems when the reactions are done at 50˚C or higher temperatures.

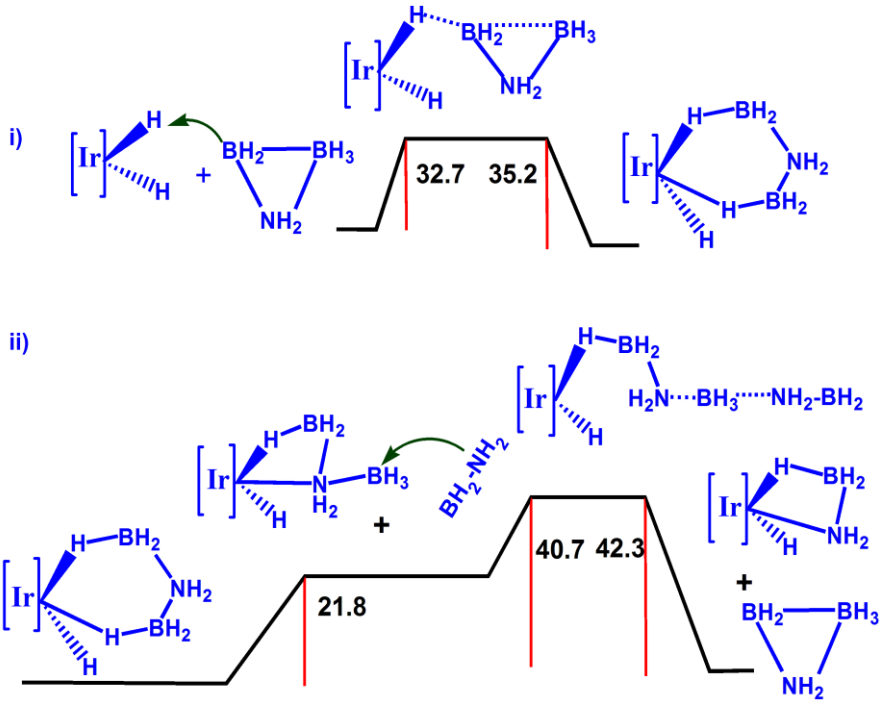

Figure 3.4 The free energy surface for the formation of the [Ir](NH_2BH_2) species from the reactants [Ir], $BH_2NH_2BH_3$ and BH_2NH_2; all values are in kcal./mol.

Thus, even though it is likely that BH_2NH_2 can be separated from the iridium catalyst at higher temperatures, it would still be possible for the iridium catalyst to re-form the [Ir](NH_2BH_2) complex. The values of the barriers obtained for the different reactions in this mechanism, as well as the relatively high concentration of the employed iridium catalyst (0.5 M),[27] indicate the likelihood of this possibility. What is also interesting to note is that the the cyclic $BH_2NH_2BH_3$ species is re-formed at the end of this reaction cycle, available for attack by another [Ir] molecule to give rise to another [Ir](NH_2BH_2) complex. The overall mechanism for this reaction is shown in **Fig. 3.5** below. Thus, even though free NH_2BH_2 species would exist in solution for

the case of the [Ir] catalyst at elevated temperatures, the NH_2BH_2 can be "recaptured" by the iridium catalyst to give back the [Ir](NH_2BH_2) complex.

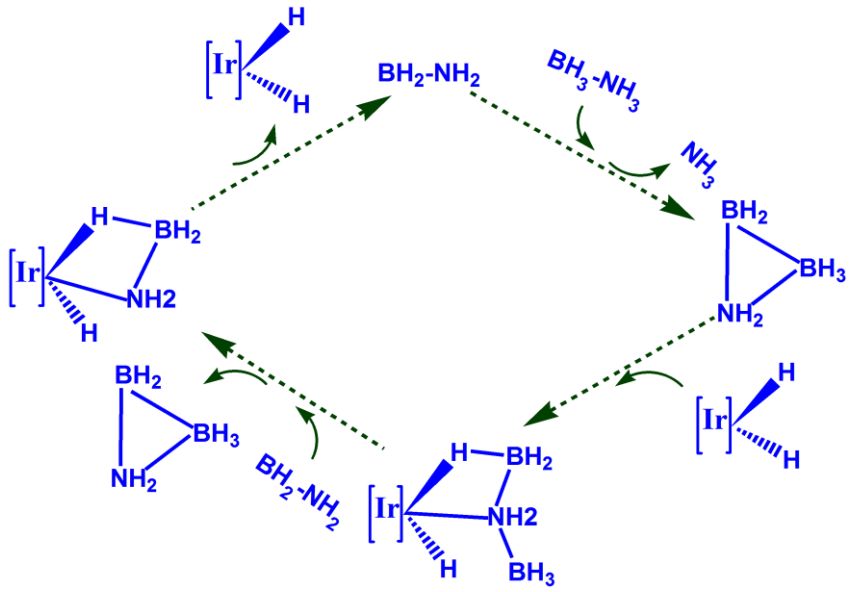

Fig. 3.5 The cycle by which [Ir] loses and is then able to recapture the NH_2BH_2 species.

3.3.2 Interaction of Iridium Catalyst with Oligomer Intermediates

The previous section showed that free NH_2BH_2 can eventually return to the iridium centre, so that the species [Ir](NH_2BH_2) can still exist in solution during the catalysis process at the elevated temperatures of 60 ˚C and above. However, apart from the cyclic $BH_2NH_2BH_3$ species and the sp3 linear dimer, discussed in the previous section, it is possible that the free NH_2BH_2 species can react and form other oligomeric intermediates in the absence of the iridium catalyst. What is discussed in this section is the possibility of such oligomeric intermediates also interacting with the iridium catalyst.

One such oligomeric intermediate that will be likely to be formed is the cyclic dimer: $(NH_2BH_2)_2$. Previous computational studies by Nutt *et al.*[60] and Zimmerman *et al.*[34] have shown that free NH_2BH_2 can, in solution, readily dimerize to yield the cyclic species $(NH_2BH_2)_2$: the barriers that they have obtained and reported for this

reaction is below 10.0 kcal/mol. It is therefore likely that the cyclic dimeric species will be formed during the catalysis process, especially at higher temperatures when free NH_2BH_2 will be available in the solution. Given the high concentration of the employed iridium catalyst (0.5 M),[27] during the reaction, a reaction between the cyclic dimeric species and the iridium complex is a likely possibility. The free energy surface for this reaction has been calculated and is shown in **Fig. 3.6** below. The product of this reaction is the complex: $[Ir](NH_2BH_2)_2$. The barrier is found to be 40.9 kcal/mol, which, as discussed earlier, indicates that the reaction could occur at higher temperatures: at 60 ˚C.

In their work, Zimmerman *et al.*[34] had also discussed the possibility of the cyclic trimeric species: $(NH_2BH_2)_3$ being formed, although their studies indicated that such a reaction would have a high barrier. As **Fig. 3.6** indicates, such a trimeric species, if formed, would be unlikely to react with the iridium catalyst complex: the barrier for the reaction between iridium and the $(NH_2BH_2)_3$ trimer was found to have a barrier of 65.9 kcal/mol (see **Fig. 3.6**). This suggests that the $(NH_2BH_2)_3$ species, if formed, would be likely to remain in solution. However, the fact that no cyclic trimer has been experimentally observed as a by-product or final product during AB dehydrogenation by the iridium catalyst, coupled with the results from the calculations by Zimemrman *et al.*[34] that indicate a high barrier to forming the cyclic trimer suggests that the cyclic trimer species is not formed during AB dehydrogenation by the iridium catalyst.

Another species that may be formed if free NH_2BH_2 is available in solution is the species $N_2B_2H_7$-NH_2BH_3: the "ECB" complex. Calculations done by Zimmerman *et al.*[34] show that the formation of this species from the reaction of two molecules of free NH_2BH_2 in solution is quite feasible, with the barriers for the reaction being less

than 10.0 kcal/mol (ΔE values). Hence, for the iridium based catalyst system the ECB complex is likely to be formed at higher temperatures, when free NH_2BH_2 would be available. As **Fig. 3.7** indicates, this complex can also react with the iridium complex to yield $[Ir](NH_2BH_2)_2$: the same complex that is formed when the cyclic dimer $(NH_2BH_2)_2$ reacts with the iridium catalyst (see the **Fig. 3.6 and Fig. 3.7**). The barrier for the reaction between ECB and the iridium complex is 39.5 kcal/mol, which suggests, as discussed earlier, that this reaction would also be feasible at the elevated temperatures of 60 ˚C and above. It is noted here that there may be two barriers for the reaction leading to the formation of the $[Ir](NH_2BH_2)_2$. The first barrier of 39.5 kcal/mol, shown in **Fig. 3.7**, would lead to the formation of a complex termed as [Ir][ECB] in the figure. After the formation of this intermediate complex, it is possible that another barrier would exist for the reaction leading to the dissociation of NH_2BH_2 from [Ir][ECB] to yield $[Ir](NH_2BH_2)_2$. Attempts to find the transition state for this reaction proved unsuccessful. However, a linear transit approach: incrementally distancing the NH_2BH_2 species in the [Ir][ECB] complex till the final products are formed, led to the estimation of an upper bound for the barrier for the reaction. This value was found to be 35.4 kcal/mol, which indicates that the overall reaction between ECB and the iridium catalyst leading to the formation of $[Ir](NH_2BH_2)_2$ would be quite feasible at elevated temperatures.

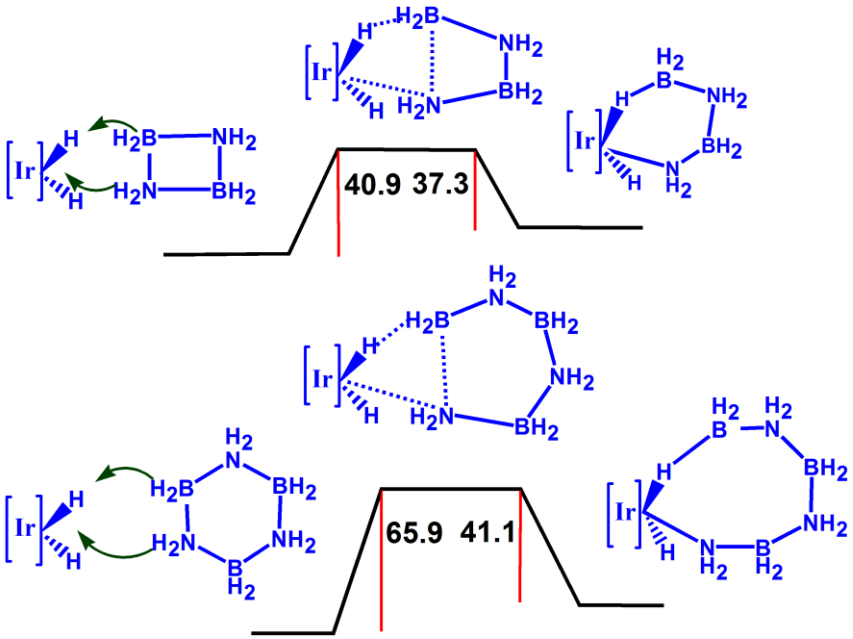

Figure 3.6 The free energy surfaces for the reaction between the cyclic dimer $(NH_2BH_2)_2$ and the cyclic trimer $(NH_2BH_2)_3$ with the iridium catalyst; all values are in kcal/mol.

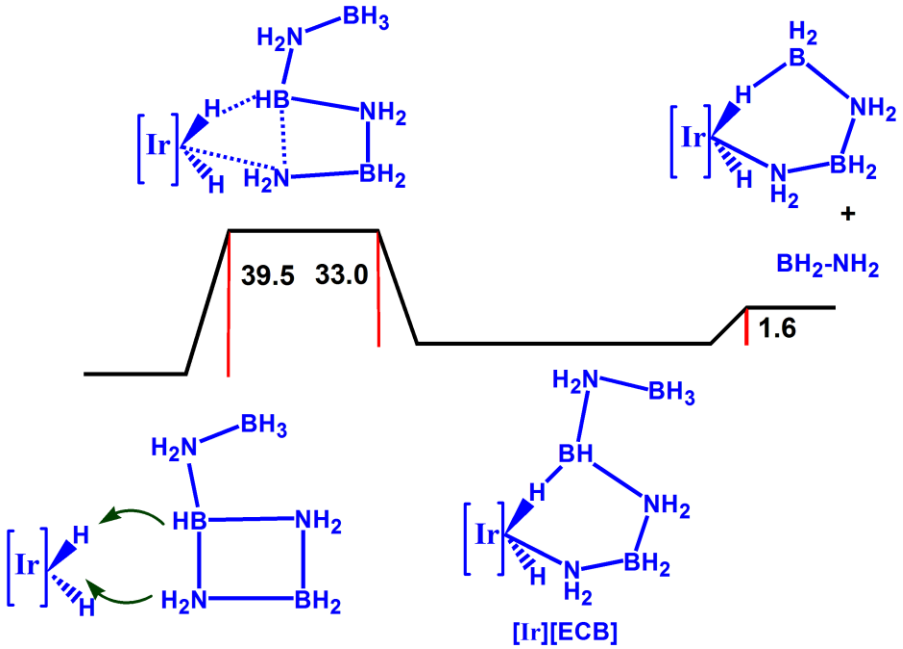

Figure 3.7 The free energy surface for the reaction between the $N_2B_2H_7$-NH_2BH_3 (ECB) complex and the iridium catalyst; all values are in kcal/mol.

3.3.3 $[Ir](NH_2BH_2)_2$ from $[Ir](NH_2BH_2)$

What was shown in the previous section is how the species $[Ir](NH_2BH_2)_2$ would be formed from the interaction between the iridium catalyst and the different oligomeric intermediates that can exist due to the presence of free NH_2BH_2 in solution. What is discussed in this section are further reaction pathways that have been found to also lead to the formation of the $[Ir](NH_2BH_2)_2$ species, beginning from the $[Ir](NH_2BH_2)$ which, as has been shown in a previous section, is likely to be a very prevalent species during the catalysis process, even at elevated temperatures. The two possibilities considered here are the reactions of (i) free NH_2BH_2 and (ii) with AB, NH_3BH_3 with the $[Ir](NH_2BH_2)$ complex. Indeed, if one considers the $[Ir](NH_2BH_2)$ complex as the precursor to forming complexes of the type $[Ir](NH_2BH_2)_x$ (x = 2,3,4 etc.), then case (i) could be considered the first step of an oligomerization process at the iridium centre. **Fig. 3.8(i)** shows the reaction profile when NH_2BH_2 reacts with $[Ir](NH_2BH_2)$: this leads to an "insertion step" having a barrier of 40.5 kcal/mol, with the product being $[Ir](NH_2BH_2)_2$, lying a stable 42.4 kcal/mol below this transition state [see **Fig. 3.8(i)**]. In contrast, the approach and attack by an NH_3BH_3 molecule would also lead to the formation of the same product and yield H_2 as a by-product of the reaction, but with a higher barrier of 49.4 kcal/mol [see **Fig. 3.8(ii)**]. The reason for the higher barrier is because the formation of H_2 has to take place away from the stabilizing influence of the iridium centre in this reaction. Attempts to involve the iridium centre in the dehydrogenation process for this case proved unsuccessful due to the increased steric demands of accommodating both the BH_2NH_2 and the BH_3NH_3 species near the iridium centre. It was found that the BH_2NH_2 species was displaced completely from the iridium in these attempts. Hence the only feasible route to obtaining the $[Ir](NH_2BH_2)_2$ species by the attack of

NH_3BH_3 requires a higher barrier than that required for the attack by NH_2BH_2. However, because NH_3BH_3, the reactant, is present at a higher concentration than NH_2BH_2, the pathway shown in **Fig. 3.8(ii)** would still be a competitive route to forming the $[Ir](NH_2BH_2)_2$ intermediate, and it is possible that it is this route that may be influential for the oligomerization process at room temperature, where free NH_2BH_2 species would not be available. Since the current investigation is principally focused on understanding the influence of the free NH_2BH_2 species on the oligomerization process, an influence that would be manifest at elevated temperatures, what is discussed in the next section is the mechanism for the oligomerization process involving the reaction of free NH_2BH_2 with intermediate species such as $[Ir](NH_2BH_2)_x$, leading finally to the cyclic pentamer, $(NH_2BH_2)_5$.

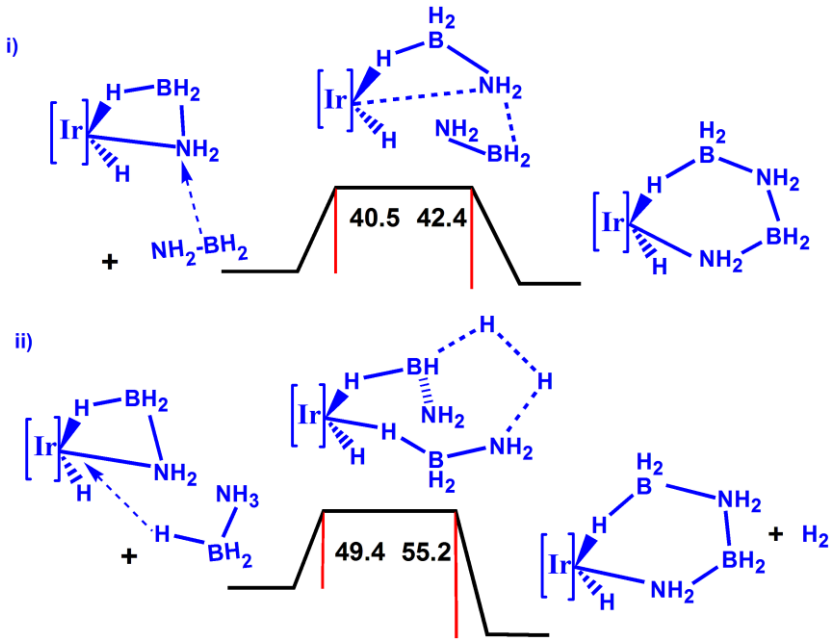

Figure 3.8 The energy (ΔG) comparison between the formation of the $[Ir](NH_2BH_2)_2$ species by attack of [Ir] by (i) NH_2BH_2 or by (ii) NH_3BH_3; all values are in kcal./mol.

3.3.4 The Oligomerization Process

What has been discussed in the previous section are the reactions that will give rise to the complex $[Ir](NH_2BH_2)_2$: the NH_2BH_2 dimer bound to the iridium centre.

From this point on, further attack by NH_2BH_2 would lead to the increase of the $(NH_2BH_2)_n$ ring size at the iridium centre, a process that would compete with the alternative possibility of the cyclization and separation of the $(NH_2BH_2)_n$ from the iridium centre. This is illustrated in **Fig. 3.9** below. At any point during the oligomerization process, the complex: $[Ir](NH_2BH_2)_n$ (shown in blue in **Fig. 3.9**) can either undergo insertion (indicated in blue) of NH_2BH_2 to yield $[Ir](NH_2BH_2)_{n+1}$ or undergo termination of the existing chain (indicated in red) to yield the original [Ir] catalyst and the cyclic oligomer $(NH_2BH_2)_n$. Of the two, the pathway that will be chosen, for any given value of n, will depend on which of the two barrier heights is lower.

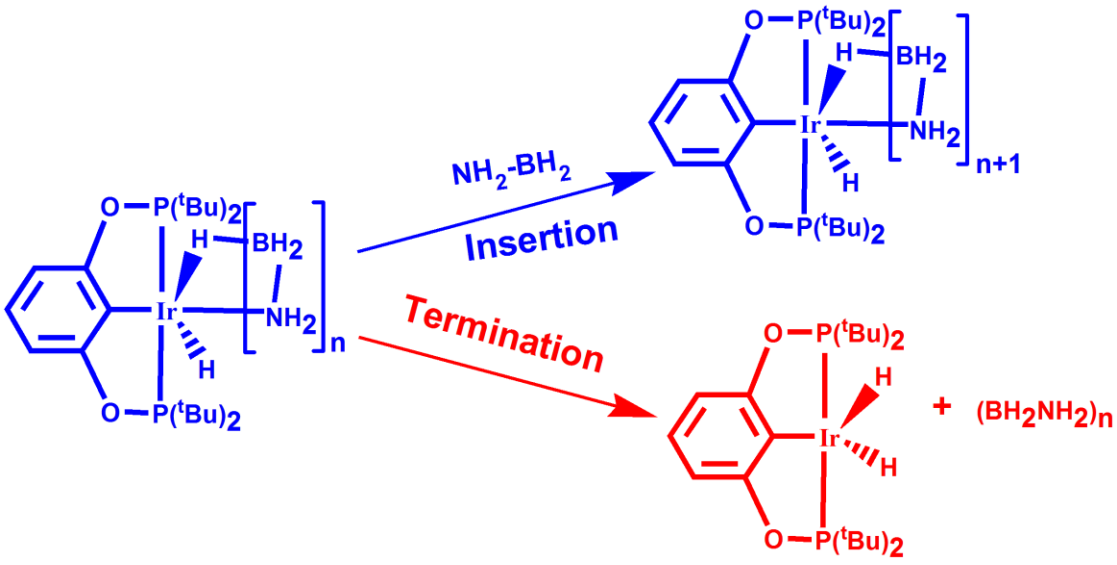

Figure 3.9 The competition between insertion and termination during the oligomerization process at the iridium centre of the [Ir] catalyst.

The insertion and termination pathways are described further in **Fig. 3.10**. It is proposed that the $[Ir](NH_2BH_2)_n$ complex can exist in two different resting states. The structures of the two resting states, labeled as A and B, are indicated in **Fig. 3.10** for the representative case of $[Ir](NH_2BH_2)_n$ where n = 3. As illustrated in **Fig. 3.10**, the resting state A would facilitate insertion while B would be a pre-requisite to termination. The principal difference between A and B lies in the coordination of the

$(NH_2BH_2)_n$ group to the iridium complex. In A, the $(NH_2BH_2)_n$ chain is attached through a boron atom to one of the axial hydrides coordinated to the iridium, while the nitrogen at the other end of the $(NH_2BH_2)_n$ chain is directly attached to the iridium centre as one of the equatorial ligands of the octahedral complex (see **Fig. 3.10**). In B, the attachment of the boron atom to the axial hydride remains, but the terminal nitrogen now lies free while one of the two hydrogen atoms of the BH_2 group attached to the axial, terminal BH_2NH_2 unit now acts as the equatorial ligand to the iridium centre (see **Fig. 3.10**). The optimized structures of A and B for the $[Ir](NH_2BH_2)_n$ complex where n = 3, are shown in **Fig. 3.11**.

A comparison of the relative energies of the structures A and B for the complexes $[Ir](NH_2BH_2)_n$ (n=3, 4 and 5) is shown in **Table 3.3**. The relative energies of A and B for the different complexes indicates that it would be possible for A to convert to B. It is to be noted that what is shown **Table 3.3** is only the thermodynamics for the interconversion between A and B. The kinetics for this process is not discussed in **Table 3.3** because it is difficult to obtain the transition state for the A-B interconversion. However, an upper bound estimate was obtained for the transition state for the A-B inter conversion by gradually removing the nitrogen attached to the iridium from the metal centre. This was achieved by fixing the iridium-nitrogen distance to different values and then optimizing the geometries. The calculations indicated that the separation of the nitrogen from the iridium centre to about 3.5 Å led to a structure that was about 24.0 kcal/mol (ΔE value) higher than A, for the complex $[Ir](NH_2BH_2)_5$. This indicates that the A-B interconversion would be a facile process, especially at elevated temperatures.

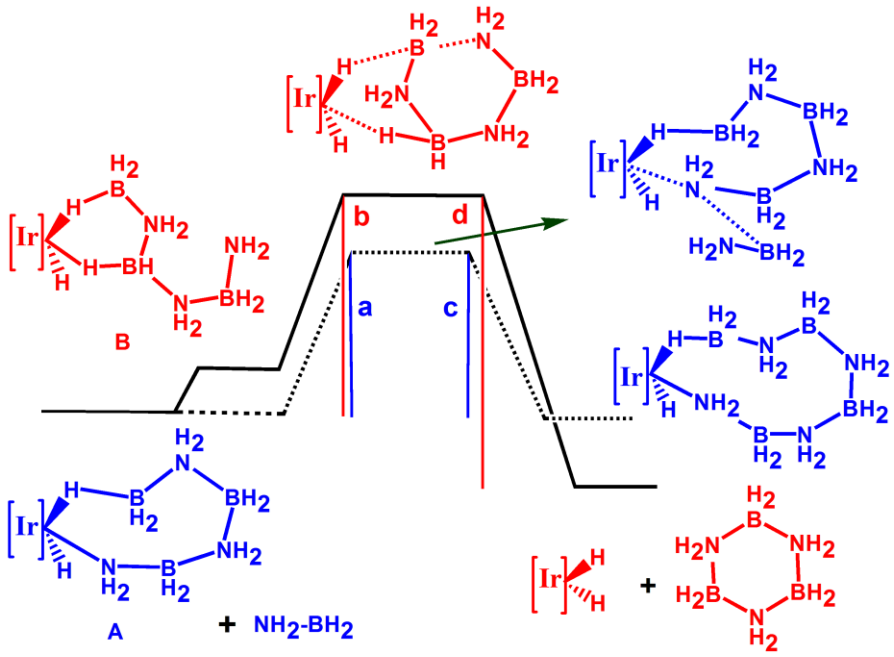

Figure 3.10 The structures of the resting states, **A** and **B**, as well as the corresponding transition states for the insertion and termination steps, for the $[Ir](NH_2BH_2)_n$ system where n = 3.

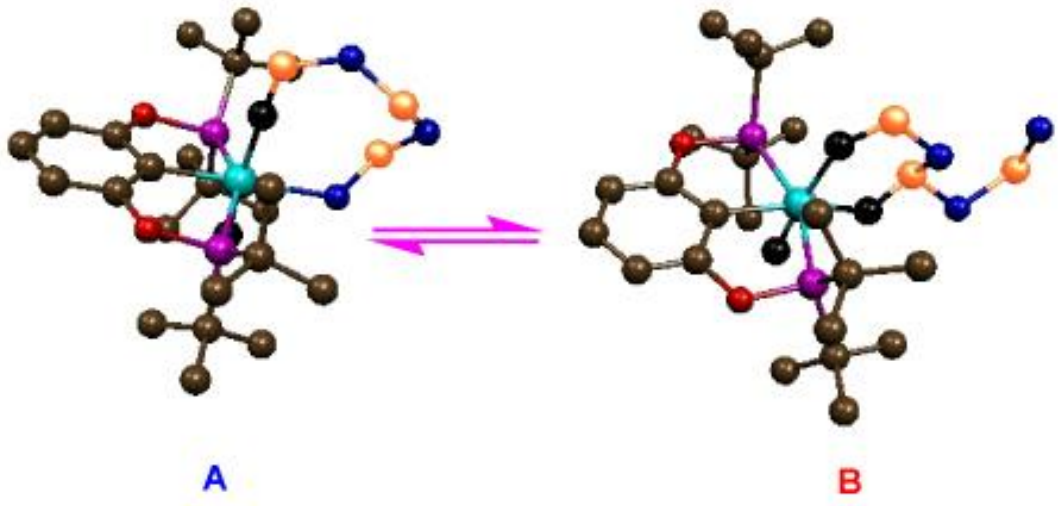

Figure 3.11 The optimized structures of "A" and "B": the two conformers which are the precursors for the formation of the extended chain and the terminated chain respectively, for the case of $[Ir]\text{-}(NH_2BH_2)_3$; only the hydrogens coordinated to the iridium are shown in black, the others have been removed for the purpose of clarity; the colour scheme for the other atoms are: iridium – light blue, phosphorus - pink, oxygen – red, nitrogen – dark blue, carbon – brown and boron – golden yellow.

It is noted here that other equilibrium structures, where a hydrogen of other BH_2 groups in $(NH_2BH_2)_n$ coordinate equatorially to the iridium centre, are also possible, but have not been considered in this study as they are unlikely to lead to either insertion or termination.

Table 3.3 The relative energies, in kcal/mol, of the two resting states "A" and "B" of the complexes: $[Ir](NH_2BH_2)_n$ (n=3,4 and 5).

$[Ir](NH_2BH_2)_n$	A	**B**
n=3	**0.0**	**0.4**
n=4	**0.0**	**5.8**
n=5	**0.0**	**12.2**

Shown in blue in **Fig. 3.10** is the mechanism for the insertion process. The resting state **A** can be subjected to insertion through the approach of a NH_2BH_2 monomer unit that displaces the equatorially coordinated nitrogen from the metal centre and leads to a new complex $[Ir](NH_2BH_2)_{n+1}$, having an additional NH_2BH_2 unit and a similar equatorial coordination of nitrogen to iridium. The barrier for the forward reaction for this process is denoted as "a" and the energetic stabilization of the product $[Ir](NH_2BH_2)_{n+1}$ downhill from the transition state is denoted as "c". The alternative termination process for the resting state **B** is shown in red in **Fig. 3.10**: the nitrogen atom at the end of the chain can approach the axially coordinated BH_2 unit to yield the cyclic oligomer structure $(NH_2BH_2)_n$ and the original catalyst [Ir]. The corresponding barriers for this process are denoted as "b" and "d" respectively.

Shown in **Table 3.4** are the values of "a", "b", "c" and "d" obtained for the complexes $[Ir](NH_2BH_2)_n$ (n = 1-5). **Table 3.4** shows that the barrier of insertion of NH_2BH_2 into the complex $[Ir](NH_2BH_2)_n$ for the cases n = 2 to n = 4 are quite similar. This is because the insertion transition states for the three cases have similar features: the nitrogen attached to the iridium is displaced due to the bond being formed with the boron of the approaching BH_2NH_2, and the displacement at the transition state is about the same in the three cases (Ir-N: 2.82 Å for n =2, 2.75 Å for n = 3, 2.86 Å for n=4). On the other hand, the displacement is greater for the cases n = 1 (Ir-N = 2.95 Å), and n = 5 (Ir-N = 3.01 Å). This higher displacement, indicating a late transition state in the two cases n =1 and n = 5, also explains why the barriers in the two cases is higher than for the cases n =2, 3 and 4.

Table 3.4 The barriers, in kcal/mol, for the insertion and the termination processes; the values in blue (**a** and **c**) indicate the barriers for the insertion process, while the values in red (**b** and **d**) indicate the barriers for the termination process.

$[Ir](NH_2BH_2)_n$	a	b	c	d
n=1	40.5	-	42.4	-
n=2	33.3	-	30.1	-
n=3	28.6	32.3	39.1	57.1
n=4	31.6	33.6	41.4	48.7
n=5	37.4	33.1	46.7	41.4

With regard to the termination process, it is noted that the termination barriers "b" and "d" are not mentioned in the table for n = 1 and 2. This is because, as is clear from **Fig. 3.10**, the termination process leading to the formation of the cyclic oligomer is not a possibility for n = 1, when there is only a single NH_2BH_2 coordinated to the metal centre, and it is sterically not possible for n = 2. For the remaining three cases, n = 3, 4 and 5, the barriers have been calculated, and have been

found to be quite similar – in the range 32.3 kcal/mol (for n =3) to 33.6 kcal/mol (for n = 4). This is because there are two factors determining the termination transition state: (i) the barrier between resting state **B** and the transition state, and (ii) the energy difference between the resting state **B** and the resting state **A**. For n = 3, factor (i) predominates, because of the steric difficulty of forming the cyclic product with three NH_2BH_2 units. For n = 5, the chain size with five NH_2BH_2 units has grown sufficiently large to ease this barrier, but, as discussed earlier and shown in **Table 3.4**, the energy difference between **B** and **A** is high in this case, leading to factor (ii) becoming important. The net effect, therefore, is that the combination of (i) and (ii) leads to the three barriers being nearly equal. However, in terms of the competition between the insertion and termination steps, it becomes clear from a perusal of the barrier values "a" and "b" in **Table 3.4** that, while insertion would be preferred for n = 1, 2, 3 and 4, for n = 5, it is termination that would be preferred. Hence the calculations indicate that the oligomerization process involving the interaction of the species $[Ir](NH_2BH_2)_n$ and NH_2BH_2 would lead to the formation of the cyclic pentamer $(NH_2BH_2)_5$. This provides validation for the experimental findings of Denney *et al.*[27] and their characterization of the insoluble white precipitate formed as the cyclic amino borane pentamer, $(NH_2BH_2)_5$. The energy profile of the entire oligomerization cycle comprising of the five insertion steps and the final termination step are shown in **Fig. 3.12** below.

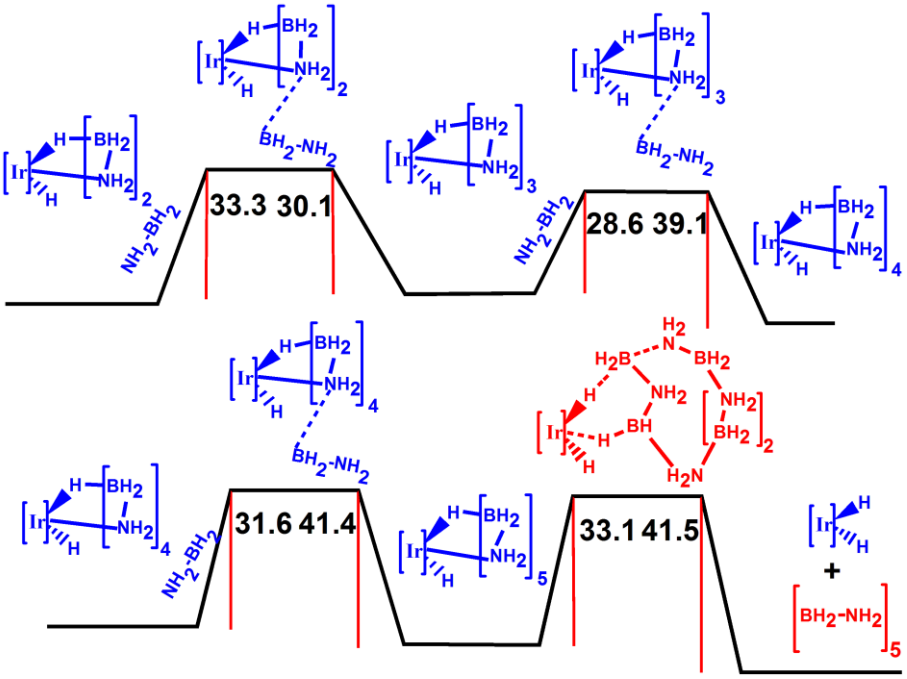

Figure 3.12 The energy profile for the complete mechanistic cycle leading to the formation of the cyclic pentamer $(NH_2BH_2)_5$.

One further point of discussion would be with regard to the formed cyclic $(NH_2BH_2)_5$ species. It is possible that this species, after it is formed, can then also interact with other existing species in solution. The most obvious candidate would be the iridium catalyst complex itself, owing to the relatively large concentration (0.5 M) of the catalyst complex employed during the catalysis. Such an interaction was studied and found to have a high barrier: 53.1 kcal/mol. Furthermore, the pentamer could also interact with free NH_2BH_2 to yield higher cyclic oligomers of the type $(NH_2BH_2)_6$. **Fig. 3.13** shows the calculations done to investigate this possibility. What has been found is that such an interaction would need a barrier of 41.6 kcal/mol, which suggests that such a reaction may indeed be feasible at elevated temperatures. There is, however, the issue of the solubility of the pentamer species: as Paul *et al*[33] have pointed out, the low solubility of the pentamer in THF may lead to the pentamer precipitating out of the solution before it can get approached by an NH_2BH_2 species, which, as discussed in previous sections, is likely to be less available for reaction with

the pentamer even at higher temperatures, owing to the possibility of it getting "recaptured" by the iridium catalyst species.

It is pertinent to note in this context that studies by Manners *et al.*[61], suggest that the insoluble product formed may contain more than five NH_2BH_2 units, though their results in this regard are not conclusive and subject to experimental error. Keeping this in mind, the possibility of the cyclic pentamer undergoing further reactions has also been considered. As shown in **Fig. 3.13** below, the pentamer, once released into the solution from the iridium centre can potentially interact with other species present such as free NH_2BH_2. This, however, would only occur if the pentamer is soluble in the THF solvent and not insoluble, as stated in previous reports [27, 33]. Subject to this condition, the reaction between the pentamer and NH_2BH_2 can produce longer cyclic chains such as $(NH_2BH_2)_6$.The barrier for such a reaction is 41.6 kcal/mol, which indicates that such processes should be feasible at elevated temperatures.

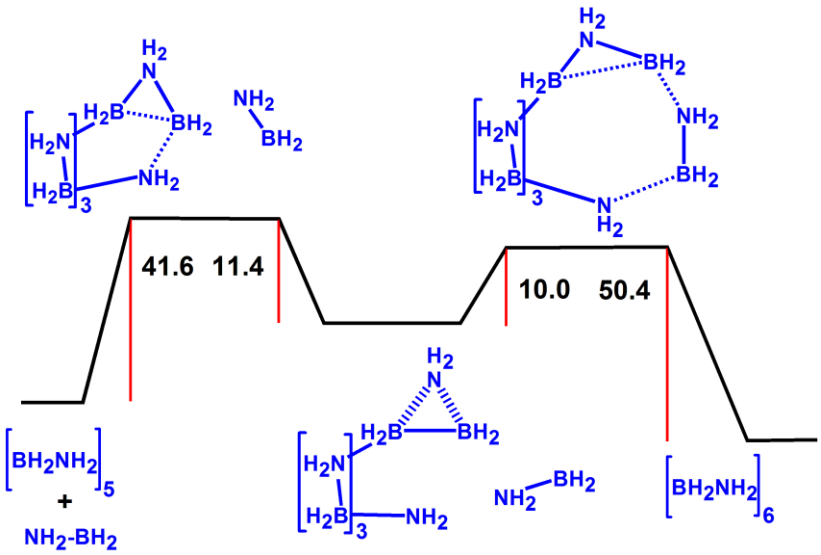

Figure 3.13 The free energy surface for the reaction between the pentamer $(NH_2BH_2)_5$ and amino borane, NH_2BH_2; all values are in kcal/mol.

It is also to be noted here that the proposed mechanistic cycle for the

oligomerization depends on the ready availability of the NH_2BH_2 species. It is possible that at room temperature, where such a species would less available[37], an alternate mechanistic cycle involving the [Ir] species would take precedence and eventually also lead to the formation of $(NH_2BH_2)_5$. The most likely co-reactant in such a mechanism is AB itself. Even though my calculations indicate that AB would be less reactive with the iridium centre than NH_2BH_2 (see **Fig. 3.8**), in the absence of free NH_2BH_2, its interaction with $[Ir](NH_2BH_2)_x$ species may lead to the release of hydrogen and the formation of the $(NH_2BH_2)_5$. An argument against this is the high barrier for the reaction: as shown in **Fig. 3.8(ii)**, the barrier for such a reaction was found to be 49.4 kcal/mol, which may make this reaction untenable at room temperature. However, the fact that the transition state for such a process involves the formation of an H-H bond, involving two light atoms [see **Fig. 3.8 (ii)**] suggests that effects such as tunneling cannot be ruled out. It is also possible that the oligomerization may involve the interaction of more than one $[Ir](NH_2BH_2)$ species. Furthermore, the possibility of the solvent, THF, playing a role and interacting with the $[Ir](NH_2BH_2)_x$ species also cannot be ruled out. Such alternate mechanistic possibilities are currently under investigation.

3.3.5 Modifications to the Catalyst, Substrate and Reaction Conditions to Reduce or Eliminate $(NH_2BH_2)_5$ Formation

The proposed mechanism therefore indicates that the cyclic pentamer $(NH_2BH_2)_5$ can be formed as the by-product during ammonia borane dehydrogenation in [Ir] system by the interaction between the [Ir] and NH_2BH_2 species and illustrates the importance of the iridium complex in the oligomerization process. Now, since the formation of $(NH_2BH_2)_5$ is undesirable and the formation of polyborazylene (PB)

would be significantly more preferable, especially since recent work shows that PB can be reconverted to AB in a facile manner,[36] it is important to consider avenues by which one could reduce or completely suppress the formation of $(NH_2BH_2)_5$ in favour of PB, for the [Ir] catalyst system. The mechanistic insights that have been gained from the current studies can help us in this regard.

One possible way to eliminate the oligomerization process entirely would be to increase the steric bulk on the ancillary phosphorus based ligands of the iridium catalyst, thereby reducing or eliminating the possibility of NH_2BH_2, or of the cyclic $NH_2BH_2BH_3$ species, coordinating to the iridium centre. This would lead to NH_2BH_2 being freed into the solution more easily and, therefore, to the formation of polyborazylene (PB) and/or related oligomeric species, as in the case of all the other catalysts employed to dehydrogenate ammonia borane. Since the process of producing PB would release more equivalents of hydrogen,[37] this is quite an attractive option. Another route to forming PB, also based on reducing the coordination of the dehydrogenation product to the metal centre, would be to use amine boranes, i.e., complexes of the type RNH_2BH_3 and $RR'NHBH_3$ instead of ammonia borane. The increased steric strain of the four membered Ir-H-B-N ring in the [Ir]($RNHBH_2$) and the [Ir]($RR'NBH_2$) complexes would ensure that the competition between the dissociation of RNH_2BH_3 and the insertion of a second RNH_2BH_3 at the metal centre would shift in favour of dissociation and therefore the formation of PB and PB-type soluble oligomers would be increased. Indeed recent work by Dietrich *et al.*[62] shows that, for dehydrogenation with the [Ir] catalyst, using a mixture of NH_3BH_3 and $CH_3NH_2BH_3$ produces soluble cyclic and linear oligomers as by-products, instead of the insoluble white precipitate.

Another means of avoiding the formation of $(NH_2BH_2)_5$ would be to increase the temperature: this would increase the dissociation of NH_2BH_2 from the iridium metal centre. Moreover, increasing the temperature will also increase the possibility of forming the sp3-linear dimer – a species with which the iridium would be likely to only form a dormant complex, therefore not leading to $(NH_2BH_2)_5$ formation.

Another suggestion that could be made to reduce the interaction between the [Ir] complex and NH_2BH_2 would be to increase the dielectric constant of the solvent. This is because there is a significant electrostatic component to the interaction between the two moieties. A natural population analysis[63] conducted for the structure [Ir](NH_2BH_2) shows that the charges on N_{NH2BH2} and the iridium metal to which the nitrogen is coordinated, are -0.95 and +0.04 respectively, which indicates favourable electrostatic interaction between the two atoms. If this electrostatic interaction could be reduced, then it would ease the separation of the coordinating nitrogen from the metal centre and thus reduce the stability of the [Ir](NH_2BH_2) species. Such reduction in electrostatic interaction between the atoms is possible if a solvent that is more polar than THF ($\varepsilon = 7.5$), such as dichloromethane ($\varepsilon = 9.1$) or acetone ($\varepsilon = 21.0$), is employed.

3.4 Conclusions

Full quantum mechanical calculations employing density functional theory (DFT) and MP2 methods reveal that the iridium dihydrogen pincer complex [Ir], which acts as a catalyst for the dehydrogenation of ammonia borane (AB), is also actively involved in converting NH_2BH_2, the immediate product of AB dehydrogenation, into the experimentally observed[27] cyclic pentameric species $(NH_2BH_2)_5$. Experimental studies[37] had shown that NH_2BH_2 is bound to the [Ir] catalyst at room temperature, but is released from the catalyst into the solution at

temperatures of around 60˚C. My calculations indicate that at elevated temperatures, the freed NH_2BH_2 can be "recaptured" by the iridium catalyst through a cycle involving the interaction of [Ir] with the intermediate $NH_2BH_2BH_3$: the product of the interaction of NH_2BH_2 with AB. This suggests that the species [Ir](NH_2BH_2) is likely to be prevalent in solution during the dehydrogenation catalysis, not only at room temperature but also at higher temperatures. Furthermore, a mechanism has been proposed involving [Ir]$(NH_2BH_2)_n$ (n = 1-5) and NH_2BH_2, leading to the cyclic oligomerization of the NH_2BH_2 species at the metal centre. The calculated energetics of the proposed oligomerization cycle indicate that it would terminate after five insertion steps to yield the cyclic pentamer $(NH_2BH_2)_5$, thus corroborating and explaining the experimental observations[27, 37] of the formation of the cyclic $(NH_2BH_2)_5$ species during AB dehydrogenation. In the case of the pentamer, now released from the metal centre, being soluble in the employed THF solvent, further interactions with species such as NH_2BH_2 can occur, leading to the extension of the cyclic chain.

The work thus illustrates the dual role of the [Ir] complex: in (i) first catalyzing the dehydrogenation of AB, and then in (ii) being instrumental in oligomerizing NH_2BH_2 the immediate product of the AB dehydrogenation, to form the experimentally observed $(NH_2BH_2)_5$. Since $(NH_2BH_2)_5$ is an undesired by-product of the reaction, a means of improving the [Ir] catalyst system would be to reduce or eliminate role (ii) played by the [Ir] complex without significantly impacting its primary role of dehydrogenating AB. Some possible means of achieving this have also been discussed in this chapter. It is to be expected that a thorough understanding of the interaction of the [Ir] complex with *all* the species present during AB dehydrogenation, a work that requires further computational investigations, will

successfully lead to its improvement to the point that it would be effective at producing more than two equivalents of H_2 from AB, while also producing the desirable polyborazylene (PB) and completely eliminating the formation of the undesired cyclic pentamer: $(NH_2BH_2)_5$.

3.5 References

[1] U. Eberle, M. Felderhoff, F. Schueth *Angewandte Chemie, International Edition*. **2009**, 48, 6608-6630.
[2] J. Zhang, T. S. Fisher, P. V. Ramachandran, J. P. Gore, I. Mudawar *J. Heat Transfer*. **2005**, 127, 1391-1399.
[3] J. Weitkamp, M. Fritz, S. Ernst *Int. J. Hydrogen Energy*. **1995**, 20, 967-970.
[4] M. Dinca, J. R. Long *Angew. Chem., Int. Ed.* **2008**, 47, 6766-6779.
[5] J. L. C. Rowsell, O. M. Yaghi *Angew. Chem., Int. Ed.* **2005**, 44, 4670-4679.
[6] B. Sakintuna, F. Lamari-Darkrim, M. Hirscher *Int. J. Hydrogen Energy*. **2007**, 32, 1121-1140.
[7] S.-i. Orimo, Y. Nakamori, J. R. Eliseo, A. Zuettel, C. M. Jensen *Chem. Rev. (Washington, DC, U. S.)*. **2007**, 107, 4111-4132.
[8] A. Staubitz, A. P. M. Robertson, I. Manners *Chem. Rev. (Washington, DC, U. S.)*. **2010**, 110, 4079-4124.
[9] N. C. Smythe, J. C. Gordon *Eur. J. Inorg. Chem.* **2010**, 509-521.
[10] F. H. Stephens, V. Pons, R. T. Baker *Dalton Transactions*. **2007**, 2613-2626.
[11] T. B. Marder *Angewandte Chemie, International Edition*. **2007**, 46, 8116-8118.
[12] S. S. Mal, F. H. Stephens, R. T. Baker *Chemical Communications*. **2011**, 47, 2922-2924.
[13] A. B. Chaplin, A. S. Weller *Inorganic Chemistry*. **2010**, 49, 1111-1121.
[14] C. A. Jaska, K. Temple, A. J. Lough, I. Manners *Chemical Communications (Cambridge, United Kingdom)*. **2001**, 962-963.
[15] C. A. Jaska, K. Temple, A. J. Lough, I. Manners *J. Am. Chem. Soc.* **2003**, 125, 9424-9434.
[16] T. J. Clark, C. A. Russell, I. Manners *J. Am. Chem. Soc.* **2006**, 128, 9582-9583.
[17] D. Pun, E. Lobkovsky, P. J. Chirik *Chemical Communications (Cambridge, United Kingdom)*. **2007**, 3297-3299.
[18] T. D. Forster, H. M. Tuononen, M. Parvez, R. Roesler *J. Am. Chem. Soc.* **2009**, 131, 6689-6691.
[19] R. J. Keaton, J. M. Blacquiere, R. T. Baker *J. Am. Chem. Soc.* **2007**, 129, 1844-1845.
[20] M. E. Sloan, T. J. Clark, I. Manners *Inorganic Chemistry (Washington, DC, United States)*. **2009**, 48, 2429-2435.
[21] M. Kaess, A. Friedrich, M. Drees, S. Schneider *Angew. Chem., Int. Ed.* **2009**, 48, 905-907.
[22] N. Blaquiere, S. Diallo-Garcia, S. I. Gorelsky, D. A. Black, K. Fagnou *J. Am. Chem. Soc.* **2008**, 130, 14034-14035.
[23] B. L. Conley, T. J. Williams *Chemical Communications*. **2010**, 46, 4815-4817.
[24] B. L. Conley, D. Guess, T. J. Williams *J Am Chem Soc*. **2011**, 133, 14212-14215.
[25] W. R. H. Wright, E. R. Berkeley, L. R. Alden, R. T. Baker, L. G. Sneddon *Chemical Communications*. **2011**, 47, 3177-3179.

[26] A. Rossin, M. Caporali, L. Gonsalvi, A. Guerri, A. Lledos, M. Peruzzini, F. Zanobini *Eur. J. Inorg. Chem.* **2009**, 3055-3059.
[27] M. C. Denney, V. Pons, T. J. Hebden, D. M. Heinekey, K. I. Goldberg *J. Am. Chem. Soc.* **2006**, 128, 12048-12049.
[28] R. P. Shrestha, H. V. K. Diyabalanage, T. A. Semelsberger, K. C. Ott, A. K. Burrell *Int. J. Hydrogen Energy*. **2009**, 34, 2616-2621.
[29] X. Yang, M. B. Hall *J. Am. Chem. Soc.* **2008**, 130, 1798-1799.
[30] X. Yang, M. B. Hall *Journal of Organometallic Chemistry*. **2009**, 694, 2831-2838.
[31] P. M. Zimmerman, A. Paul, C. B. Musgrave *Inorganic Chemistry (Washington, DC, United States)*. **2009**, 48, 5418-5433.
[32] P. M. Zimmerman, A. Paul, Z. Zhang, C. B. Musgrave *Angewandte Chemie, International Edition*. **2009**, 48, 2201-2205.
[33] A. Paul, C. B. Musgrave *Angew. Chem., Int. Ed.* **2007**, 46, 8153-8156.
[34] P. M. Zimmerman, A. Paul, Z. Zhang, C. B. Musgrave *Inorganic Chemistry (Washington, DC, United States)*. **2009**, 48, 1069-1081.
[35] B. L. Davis, D. A. Dixon, E. B. Garner, J. C. Gordon, M. H. Matus, B. Scott, F. H. Stephens *Angewandte Chemie, International Edition*. **2009**, 48, 6812-6816, S6812/6811-S6812/6818.
[36] A. D. Sutton, A. K. Burrell, D. A. Dixon, E. B. Garner, J. C. Gordon, T. Nakagawa, K. C. Ott, J. P. Robinson, M. Vasiliu *Science*. **2011**, 331, 1426-1429.
[37] V. Pons, R. T. Baker, N. K. Szymczak, D. J. Heldebrant, J. C. Linehan, M. H. Matus, D. J. Grant, D. A. Dixon *Chemical Communications (Cambridge, United Kingdom)*. **2008**, 6597-6599.
[38] K. W. Boeddeker, S. G. Shore, R. K. Bunting *J. Am. Chem. Soc.* **1966**, 88, 4396-4401.
[39] R. Ahlrichs, M. Baer, M. Haeser, H. Horn, C. Koelmel *Chem. Phys. Lett.* **1989**, 162, 165-169.
[40] A. D. Becke *Phys. Rev. A Gen. Phys.* **1988**, 38, 3098-3100.
[41] J. P. Perdew *Physical Review B*. **1986**, 33, 8822-8824.
[42] F. Weigend *Physical Chemistry Chemical Physics*. **2002**, 4, 4285-4291.
[43] F. Weigend, R. Ahlrichs *Physical Chemistry Chemical Physics*. **2005**, 7, 3297-3305.
[44] A. Schaefer, H. Horn, R. Ahlrichs *Journal of Chemical Physics*. **1992**, 97, 2571-2577.
[45] A. Schaefer, C. Huber, R. Ahlrichs *Journal of Chemical Physics*. **1994**, 100, 5829-5835.
[46] J. P. Perdew, K. Burke, M. Ernzerhof *Phys. Rev. Lett.* **1996**, 77, 3865-3868.
[47] K. Eichkorn, O. Treutler, H. Oehm, M. Haeser, R. Ahlrichs *Chem. Phys. Lett.* **1995**, 240, 283-290.
[48] M. Sierka, A. Hogekamp, R. Ahlrichs *The Journal of Chemical Physics*. **2003**, 118, 9136-9148.
[49] C. Hattig, F. Weigend *Journal of Chemical Physics*. **2000**, 113, 5154-5161.
[50] A. Klamt *J. Phys. Chem.* **1995**, 99, 2224-2235.
[51] M. Mammen, E. I. Shakhnovich, G. M. Whitesides *Journal of Organic Chemistry*. **1998**, 63, 3168-3175.
[52] G. Alcaraz, L. Vendier, E. Clot, S. Sabo-Etienne *Angewandte Chemie, International Edition*. **2010**, 49, 918-920, S918/911-S918/914.
[53] R. Dallanegra, A. B. Chaplin, J. Tsim, A. S. Weller *Chemical Communications (Cambridge, United Kingdom)*. **2010**, 46, 3092-3094.

[54] R. Dallanegra, A. B. Chaplin, A. S. Weller *Angewandte Chemie, International Edition*. **2009**, 48, 6875-6878, S6875/6871-S6875/6815.
[55] S. Gancher, J. Nutt, D. Mckee *Movement Disord*. **1991**, 6, 275-276.
[56] M. P. Caulfield, R. L. Mckee, M. E. Goldman, L. T. Duong, J. E. Fisher, C. T. Gay, P. A. Dehaven, J. J. Levy, E. Roubini, R. F. Nutt, M. Chorev, M. Rosenblatt *Endocrinology*. **1990**, 127, 83-87.
[57] Z. Li, G. Zhu, G. Lu, S. Qiu, X. Yao *J Am Chem Soc*. **2010**, 132, 1490-1491.
[58] W. J. Shaw, J. C. Linehan, N. K. Szymczak, D. J. Heldebrant, C. Yonker, D. M. Camaioni, R. T. Baker, T. Autrey *Angewandte Chemie, International Edition*. **2008**, 47, 7493-7496.
[59] M. T. Nguyen, V. S. Nguyen, M. H. Matus, G. Gopakumar, D. A. Dixon *Journal of Physical Chemistry A*. **2007**, 111, 679-690.
[60] W. R. Nutt, M. L. McKee *Inorganic Chemistry (Washington, DC, United States)*. **2007**, 46, 7633-7645.
[61] A. Staubitz, M. E. Sloan, A. P. M. Robertson, A. Friedrich, S. Schneider, P. J. Gates, J. S. a. d. Günne, I. Manners *J Am Chem Soc*. **2010**, 132, 13332-13345.
[62] B. L. Dietrich, K. I. Goldberg, D. M. Heinekey, T. Autrey, J. C. Linehan *Inorg. Chem. (Washington, DC, U. S.)*. **2008**, 47, 8583-8585.
[63] A. E. Reed, R. B. Weinstock, F. Weinhold *J. Chem. Phys.* **1985**, 83, 735-746.

Chapter 4: Efficiency of Bidentate Analogue of the Ir-pincer Catalyst [(Ir)(POC)H_2)] over the Tridentate Ir-pincer Catalyst [(Ir)(POCOP)H_2)]

Abstract

Full quantum mechanical calculations demonstrate that cooperativity in the form of the activation of the M–C bond (M: transition metal or boron, C: the *ipso* carbon of the coordinated phenyl group) can lead to effective catalysis pathways. Calculations show that the presence of an aromatic bidentate ligand attached to a transition metal, or even a main group element such as boron, can lead to effective catalysts for a range of important reactions, such as the dehydrogenation of ammonia borane and formic acid and the activation of the N–H bond in aromatic amines. Moreover, it is shown that the design of tridentate pincer complexes with the aromatic group at a terminal end can lead to effective M–C cooperativity. As such, the current work introduces a new concept in cooperativity and bond activation chemistry.

4.1 Introduction

Non-oxidative addition and elimination reactions using organometallic complexes that demonstrate metal-ligand cooperativity are of great practical significance, especially if the reactions can occur reversibly over a small span of time. Complexes having tridentate "pincer ligands" such as PCP [$C_6H_3(R')(P(R)_3CH_2)_2$–1,2,6], POCOP [$C_6H_3(R')(P(R)_3O)_2$–1,2,6], NCN [$C_6H_3(R')(N(R)_2CH_2)_2$–1,2,6], PCN [$C_6H_3((R'')P(R)_3CH_2)(N(R')_2CH_2)$–1,2,6], PNP [$C_5H_3N(R)(P(R')_3CH_2)_2$-1,2,6] and others[1, 2] have proved to be very versatile and effective ligands in facilitating such reactions, in conjunction with transition metals such as iridium, platinum, rhodium, osmium and ruthenium. The group of David Milstein has exploited the cooperativity between the metal and pincer ligands in order to obtain a stable platinum oxo complex exhibiting interesting reactivity[3] and to split water and obtain molecular oxygen and hydrogen[4]. Ahuja *et al.*[5] have used different pincer-ligated iridium complexes in order to convert linear alkanes to aromatic compounds. Pincer ligand coordinated

organometallic complexes have also been effective at N–H, N–C, C–C, C–H, H–H and O–H activation.[2, 6-8] Such complexes have been also been found to be important for reactions such as the highly efficient dehydrogenation of ammonia borane, due to the hemi–labile nature of the nitrogen-metal bond.[9]

The rich and varied chemistry that has emerged from the effective use of pincer ligand complexes gives reason to believe that further exploitation of metal–ligand cooperativity using such complexes is likely in the near future. However, it is interesting to note that cooperativity between the metal centre and a coordinated carbon atom in pincer ligand complexes has not been explored. To the best of my knowledge, the only reported example of the non-innocent behaviour of a metal-carbon bond in a pincer complex is by Musa *et al.*[10] for C(sp^3) metalated pincer compounds. Moreover, the reactions that were studied with this complex were found to require a significant amount of time, and needed extra heating over a period of twelve hours to ensure completion. Also, to date, no pincer ligated metal complexes having an aromatic group as one of the arms of the pincer have been reported to display metal–C(sp^2) cooperativity through activation of the metal–*ipso* carbon bond.

I postulate here that the reason pincer ligand containing complexes do not exhibit metal-carbon cooperativity is because of the steric constraints imposed by the tridentate nature of the ligand coordination, and, further, that employing analogous aromatic bidentate ligands in place of the tridentate pincer ligands (see **Fig. 4.1**), or tridentate pincers where the phenyl ring is at a terminal end of the ligand, would reduce the steric restrictions. This would serve to make the bidentate or tridentate complexes efficient catalysts due to the emergence of cooperativity between the metal and the *ipso* carbon of the attached phenyl group. An example for such a possibility is shown in **Fig. 4.2** below, where the catalysis of dehydrogenation reactions is

discussed, for a complex with an aromatic bidentate ligand coordinated to the metal center. The dehydrogenation would proceed with the loss of two hydrogen atoms from the substrate molecule H–A–B–H, with the protic hydrogen being taken up by the *ipso*-carbon of the phenyl ring and the hydridic hydrogen forming a bond with the metal centre (see **Fig. 4.2**). Following this, the oxidative metalation step would complete the catalytic cycle, releasing hydrogen gas, H_2, and regenerating the original catalyst species. The facile activation of the metal–*ipso* carbon bond would make the first step kinetically and thermodynamically favourable, and the likely ready re-coordination of the phenyl ring back to the metal centre in the second step would complete the cycle. Likewise, analogous to the dehydrogenation reaction discussed in **Fig. 4.2**, one could envisage other possible reactions that could be effectively catalyzed by the use of the aromatic bidentate complexes, or tridentate complexes having the phenyl ring at a terminal end and not at the center.

The reason the catalytic pathway, illustrated in **Fig. 4.2**, involving metal-carbon activation has been considered for aromatic ligands, and not for their aliphatic analogues, is because of the possibility of an agostic interaction between the $C(sp^2)$–H bond and the metal, as experimentally observed and reported in several complexes containing an aromatic ligand.[11-15] Such an interaction would pre-activate the $C(sp^2)$–H bond in this step and thus aid in reducing the barrier to metalation, thereby ensuring the efficiency of the catalysis process.

Figure 4.3 Tridentate and bidentate aromatic ligand complexes.

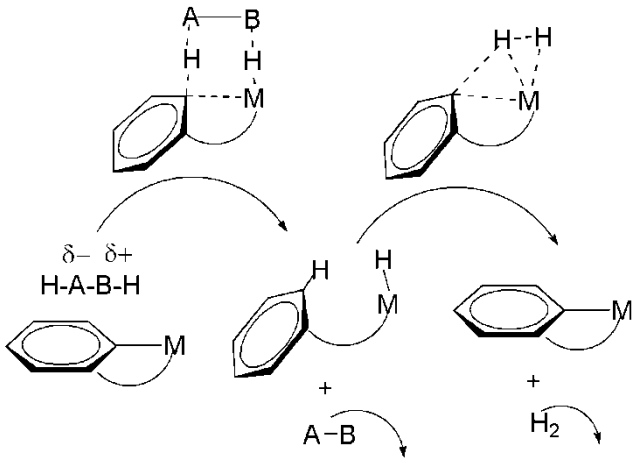

Figure 4.2 The catalysis of dehydrogenation reactions through the use of metal-*ipso* carbon cooperativity in aromatic bidentate complexes.

The effectiveness of the proposed metal-carbon cooperative catalytic pathway will be demonstrated in the Results and Discussion section, by considering the example of the tridentate pincer ligand complex: (POCOP)IrH_2, one of the most efficient catalysts for dehydrogenating ammonia borane[16] (AB). It will be shown that the bidentate analogue of the tridentate (POCOP)IrH_2, if synthesized: "(POC)IrH_2", would be considerably more effective at catalyzing the same reaction. I will also demosntrate computationally that employing tridentate ligands with the aromatic ring at the terminal end would also lead to the emergence of metal-carbon cooperativity. The potential of metal-carbon cooperativity in bidentate complexes will be further discussed for other cases, such as the experimentally synthesized real system: Ta(=CH–*t*–Bu)[$C_6H_3(CH_2NMe_2)_2$–2,4](Cl)(O–*t*–Bu) and even for non-metal based complexes such as B(Et)[$C_6H_4(CH_2CH_2)$]. Moreover, it will be shown that the catalysis of other important reactions, such as the dehydrogenation of formic acid, as well as the activation of the N–H bond in aromatic amines, will become feasible through the proposed route of metal–carbon cooperativity.

4.2 Computational details

All the DFT calculations were carried out using the Turbomole 6.0 suite of programs[17]. Geometry optimizations were performed using the Becke Perdew 86 (BP–86) functional[18, 19]. The electronic configuration of the atoms was described by a triple-zeta basis set augmented by a polarization function (Turbomole basis set TZVP)[20]. The basis set employed for iridium includes relativistic effective core potentials (RECP). The resolution of identity (RI)[21], along with the multipole accelerated resolution of identity (MARIJ)[22] approximations were employed for an accurate and efficient treatment of the electronic Coulomb term in the density functional calculations. Since it is possible that the geometry optimization procedure with DFT may be sensitive to the nature of the functional, a further test has been done to ensure the reliability of the obtained geometry optimised structures: all the minima and transition state structures were also optimised with the Perdew, Burke, and Erzenhof density functional (PBE)[23] at the same, TZVP, basis set level. A comparison was then done between the corresponding structures obtained with the BP–86 and the PBE functionals. The comparison showed very little difference in bond lengths, angles and dihedral values between the corresponding structures for all the cases. A further corroboration of the small difference between the structures obtained from the two functionals comes from comparison of the potential energy surfaces for the different reactions. The ΔE values obtained from the two separate set of DFT calculations are almost similar in most of the cases (see the **Tables 4.1** –**4.5** in the Supporting Information File) thus providing further proof of the reliability of the BP-86 functional in obtaining optimised geometries and transition states. Care was taken to ensure that the obtained transition state structures possessed only one imaginary frequency corresponding to the correct normal mode. The validity of the

obtained transition states was further confirmed by doing IRC[24] calculations: the correct reactant and product structures were obtained for every transition state obtained. In order to do the IRC calculations, Turbomole 6.4 was employed. Subsequent to obtaining the reliable optimized minima and transition states as discussed here, single point calculations were done with the hybrid B3-LYP functional[25, 26] in order to obtain more reliable energy values for the potential energy surfaces for the different investigated reactions. Solvent effects were incorporated through single point calculations using the COSMO model[27], with tetrahydrofuran (ε = 7.52) as the solvent. Moreover, dispersion corrections were also included through single point calculations. The contributions of internal energy and entropy were obtained from frequency calculations done on the DFT structures at 298.15 K: thus, the energies reported in the figures are the ΔG values. In order to account for the fact that all the species are in solution, the translational entropy term in the calculated structures was corrected through a free volume correction introduced by Mammen *et al.*[28].

Table 4.1 The comparison of the barriers, in kcal/mol, between the values obtained from the calculations done with the BP–86 and the PBE functionals for the (POCOP)IrH_2 real case; the second and the third columns compare the "forward barriers" the difference between the transition states and the reactants, while the fourth and the fifth columns compare the "reverse barriers" - the difference between the transition states and the products of the individual reactions considered.

Transition States for the Tridentate Case	ΔE BP-86 Value for the Forward Barrier (kcal/mol)	ΔE PBE Value for the Forward Barrier (kcal/mol)	ΔE BP-86 Value for the Reverse Barrier (kcal/mol)	ΔE PBE Value for the Reverse Barrier (kcal/mol)
The proposed M-C activation pathway 1st trans state	23.8	24.1	19.5	16.9
The proposed M-C activation pathway 2nd trans state	0.9	0.7	9.8	9.4
The proposed M-C activation pathway 3rd Trans state	13.6	13.5	8.4	6.7
Paul-Musgrave mechanism 1st trans state	11.5	12.0	16.1	13.5
Paul-Musgrave mechanism 2nd trans state	18.9	19.1	13.7	12.2

It is to be noted that the entropic term is likely to be mis–represented when the reactants are considered separately in a reaction pathway: it is well known that the translational entropy is artificially increased in such cases.[28] Though the use of the free volume correction[28], as done in all calculations reported in this chapter, can mitigate this problem to some extent, it is still likely to be an issue and provide heightened values for the barriers for all the reactions. Hence, in order to avoid this problem, all the reaction pathways have been determined starting with the reactants having formed a complex, instead of beginning from the separated reactant species, a procedure that has also been followed by other groups.[29-35]

Table 4. 2 The comparison of the barriers, in kcal/mol, between the values obtained from the calculations done with the BP–86 and the PBE functionals for the (POC)IrH_2 case; the second and the third columns compare the "forward barriers" – the difference between the transition states and the reactants, while the fourth and the fifth columns compare the "reverse barriers" - the difference between the transition states and the products of the individual reactions considered.

Transition States for the Bidentate Case	ΔE BP-86 Value for the Forward Barrier (kcal/mol)	ΔE PBE Value for the Forward Barrier (kcal/mol)	ΔE BP-86 Value for the Reverse Barrier (kcal/mol)	ΔE PBE Value for the Reverse Barrier (kcal/mol)
The proposed M-C activation pathway 1st trans state	13.8	14.2	19.4	16.1
The proposed M-C activation pathway 2nd trans state	9.8	9.3	5.2	5.0
The proposed M-C activation pathway 3rd Trans state	13.7	13.5	5.9	4.2
Paul-Musgrave mechanism 1st trans state	18.0	18.2	19.0	15.8
Paul-Musgrave mechanism 2nd trans state	21.0	20.9	13.2	11.5

Table 4.3 The comparison of the barriers, in kcal/mol, between the values obtained from the calculations done with the BP–86 and the PBE functionals for the (PPC)IrH_2 case; the second and the third columns compare the "forward barriers" – the difference between the transition states and the reactants, while the fourth and the fifth columns compare the "reverse barriers" - the difference between the transition states and the products of the individual reactions considered.

Transition States for the (PPC)Ir(H_2) catalyst	ΔE BP-86 Value for the Forward Barrier (kcal/mol)	ΔE PBE Value for the Forward Barrier (kcal/mol)	ΔE BP-86 Value for the Reverse Barrier (kcal/mol)	ΔE PBE value for the Reverse Barrier (kcal/mol)
The proposed M-C activation pathway 1st trans state	20.7	20.9	6.9	4.0
The proposed M-C activation pathway 2nd trans state	5.5	5.1	14.4	14.0
The proposed M-C activation pathway 3rd Trans state	14.3	14.8	0.4	-0.4
Paul-Musgrave mechanism 1st trans state	20.4	20.7	15.5	12.6
Paul-Musgrave mechanism 2nd trans state	26.7	27.1	12.9	11.8

Table 4.4 The comparison of the barriers, in kcal/mol, between the values obtained from the calculations done with the BP-86 and the PBE functionals for the Ta(H)(CH_2-*t*-Bu)[C_6H_3(CH_2NMe_2)$_2$-2,6](Cl)(O-*t*-Bu) case; the second and the third columns compare the "forward barriers" – the difference between the transition states and the reactants, while the fourth and the fifth columns compare the "reverse barriers" - the difference between the transition states and the products of the individual reactions considered.

Transition States for the Tantalum Case	ΔE BP-86 Value for the Forward Barrier (kcal/mol)	ΔE PBE Value for the Forward Barrier (kcal/mol)	ΔE BP-86 Value for the Reverse Barrier (kcal/mol)	ΔE PBE Value for the Reverse Barrier (kcal/mol)
The proposed M-C activation pathway 1st trans state	15.9	16.0	21.3	17.6
The proposed M-C activation pathway 2nd trans state	20.0	19.2	13.0	12.7
The proposed M-C activation pathway 3rd trans state	1.9	1.9	8.8	7.3

Table 4.5 The comparison of the barriers, in kcal/mol, between the values obtained from the calculations done with the BP-86 and the PBE functionals for the B(Et)[$C_6H_3(CH_2CH_2)$-2] case; the second and the third columns compare the "forward barriers" – the difference between the transition states and the reactants, while the fourth and the fifth columns compare the "reverse barriers" - the difference between the transition states and the products of the individual reactions considered.

Transition States for the Boron Case	ΔE BP-86 Value for the Forward Barrier (kcal/mol)	ΔE PBE Value for the Forward Barrier (kcal/mol)	ΔE BP-86 Value for the Reverse Barrier (kcal/mol)	ΔE PBE Value for the Reverse Barrier (kcal/mol)
The proposed M-C activation pathway 1st trans state	25.2	24.7	23.6	19.7
The proposed M-C activation pathway 2nd trans state	23.1	20.6	21.7	18.7
The proposed M-C activation pathway *p*-OMe 1st trans state	23.2	22.8	19.8	16.0
The proposed M-C activation pathway *p*-OMe 2nd trans state	22.3	19.8	22.5	19.6
The proposed M-C activation pathway *o*-OMe , p-OMe 1st trans state	20.8	20.3	19.8	16.0
The proposed M-C activation pathway *o*-OMe , p-OMe 2nd trans state	22.0	19.4	22.5	19.6

4.3 Results and Discussion

4.3.1 Comparison of Ammonia Borane Dehydrogenation using Bidentate and Tridentate Iridium Catalysts

The pincer ligand containing complex, (POCOP)IrH_2, has been found to be a very efficient catalyst for the dehydrogenation of ammonia borane: NH_3BH_3 (AB)[16]. The structure of (POCOP)IrH_2 is shown in **Fig. 4.3** below. Ammonia borane (AB), it may be noted, is one of the most promising candidates for the chemical storage of hydrogen[36], and, therefore, the efficient catalysis of AB dehydrogenation is an important problem in hydrogen storage research. The mechanism for the dehydrogenation of AB using the (POCOP)IrH_2 catalyst has been reported by Paul and Musgrave[37]. As shown in **Fig. 4.4**, the Paul-Musgrave dehydrogenation mechanism proceeds through the coordination of AB to the (POCOP)IrH_2 catalyst, followed by removal of NH_2BH_2 from the vicinity of the catalyst. The (POCOP)IrH_4 intermediate thus formed is then converted to the (POCOP)IrH_2 catalyst by the loss of H_2, thereby completing the catalytic cycle[37]. The competing pathway for the (POCOP)IrH_2 catalyst, involving the proposed metal-carbon cooperativity, is shown in **Fig. 4.5**. This pathway is found not to compete, having a slowest step barrier that is higher by 14.5 kcal/mol than the slowest step of the Paul-Musgrave pathway.

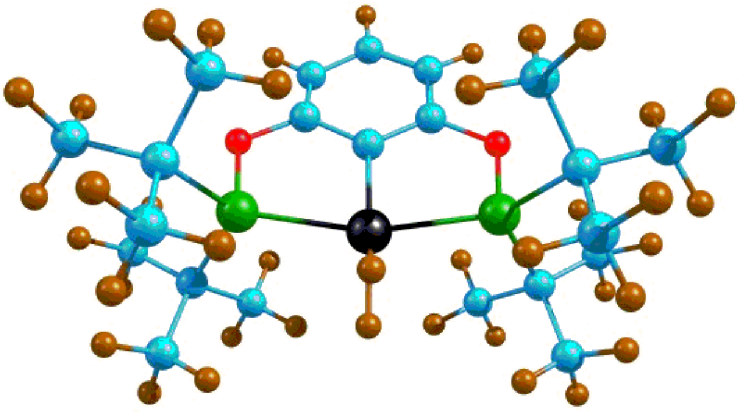

Figure 4.3 Structural parameters in Rh_6, Rh_4Ru_2 clusters (golden coloured atom: Rh; purple Structure of tridentate (POCOP)IrH_2 pincer catalyst; the color scheme is as follows: iridium- black, carbon - blue, phosphorus – green, oxygen – red and hydrogen – brown.

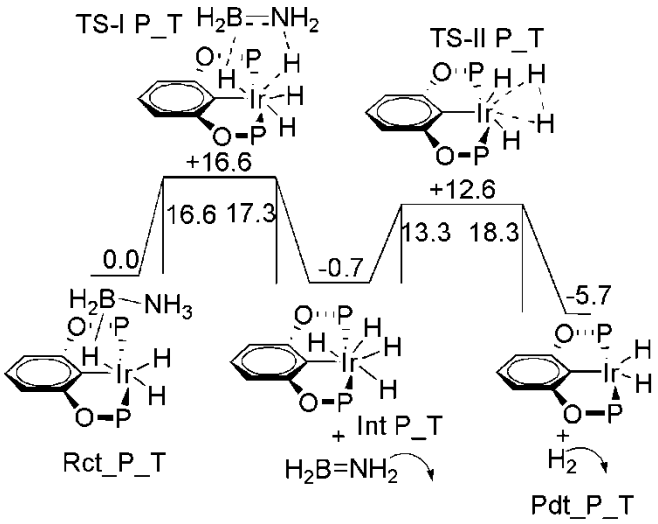

Figure 4.4 The free energy profile for the Paul-Musgrave reaction pathway for the dehydrogenation of ammonia borane by the (POCOP)IrH_2 catalyst; all energies are in kcal/mol.

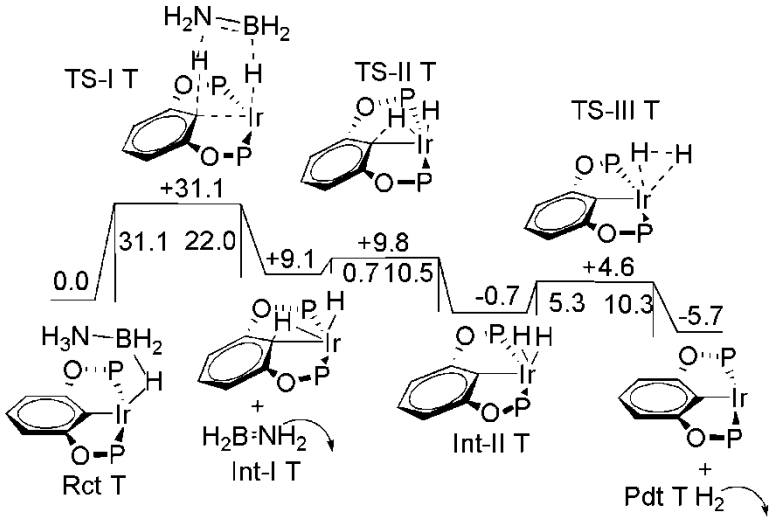

Figure 4.5 The free energy profile for the dehydrogenation of ammonia borane through the proposed M-C activation pathway, for the (POCOP)IrH_2 catalyst; all values are in kcal/mol.

However, However, it is likely that the metal-ligand cooperative pathway might become more competitive if the steric restrictions, imposed by the tridentate nature of the bonding of the ligand at the metal center, could be reduced. This would be possible if the catalyst employed were to have an *aromatic bidentate ligand coordination to begin with*. This point is underlined through calculations with the bidentate analogue of (POCOP)IrH_2: the "(POC)IrH_2" complex. The optimized structure for (POC)IrH_2 is shown in **Fig. 4.6** below: the complex has a monodentate phosphine (with tertiary butyl groups), and a bidentate ligand with an aromatic ring as one of the arms and a phosphine as the other, of the bidentate ligand. The fact that this system would be stable in solution was confirmed through calculations investigating the dissociation of the phosphine from this complex and the replacement of the same with a solvent (THF) molecule. As shown in **Fig. 4.7**, it was found that such a reaction would be highly unlikely, being endothermic by 104.8 kcal/mol. Hence, the complex (POC)IrH_2 would be stable in solution.

For this system, the catalysis of AB dehydrogenation would prefer the

pathway of metal-*ipso* carbon cooperativity, as is made clear from **Fig. 4.8** and **Fig. 4.9**. The slowest step barrier for the reaction, 15.3 kcal/mol, through the proposed metal – *ipso* carbon cooperative pathway, is lower by 1.6 kcal/mol than the slowest step for the Paul-Musgrave pathway in this case, and lower by 1.3 kcal/mol to the slowest step barrier (16.6 kcal/mol) for the Paul-Musgrave pathway obtained for the tridentate iridium analogue. These computational results therefore underline the potential of metal-carbon cooperativity, which is dormant in the pincer ligand complex but is unlocked in the bidentate analogue.

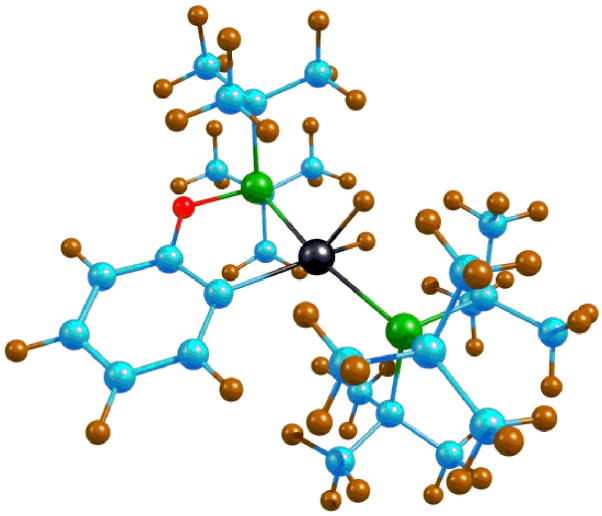

Figure 4.6 The optimized geometry of the iridium bidentate complex: (POC)IrH_2 complex; the colour scheme is the same as in Figure 4.3.

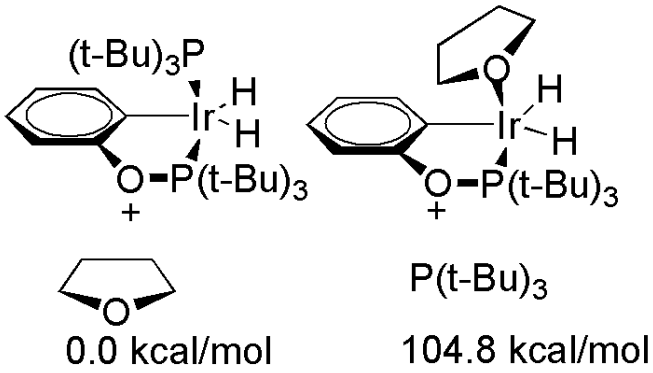

Figure 4.7 The comparison of the optimized structures of non dissociated bidentate catalyst with the separate solvent molecule (THF) and dissociated catalyst (in coordination with the solvent molecule) with separate phosphine; all values are in kcal/mol.

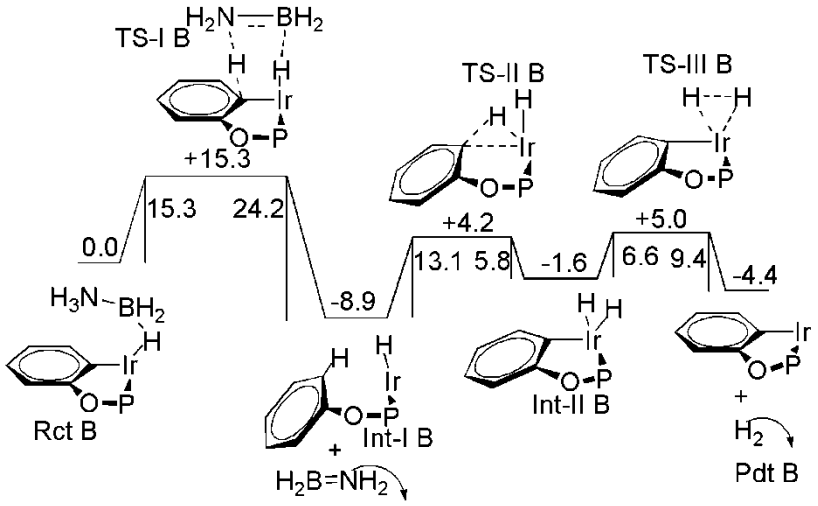

Figure 4.8 The free energy profile for the proposed M-C activation pathway for the dehydrogenation of ammonia borane by the (POC)IrH_2 catalyst; all energies are in kcal/mol.

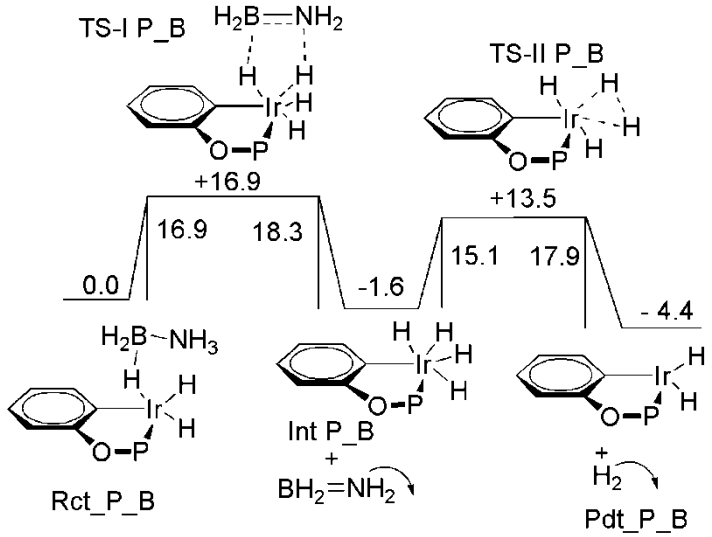

Figure 4.9 The free energy profile for the dehydrogenation of ammonia borane through the Paul-Musgrave pathway, for the (POC)IrH_2 catalyst; all energies are in kcal/mol.

The reasons the bidentate catalyst is determined to be more effective than the corresponding tridentate complexes are two-fold: (i) the reduction of steric hindrance for the motion of the phenyl ring out of the POC plane, and (ii) the low barrier for the second transition state because of the pre-activation of the *ipso*-carbon-hydrogen bond due to the aromatic agostic interaction of the bond with the iridium metal centre. There have been experimental reports in the literature that have hypothesized the existence of such an interaction, for rhodium[11],[12],[13] and ruthenium metal[14],[15] complexes. The presence of the aromatic agostic interaction in the (POC)IrH_2 complex is made evident from the geometric features obtained for the intermediate: **Int-I B** (see **Fig. 4.8**) along the catalytic path. The structure of **Int-I B** is shown in **Fig. 4.10** below. The *ipso* carbon–hydrogen bond length in **Int-I B** is found to be 1.12 Å, which is greater than the standard aromatic C-H bond length (1.09 Å). Moreover, the hydrogen of the pre-activated C-H bond is found to lie out of the plane of the aromatic ring by 11.25º. Furthermore, the Ir-H distance is found to be 2.10 Å and the Ir-H-C angle is observed to be 116.81º, both falling in the range of typical agostic interactions. To further underline the agostic nature of the interaction, another conformer of **Int-I B: Int-I B′** was optimized – having the aromatic ring turned away from the iridium metal centre, thereby denying the system the possibility of an aromatic agostic interaction. The two conformers: **Int-I B** and **Int-I B′** are shown juxtaposed in **Fig. 4.11**. As the figure shows, **Int-I B′** is less stable by 8.1 kcal/mol (ΔE) than **Int-I B**, providing further evidence of the stabilizing influence of the aromatic agostic interaction in **Int-I B**. Hence the cumulative evidence points to the pre-activation of the C(sp^2)-H bond, which provides the explanation as to why the second barrier the barrier for the oxidative metalation step is 13.1 kcal/mol , thereby making the catalytic cycle a feasible process.

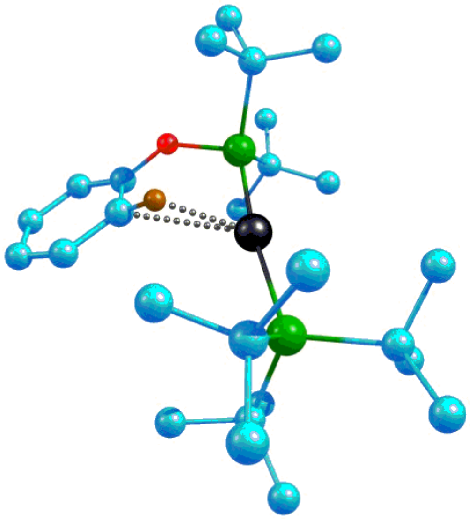

Figure 4.10 The optimized structure of **Int-I B**: the hydrogenated (POC)IrH_2 catalyst; the colour scheme is the same as in Figure 4.3; only the hydrogen coordinated to the *ipso* carbon is shown, the rest of the hydrogens have been removed for the purpose of clarity.

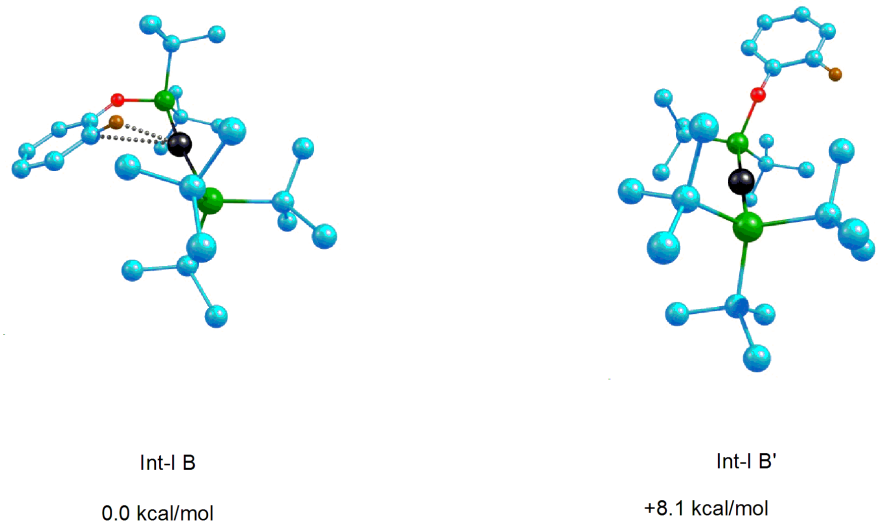

Figure 4.11 The optimized The comparison of the stabilities of the two optimized structures: **Int-I B –** the (POC)IrH_2 complex with an agostic interaction between the *ipso* C-H bond and the iridium, and **Int-I B′ –** the (POC)IrH_2 complex without the agostic interaction; the colour scheme is as follows: iridium- black, carbon - blue, phosphorus – green, oxygen – red and hydrogen – brown; only the hydrogen coordinated to the ipso carbon is shown, the rest of the hydrogens have been removed for the purpose of clarity.

It is also interesting to note that an aromatic agostic interaction with the metal centre is more likely than an aliphatic agostic interaction: no structural evidence for an agostic interaction is observed in the optimized complex $Ir(H)_3[P(CH_3)_3][P(Me)_3OCH_2CH_2(CH_3)]$ – a structure, shown in **Fig. 4.12**, where the aromatic phenyl ring has been replaced with an aliphatic CH_2CH_2 group. Thus, the corresponding metalation step for the aliphatic complex has been calculated to be 23.4 kcal/mol (ΔE value), higher than the corresponding step in the aromatic complex, by 9.6 kcal/mol (ΔE value). These investigations therefore reveal that the bidentate complexes would be more effective for aromatic ligands, and not for their aliphatic analogues.

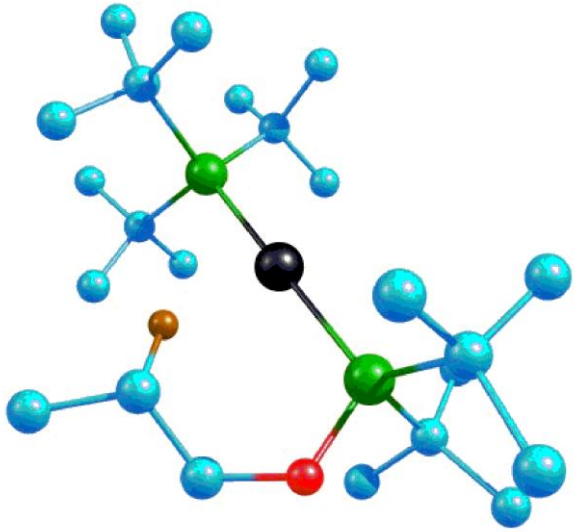

Figure 4.12 The optimized structure for the aliphatic analogue of the (POC)IrH_2 complex; the colour scheme is same as Figure 4.3; only the hydrogen coordinated to the ipso carbon is shown, the rest of the hydrogens have been removed for the purpose of clarity.

The results discussed in this section therefore indicate that the iridium bidentate complex, (POC)IrH_2, if synthesized, would be a more effective catalyst for ammonia borane (AB) dehydrogenation than the tridentate complex, (POCOP)IrH_2,

because of Ir-*ipso* carbon cooperativity, discussed here, for the bidentate complex, which gives it an edge over the original mechanism, described by Paul and Musgrave for the tridentate complex[37]. This computational demonstration of the potential for metal-carbon cooperativity in bidentate complexes can lead to significant improvements in catalyst design for important chemical transformations.

It is important to mention here that it may also be possible to observe metal-carbon cooperativity in tridentate pincer ligand complexes. This would be possible if the steric contraints were to be reduced by the putting of the aromatic phenyl ring at the terminal end of the ligand, instead of in the center. An example of a model tridentate pincer ligand with such a linkage is shown in **Fig. 4.13** below. The ligand coordinated to the iridium center has two consecutive phosphine linkages, followed by a phenyl linkage. This ligand is henceforth termed as "PPC": thus the complex would be (PPC)IrH_2. This complex would provide a "bidentate" environment to the phenyl ligand, and thus could allow the emergence of metal-carbon cooperativity. This is further illustrated by doing AB dehydrogenation catalysis with this (PPC)IrH_2. As **Figs. 4.14** and **4.15** indicate, the metal-carbon activation pathway (slowest step barrier: 22.2 kcal/mol) is seen to be competitive in comparison to the Paul-Musgrave pathway (slowest step barrier: 21.2 kcal/mol). Tridentate pincer ligand complexes having the phenyl ring at a terminal end, instead of in the center, have already been prepared.[38] The current work therefore provides an example of the potential of such complexes for catalysis. The focus of the remainder of this chapter, however, is on aromatic bidentate ligand complexes.

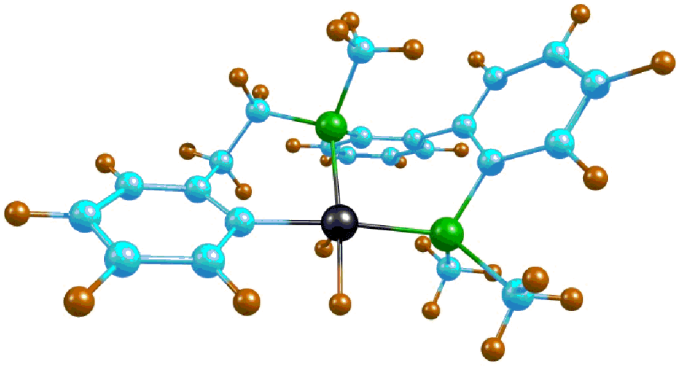

Figure 4.13 The optimized geometry of (PPC)IrH_2 complex; the colour scheme is the same as in Figure 4.3.

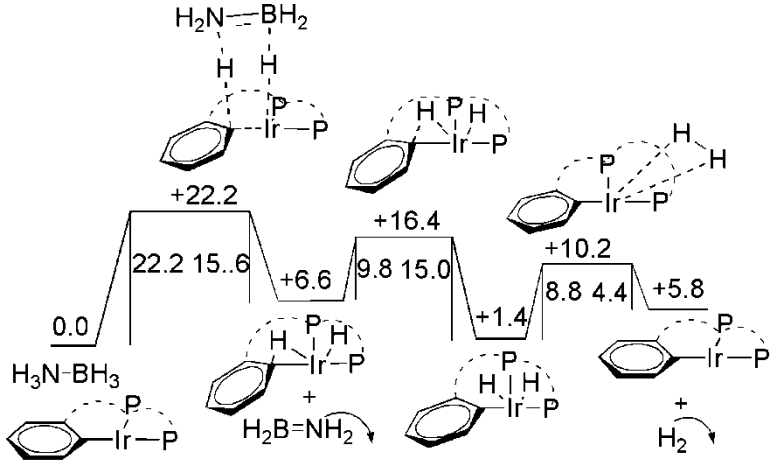

Figure 4.14 The free energy profile for the proposed M-C activation pathway for the dehydrogenation of ammonia borane by a (PPC)IrH_2 complex; all energies are in kcal/mol.

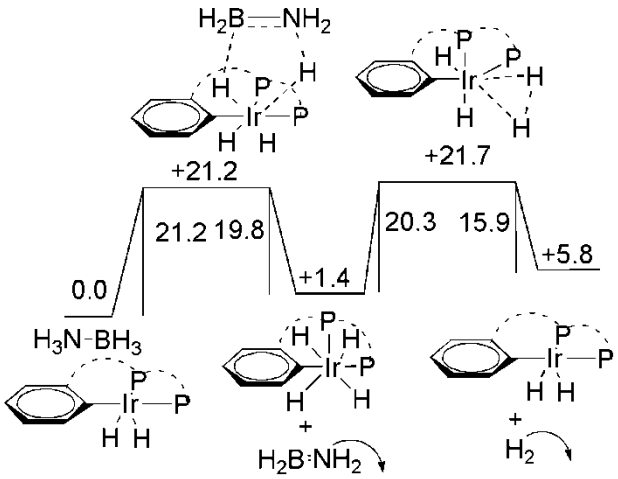

Figure 4.15 The free energy profile for the Paul-Musgrave pathway for the

dehydrogenation of ammonia borane by a (PPC)IrH_2 complex; all energies are in kcal/mol.

Since there already exist metal complexes having aromatic bidentate ligands, they can be considered candidates for the catalysis processes. The next section focuses on one such existing complex: the bidentate tantalum based carbene complex: Ta(=CH-*t*-Bu)[$C_6H_3(CH_2NMe_2)_2$-2,4](Cl)(O-*t*-Bu), and shows how this complex could potentially display metal-carbon cooperativity.

4.3.2 Ammonia Borane Dehydrogenation using a Bidentate Tantalum Catalyst

The Ta(=CH-*t*-Bu)[$C_6H_3(CH_2NMe_2)_2$-2,4](Cl)(O-*t*-Bu) (**Ta-bid**) complex, synthesized in 1997[39], is considered in this section for the catalysis of the AB dehydrogenation reaction. This is a carbene complex and it is likely that in the presence of a hydrogenating agent such as ammonia borane, the first reaction that would occur is the hydrogenation of the Ta-carbene double bond, rather than the activation of the metal-*ipso* carbon bond of the coordinated aromatic ring. Calculations done with a model system (shown in **Fig. 4.16**) bear out this view. However, as the hydrogenation of the Ta=C bond would lead to a stable product (the product is found to be 8.6 kcal/mol more stable than the reactants for the model system), the hydrogenated species is likely to be long-lasting in the reaction vessel and can therefore act as the catalyst for ammonia borane dehydrogenation. The optimized structure of the hydrogenated form of the real system: Ta(H)(CH_2-*t*-Bu)[$C_6H_3(CH_2NMe_2)_2$-2,4](Cl)(O-*t*-Bu), **Ta-bid-H_2**, is shown **Fig. 4.17**. As shown in **Fig. 4.18** below, calculations done with **Ta-bid-H_2** indicate that the barriers for the dehydrogenation process are comparable to the bidentate iridium catalyst case. These results thus indicate that complexes that have already been synthesized may become

active and efficient catalysts for this important dehydrogenation reaction.

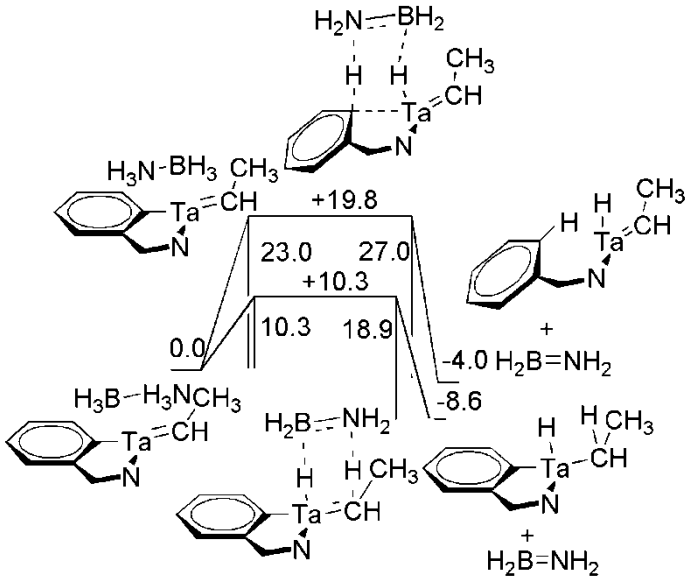

Figure 4.16 The comparison of the free energy profiles for hydrogenation by ammonia borane of the tantalum complex: Ta(=CH-Me)[$C_6H_3(CH_2NMe_2)$-2](Cl)(O-Me): the ammonia borane may hydrogenate the tantalum carbene bond or the tantalum–*ipso* carbon bond of the aromatic ligand; all values are in kcal/mol.

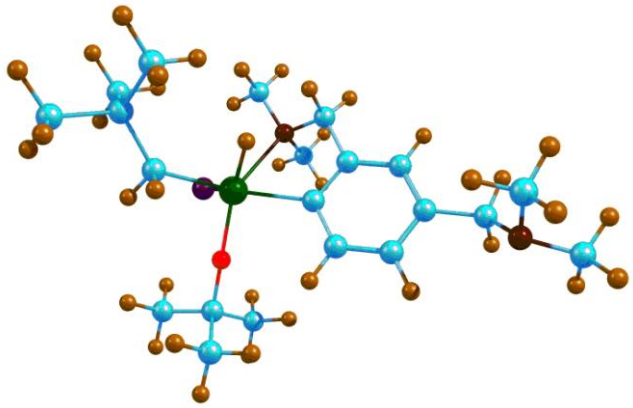

Figure 4.17 The optimized structure for the Ta(H)(CH_2-*t*-Bu)[$C_6H_3(CH_2NMe_2)_2$-2,4](Cl)(O-*t*-Bu) complex; the colour scheme is as follows: tantalum- green, carbon - blue, nitrogen – maroon, oxygen – red, chlorine - purple and hydrogen – brown.

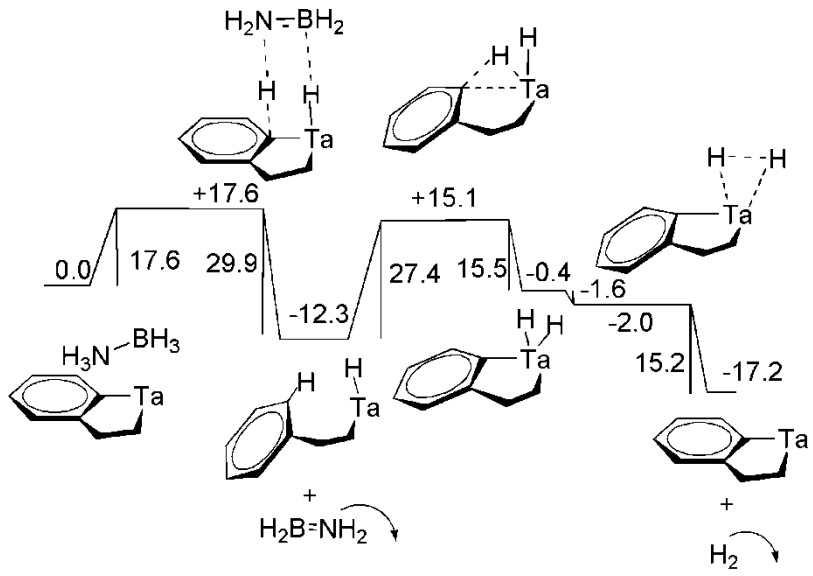

Figure 4.18 The free energy profile for the proposed M-C activation pathway for the dehydrogenation of ammonia borane by a tantalum complex; all energies are in kcal/mol.

4.3.3 Ammonia Borane Dehydrogenation using a Boron Complex

I have also considered the interesting possibility of *non-metal complexes with an aromatic bidentate linkage* also proving to be effective at catalysis processes through the proposed cooperativity pathway. The complex that has been considered for this is the boron containing molecule: B(Et)[$C_6H_4(CH_2CH_2)$] (**B-cat**). It is to be noted that the analogous complex, B(Pr)[$C_6H_4(CH_2CH_2)$][40], has already been synthesized, and therefore the synthesis of B(Et)[$C_6H_4(CH_2CH_2)$] should be feasible.

There are several excellent reasons for investigating boron containing complexes:

(a) like metal centres, boron is also known to be acidic, and so would be susceptible to attack from a complex of the type HABH, shown earlier in **Fig. 4.2**.

(b) The second step, which involves the elimination of hydrogen, H_2, from the complex to complete the cycle, requires the increase in coordination number at the acidic centre. Like transition metals, boron, too, has displayed the ability to increase its coordination number by two units[41, 42].

(c) A further motivation is the need to develop non-metal based catalyst systems for important reactions such as ammonia borane dehydrogenation. Non-metal catalyst systems are likely to be less toxic, and therefore more environmentally friendly, as well as cheaper, than their metal analogues[43]. A phosphorus based analogue of pincer ligated transition metal complexes has recently been prepared,[44] for instance, and is considered a promising harbinger for furture work in preparing non-metal analogues to transition metal complexes.[45]

Keeping these factors in mind, the complex **B-cat** (shown in **Fig. 4.19)** was considered for the AB dehydrogenation process. As **Fig. 4.20** shows below, the catalysis cycle contains two barriers of 35.9 kcal/mol and 30.9 kcal/mol respectively. A further advantage of investigating the non-metal boron complex is that the relative smallness of its size, in comparison to the larger, metal containing complexes, allows for further computational investigations which would be prohibitively expensive computationally for the metal based systems. Hence, for the boron complex, the effect of modification of the catalyst by the addition of functional groups has also been considered. Electron donating OCH_3 group were added at the *ortho* and *para* positions of the complex and this was found to lead to a reduction of the barriers by 6.7 kcal/mol (see **Fig. 4.20** below). These calculations also suggest that the efficiency of the catalysts can be further improved by suitable addition of functional groups, not only for the case of the boron complex considered here, but, by extension, also for the previous metal based complexes.

It is true that the barrier heights discussed here for the boron systems are still higher than those obtained in the iridium and tantalum cases considered earlier. However, it is to be noted that current effective main-group catalyst systems have been found to function well only at higher temperatures (80 °C for the phosphorus

based system mentioned above[46]) and have been seen to have high barriers, ranging from 29.1 kcal/mol to 44.3 kcal/mol[47-49] during the catalysis process. Hence the obtained values for the boron systems investigated here can be considered respectable, especially for the OCH_3 substituted case.

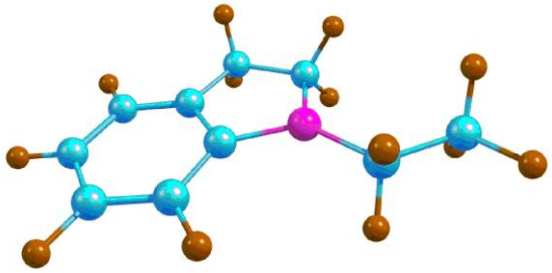

Figure 4.19 The optimized structure for the B(Et)[$C_6H_3(CH_2CH_2)$] complex; the colour scheme is as follows: boron- pink, carbon - blue and hydrogen – brown.

System	a (kcal/mol)	c (kcal/mol)	b (kcal/mol)	d (kcal/mol)
R = H R1 = H	35.9	35.7	30.9	35.9
R = H R1 = OMe	32.7	31.9	30.2	37.1
R = OMe R1 = OMe	29.2	27.1	29.2	37.1

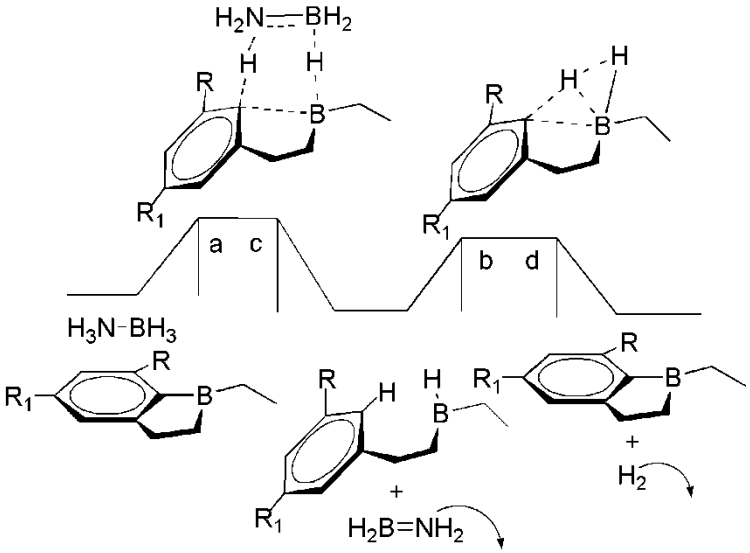

Figure 4.20 The free energy profile for the proposed M-C activation pathway for the dehydrogenation of ammonia borane by boron complexes; all energies are in kcal/mol.

4.3.4 Other Reactions with the Bidentate (POC)IrH_2 Complex: Dehydrogenation of Formic Acid and N-H Activation

The previous section discussed the potential of bidentate complexes in catalyzing the dehydrogenation of ammonia borane: an important reaction because of its relevance in the chemical storage of hydrogen[36]. It is also likely that the lability of the metal-carbon bond in bidentate complexes can be exploited for other important reactions as well. In this section, two such possibilities will be discussed: the catalysis of the dehydrogenation of formic acid (HCOOH), and the activation of the N-H bond in aromatic amines. The bidentate complex considered for these cases is the (POC)IrH_2 complex.

The dehydrogenation of formic acid has assumed importance recently because of the recognition of its potential for the chemical storage of hydrogen[49], with HCOOH having an additional advantage in that its regeneration after dehydrogenation would be a very facile process[49]. A complex that can catalyze the ready removal of hydrogens from HCOOH to yield CO_2 can thus be of great importance. Here, I discuss the possibility of the (POC)IrH_2 complex acting as a homogeneous catalyst to dehydrogenate HCOOH. Shown in **Fig. 4.21** below is the potential energy surface for the dehydrogenation process. The three barriers corresponding to – (a) the removal of the hydridic and the protic hydrogens from the carbon and oxygen atoms of HCOOH respectively, (b) the transfer of hydrogen from the *ipso* carbon of the aromatic ring to iridium and (c) the subsequent removal of the hydrogens from the catalyst, are 12.1 kcal/mol and 13.1 kcal/mol and 6.6 kcal/mol. These values are significantly lower than those obtained for systems employing the most efficient catalysts for ammonia borane dehydrogenation[9, 16, 50], which suggests that bidentate ligand containing catalysts which can exploit metal-carbon cooperativity have great potential to be

excellent catalysts for dehydrogenating HCOOH.

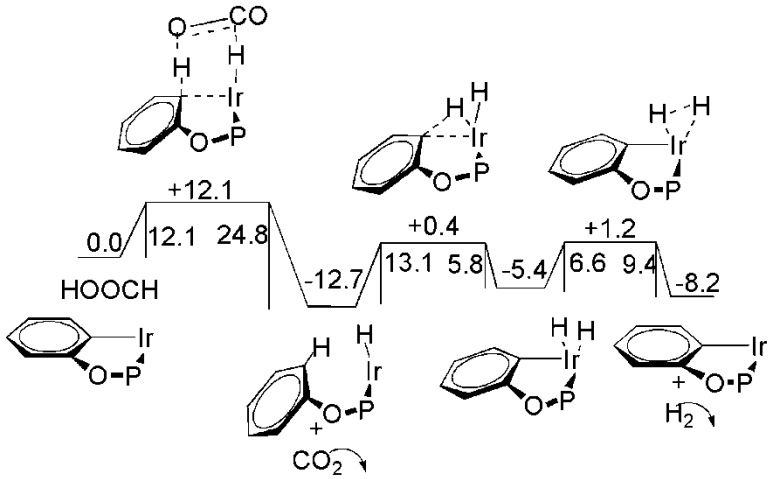

Figure 4.21 The free energy profile for the proposed M-C activation pathway for the dehydrogenation of formic acid by the (POC)IrH_2 complex; all energies are in kcal/mol.

The N-H activation of amines by metal complexes is a process that has not been widely studied, despite its potential importance in explaining a range of important metal catalyzed transformations.[51-61] Recently, Milstein's group have reported the N-H activation of aromatic amines such as $C_6H_3Cl_2NH_2$, using the concept of metal-ligand cooperativity involving pincer ligand complexes and aromatization-dearomatization.[62, 63] In order to test the efficacy of the metal-*ipso* carbon cooperativity for N-H bond activation, calculations were done with the (POC)IrH_2 catalyst and the N-H activation in $C_6H_3Cl_2NH_2$ was studied. As shown in **Fig. 4.22** below, the barrier for the N-H activation was found to be 23.4 kcal/mol, which indicates that such a process would be feasible at ambient temperature.

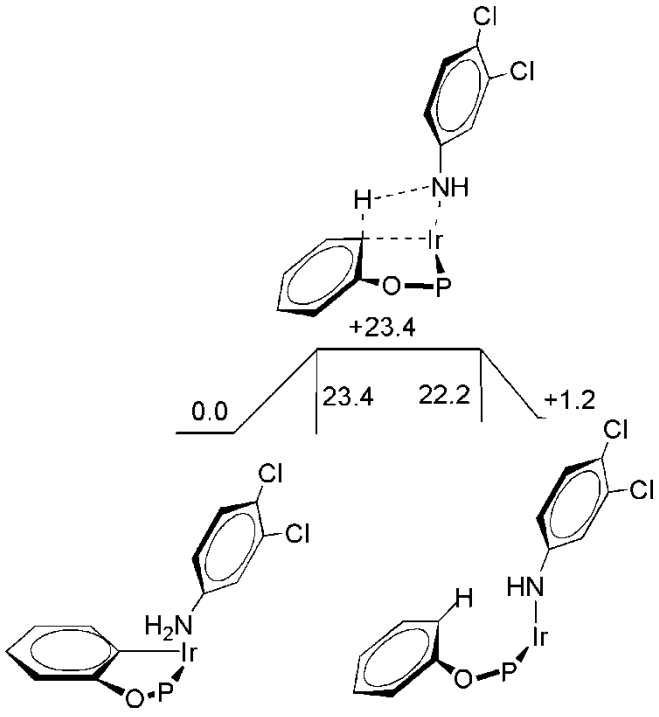

Figure 4.22 The free energy profile for the proposed M-C pathway for the activation of the N-H bond in $C_6H_3Cl_2$**.**

4.4 Conclusions

The current work, employing full quantum mechanical (QM) density functional theory (DFT) methods, demonstrates the potential of aromatic bidentate metal and non-metal complexes, as well as of tridentate pincer complexes having the aromatic linkage at a terminal end, to act as catalysts for important chemical reactions. It has been shown that such systems may even be more effective than the currently employed tridentate pincer ligand complexes, due to the possibility, absent in the currently employed pincer complexes, of exploiting metal-carbon cooperativity. What has also been shown is that metal-carbon cooperativity can be exploited in a range of different complexes, both metal and, significantly, non-metal, for catalyzing a variety of reactions, including ammonia borane dehydrogenation, formic acid dehydrogenation and N-H activation. Therefore, metal (or non-metal)-*ipso* C(sp^2) cooperativity, which has been discussed for the first time in this work, represents an

important new avenue for achieving important chemical transformations.

4.5 References

[1] M. Albrecht, G. van Koten *Angewandte Chemie International Edition*. **2001**, 40, 3750-3781.
[2] M. E. van der Boom, D. Milstein *Chemical Reviews*. **2003**, 103, 1759-1792.
[3] E. Poverenov, I. Efremenko, A. I. Frenkel, Y. Ben-David, L. J. W. Shimon, G. Leitus, L. Konstantinovski, J. M. L. Martin, D. Milstein *Nature*. **2008**, 455, 1093-1096.
[4] S. W. Kohl, L. Weiner, L. Schwartsburd, L. Konstantinovski, L. J. W. Shimon, Y. Ben-David, M. A. Iron, D. Milstein *Science (Washington, DC, United States)*. **2009**, 324, 74-77.
[5] R. Ahuja, B. Punji, M. Findlater, C. Supplee, W. Schinski, M. Brookhart, A. S. Goldman *Nat Chem*. **2011**, 3, 167-171.
[6] C. Gunanathan, D. Milstein *Accounts of Chemical Research*. **2011**, 44, 588-602.
[7] E. Balaraman, C. Gunanathan, J. Zhang, L. J. W. Shimon, D. Milstein *Nature Chemistry*. **2011**, 3, 609-614.
[8] W. Weng, C. Guo, C. Moura, L. Yang, B. M. Foxman, O. V. Ozerov *Organometallics*. **2005**, 24, 3487-3499.
[9] M. Käß, A. Friedrich, M. Drees, S. Schneider *Angewandte Chemie International Edition*. **2009**, 48, 905-907.
[10] S. Musa, R. Romm, C. Azerraf, S. Kozuch, D. Gelman *Dalton Transactions*. **2011**, 40, 8760-8763.
[11] A. Vigalok, O. Uzan, L. J. W. Shimon, Y. Ben-David, J. M. L. Martin, D. Milstein *J Am Chem Soc*. **1998**, 120, 12539-12544.
[12] M. Montag, L. Schwartsburd, R. Cohen, G. Leitus, Y. Ben-David, J. M. L. Martin, D. Milstein *Angewandte Chemie, International Edition*. **2007**, 46, 1901-1904.
[13] J. C. Lewis, J. Wu, R. G. Bergman, J. A. Ellman *Organometallics*. **2005**, 24, 5737-5746.
[14] D. G. Gusev, M. Madott, F. M. Dolgushin, K. A. Lyssenko, M. Y. Antipin *Organometallics*. **2000**, 19, 1734-1739.
[15] A. A. Koridze, A. V. Polezhaev, S. V. Safronov, A. M. Sheloumov, F. M. Dolgushin, M. G. Ezernitskaya, B. V. Lokshin, P. V. Petrovskii, A. S. Peregudov *Organometallics*, 29, 4360-4368.
[16] M. C. Denney, V. Pons, T. J. Hebden, D. M. Heinekey, K. I. Goldberg *J. Am. Chem. Soc.* **2006**, 128, 12048-12049.
[17] R. Ahlrichs, M. Baer, M. Haeser, H. Horn, C. Koelmel *Chem. Phys. Lett.* **1989**, 162, 165-169.
[18] A. D. Becke *Phys. Rev. A Gen. Phys.* **1988**, 38, 3098-3100.
[19] J. P. Perdew *Physical Review B*. **1986**, 33, 8822-8824.
[20] F. Weigend *Physical Chemistry Chemical Physics*. **2002**, 4, 4285-4291.
[21] K. Eichkorn, O. Treutler, H. Oehm, M. Haeser, R. Ahlrichs *Chem. Phys. Lett.* **1995**, 240, 283-290.
[22] M. Sierka, A. Hogekamp, R. Ahlrichs *J. Chem. Phys.* **2003**, 118, 9136-9148.
[23] J. P. Perdew, K. Burke, M. Ernzerhof *Physical Review Letters*. **1996**, 77, 3865-3868.
[24] K. Fukui *Accounts of Chemical Research*. **1981**, 14, 363-368.
[25] A. D. Becke *The Journal of Chemical Physics*. **1993**, 98, 5648-5652.
[26] C. Lee, W. Yang, R. G. Parr *Physical Review B*. **1988**, 37, 785-789.

[27] A. Klamt *The Journal of Physical Chemistry*. **1995**, 99, 2224-2235.
[28] M. Mammen, E. I. Shakhnovich, G. M. Whitesides *Journal of Organic Chemistry*. **1998**, 63, 3168-3175.
[29] E. Kelly, M. Seth, T. Ziegler *The Journal of Physical Chemistry A*. **2004**, 108, 2167-2180.
[30] H. Yin, D. Wang, M. Valiev *The Journal of Physical Chemistry A*. **2011**, 115, 12047-12052.
[31] V. M. Williams, J. R. Kong, B. J. Ko, Y. Mantri, J. S. Brodbelt, M.-H. Baik, M. J. Krische *J Am Chem Soc*. **2009**, 131, 16054-16062.
[32] W. Janse van Rensburg, C. Grové, J. P. Steynberg, K. B. Stark, J. J. Huyser, P. J. Steynberg *Organometallics*. **2004**, 23, 1207-1222.
[33] Y. Qi, Q. Dong, L. Zhong, Z. Liu, P. Qiu, R. Cheng, X. He, J. Vanderbilt, B. Liu *Organometallics*. **2010**, 29, 1588-1602.
[34] A. Bagno, W. Kantlehner, R. Kress, G. Saielli, E. Stoyanov *The Journal of Organic Chemistry*. **2006**, 71, 9331-9340.
[35] J.-N. Li, M. Pu, C.-C. Ma, Y. Tian, J. He, D. G. Evans *Journal of Molecular Catalysis A: Chemical*. **2012**, 359, 14-20.
[36] T. B. Marder *Angewandte Chemie, International Edition*. **2007**, 46, 8116-8118.
[37] A. Paul, C. B. Musgrave *Angewandte Chemie*. **2007**, 119, 8301-8304.
[38] N. Liu, X. Li, H. Sun *Journal of Organometallic Chemistry*. **2011**, 696, 2537-2542.
[39] M. H. P. Rietveld, E. G. Klumpers, J. T. B. H. Jastrzebski, D. M. Grove, N. Veldman, A. L. Spek, G. van Koten *Organometallics*. **1997**, 16, 4260-4267.
[40] B. Wrackmeyer, H. Vollrath in Ring Enlargrment by 1,1-Organoboration. Routes to Novel Dienes, Trienes, and allenes, Vol. 21 (Ed.^Eds.: Editor), City, **1998**, pp.515-526.
[41] R. Custelcean *Journal of Molecular Structure: THEOCHEM*. **2000**, 505, 95-101.
[42] J. F. Stanton, W. N. Lipscomb, R. J. Bartlett *J Am Chem Soc*. **1989**, 111, 5173-5180.
[43] T. Hügle, M. Hartl, D. Lentz *Chemistry – A European Journal*. **2011**, 17, 10184-10207.
[44] N. L. Dunn, M. Ha, A. T. Radosevich *J Am Chem Soc*. **2012**, 134, 11330-11333.
[45] E. E. Coyle, C. J. O'Brien *Nat Chem*. **2012**, 4, 779-780.
[46] A. Berkessel, J. A. Adrio *J Am Chem Soc*. **2006**, 128, 13412-13420.
[47] K. Etzenbach-Effers, A. Berkessel in *Noncovalent Organocatalysis Based on Hydrogen Bonding: Elucidation of Reaction Paths by Computational Methods, Vol. 291* (Ed. B. List), Springer Berlin Heidelberg, **2009**, pp.38-69.
[48] D. Cantillo, B. Gutmann, C. O. Kappe *J Am Chem Soc*. **2011**, 133, 4465-4475.
[49] J. F. Hull, Y. Himeda, W.-H. Wang, B. Hashiguchi, R. Periana, D. J. Szalda, J. T. Muckerman, E. Fujita *Nat Chem*. **2012**, 4, 383-388.
[50] N. Blaquiere, S. Diallo-Garcia, S. I. Gorelsky, D. A. Black, K. Fagnou *J. Am. Chem. Soc.* **2008**, 130, 14034-14035.
[51] J. L. Klinkenberg, J. F. Hartwig *Angewandte Chemie, International Edition*. **2011**, 50, 86-95.
[52] J. I. van der Vlugt *Chemical Society Reviews*. **2010**, 39, 2302-2322.
[53] S. Enthaler *ChemSusChem*. **2010**, 3, 1024-1029.
[54] J. F. Hartwig *Pure and Applied Chemistry*. **2004**, 76, 507-516.
[55] R. A. Grey, G. P. Pez, A. Wallo *J Am Chem Soc*. **1981**, 103, 7536-7542.
[56] T. Suarez, B. Fontal *Journal of Molecular Catalysis*. **1988**, 45, 335-344.
[57] D. K. Mukherjee, B. K. Palit, C. R. Saha *Journal of Molecular Catalysis*. **1994**,

88, 57-70.
[58] R. I. Storer, D. E. Carrera, Y. Ni, D. W. C. MacMillan *J. Am. Chem. Soc.* **2006**, 128, 84-86.
[59] T. C. Nugent, M. El-Shazly *Advanced Synthesis & Catalysis*. **2010**, 352, 753-819.
[60] S. Gomez, J. A. Peters, T. Maschmeyer *Advanced Synthesis & Catalysis*. **2002**, 344, 1037-1057.
[61] S. Kobayashi, H. Ishitani *Chemical Reviews (Washington, D. C.)*. **1999**, 99, 1069-1094.
[62] M. Feller, Y. Diskin-Posner, L. J. W. Shimon, E. Ben-Ari, D. Milstein *Organometallics*. **2012**, 31, 4083-4101.
[63] E. Khaskin, M. A. Iron, L. J. W. Shimon, J. Zhang, D. Milstein *J. Am. Chem. Soc.* **2010**, 132, 8542-8543.

Chapter 5: Efficiency of Pure and Ru-doped Rh_6 Clusters towards Methanol Activation

Abstract

Catalysis of molecular activation of small molecules through scission of strong chemical bonds is one of the major challenges faced by chemists. More specifically, activation of the strong C–H and O–H bonds of various alcohols, especially methanol, is one of the various important intermediate steps of key organic reactions. My present work explores a suitable metal cluster catalyst towards methanol dissociation. In particular I have examined the effect of ruthenium doping (Rh:Ru=2:1) on the catalytic activity of Rh_6 cluster towards methanol dissociation. Density functional theory based calculations illustrate two competitive pathways for methanol dissociation, which are via O–H and C–H bond breaking. Both the pathways are found to be energetically favourable in presence of bimetallic and mono-metallic clusters. Importantly, energy barrier for O–H bond dissociation reduces considerably in doped cluster as compared to pure Rh_6 cluster and is smaller than the values reported for a number of other small metallic clusters.

5.1 Introduction

Methyl alcohol, commonly known as methanol, is the simplest alcohol and one of the most versatile compound having multi-fold applications in areas such as, (a) organic synthesis,[1-3] (b) transportation fuel,[4] (c) waste water denitrification,[5-10] d) production of pure hydrogen, also known as steam reforming,[11-14] and most importantly e) in fuel cells.[15] Methanol is a liquid between -97.0 ºC to 64.7 ºC at atmospheric pressure and hence is an ideal fuel for transportation in large parts. Since it is produced from natural gases, it is cost effective and non renewable in nature. Methanol (MeOH) has higher hydrogen content as compared to H_2 stored in cylinders or hydrides leading to lower system weight and volume. A necessary step in almost all applications regarding methanol requires the activation of its O–H and C–H bonds.

Activation of strong organic bonds is one of the major challenges in chemistry due to its indispensability towards developing more and more cost-effective paths in industrial production of chemicals.[1-3, 16, 17] Among them, controlled scission of strong O-H and C-H bonds of aliphatic alcohol, especially methanol, is one of the important steps.[18-21] This is a fairly difficult process given the high energy required[22] to dissociate the C–H (~96.1 kcal/mol) and O–H (~104.6 kcal/mol) bonds. In this respect, few of the earlier works [23-27] have attempted to evaluate activation barrier for the first step of the methanol dissociation from different pathways.

In this context, many theoretical studies have focussed in identifying metal oxide and metal surfaces with moderate to low barrier towards either O–H or C–H activation. TiO_2 is the most well studied metal oxide for methanol activation. In a recent theoretical work by Sanchez et al.,[28] the dissociation of O–H on TiO_2(101) (anatase) surface is investigated, and the activation barrier for O–H bond scission is reported to be as low as 13.6 kcal/mol. Methanol decomposition on noble metal surfaces has gained importance from the point of view of heterogeneous catalysis. In spite of many successes in this field, the exact effect of surface defects and structural dependence on catalysis has not been fully understood yet. A work based on methanol activation on Pt(111) surface reports [29] substantially high barriers for both the O–H (~22 kcal/mol) and C–H (~34 kcal/mol) bond scissions, whereas slightly lower barriers of 12.7 kcal/mol (C–H scission) and 24.7 kcal/mol (O–H scission) are reported for Pd(111) surface.[30] In a very recent work,[31] stepped Pd(211) surface is shown to lower the O–H activation barrier (18.9 kcal/mol) but C–H activation barrier (14.7 kcal/mol) is seen to be slightly higher than in case of Pd(111) surface.[30] Cu surfaces are also one of the well studied metal surfaces in activating methanol. The barriers for O-H dissociation on a Cu(100) surface[32] is 14.5 kcal/mol while elevated

barrier(24.6 kcal/mol) were reported on a Cu(111) surface[30]. Recently, Wang et al.[33] reported competitive barriers for C–H (12 kcal/mol) and O–H (12.4 kcal/mol) activation on Ir(111) surface with slightly endothermic reaction energies.

Small metal clusters form another class of materials being actively explored as candidates towards methanol activation. Methanol activation studies[34, 35] on Cu_4, Co_4 and Pd_4 atomic clusters reveal that Co_4 cluster is catalytically more active having lower energy barrier towards both O–H scission (10.8 kcal/mol) and C–H scission (14.3 kcal/mol). In another work by Xie et al.,[36] combined theoretical and experimental investigation reveals O–H activation to be more favorable over C–H activation on neutral iron clusters. Al_n clusters[37] are seen to have size selective reactivity towards methanol molecule and its O–H bond dissociation. V_3^+ cluster[38] is reported to possess a moderate barrier of 13.9 kcal/mol towards O–H activation. In addition, several other metal clusters such as: Au_n,[39, 40] Ni_n^+,[41] Pt-Au,[42] and $Cu_nAu_m^+$ [43] have been explored for their potential towards methanol activation.

Rhodium clusters have been a subject of numerical experimental and theoretical studies due to their catalytic properties. Rh clusters are now well established catalysts for applications such as, a) controlling automobile exhaust emissions (CO, NO, NO_2 etc.),[44-46] b) reforming fuels such as biogas and diesel,[45, 47] c) oxidation reduction reactions,[48] d) reverse hydrogen spill over reaction,[49, 50] e) hydrogenation of alkenes,[51] f) conversion of syngas[52] etc. High activity and thermal stability make Rh based nanoclusters very attractive particularly in fuel cell electro-catalysts[48, 53] and hence, attempts are being made to synthesize extremely small Rh clusters.[54] Among various rhodium clusters, Rh_6 is an efficient cluster due to its high catalytic activity in several reactions.[50-52, 55, 56] Earlier theoretical studies suggest an octahedral ground state geometry for the same.[53, 57-60] Doping these Rh clusters further improves and

enhances the catalytic activity and also reduces the disadvantages that are present in homogeneous Rh catalysts.[61]

Rh-Pt binary clusters are the most popular catalysts towards alcohol oxidation in Direct Alcohol Fuel Cells (DAFC).[62-67] While Rh is known to inhibit the CO poisoning,[63, 66, 68-70] Ru is well known to increase the rate of methanol oxidation reactions when doped with platinum.[71-74] Hence, I explored the unique combination of Rh–Ru binary clusters to have best of both sides. In this present chapter, I have studied the properties of an octahedral Rh_6 cluster towards methanol activation. In order to explore the potential of Ru doping towards methanol activation, I have replaced two of the trans rhodium atoms by ruthenium atoms leading to a Rh_4Ru_2 (Rh:Ru = 2:1) cluster. It is of relevance here to note that bimetallic clusters having 2:1 ratio can be commonly synthesized experimentally [53, 75-78] and hence I have used this ratio in my present study. The principal objective of the study is to understand the detailed interaction of methanol molecule with these clusters and their effectiveness towards activation of C–H and O–H bonds in methanol molecule.

5.2 Computational Details

I have considered the lowest spin state for all the clusters in my study. Around ten Rh_6 conformations are considered in the lowest spin state to begin with. Optimization of these conformations revealed the octahedral geometry to be the most stable one among all the conformations. Some of the earlier reported studies also considered Rh_6 cluster in its lowest spin state.[53, 57-60, 79, 80] All the calculations in this work are performed using Density Functional Theory (DFT) as implemented in Gaussian 09 package.[81] The geometries are optimized using PBE-PBE functional with LANL2DZ basis set along with LANL2 effective core potential (pseudo potential) for the core electrons of metal atoms. TZVP basis set is used for the rest of

the atoms. PBE-PBE is widely used for transition and as well as other metal clusters and complexes.[82-89] Following geometry optimization, harmonic frequencies are calculated for all the optimized conformations. All the frequencies are found to be positive, indicating the conformations to be local minimum. The transition state conformations have one imaginary frequency (with high magnitude), signifying the first order saddle point. The transition state barriers are calculated from the corresponding free energies. As implemented in Gaussian 09 package,[90, 91] the absolute value of total free energy (G_{tot}) considered for each structure is calculated using the Gibbs free energy function in terms of enthalpy (H_{tot}) and entropy (S_{tot}) :

$$G_{tot} = H_{tot} - TS_{tot} = E_{tot} + PV - TS_{tot} \tag{5.1}$$

where E_{tot} is represented by its individual components like electronic, translational, rotational, vibrational and contribution from zero point energy correction. Hence,

$$G_{tot} = E_{elec} + E_{trans} + E_{rot} + E_{vib} + E_{ZPE} + PV - TS_{tot} = E_{elec} + G_{therm} \tag{5.2}$$

where G_{therm} is the thermal free energy.

Contribution of each component to total internal energy (E_{tot}) is calculated using the derived partition function for that particular component using the following formula:

$$E = Nk_bT^2\left(\frac{\partial \ln Z}{\partial T}\right)_V \tag{5.3}$$

where Z is the partition function of the corresponding component and k_b is the Boltzmann constant. For 1 mol of gas, N is replaced by Avogadro's number (N_A) and hence the equation reduces to

$$E = RT^2\left(\frac{\partial \ln Z}{\partial T}\right)_V \tag{5.4}$$

Similarly the total entropy S_{tot} can be written in terms of its component by the

following formula:

$$S_{tot} = S_{trans} + S_{rot} + S_{vib} + S_{elec} \tag{5.5}$$

The entropic contribution per mol for each component is derived from the following equation:

$$S = RT\left(\frac{\partial \ln Z}{\partial T}\right)_V + R\ln Z \tag{5.6}$$

Zero point energy (*ZPE*) correction for each vibrational mode is also incorporated within my calculations. Total *ZPE* correction including *3N-6* modes of vibration (*3N-5* for linear molecule) is represented as follows:

$$E_{ZPE} = \sum_{i=1}^{3N-6} \tfrac{1}{2} h\upsilon_i \tag{5.7}$$

where ν_i is the frequency of the corresponding mode of vibration. Binding Energy (BE) of the clusters is calculated using:

$$\frac{BE}{atom} = \frac{E_{cluster} - \sum_{i=1}^{N} E_i}{N} \tag{5.8}$$

where, N is the number of metal atoms in the cluster, E_i is the free energy of an atom and $E_{cluster}$ is the free energy of the total cluster. Charge analysis of the systems is based on the Mulliken partitioning scheme.

Following the structural and electronic property analysis of Rh_6 and Rh_4Ru_2 clusters, their thermal stability is examined by carrying out Born Oppenheimer Molecular Dynamics (BOMD) simulations using the deMon2K package.[92] The finite temperature simulations are carried out on Rh_6 and Rh_4Ru_2 clusters from 300 K to 700 K with a temperature interval of 100 K. Thermal stability and finite temperature behaviour of the methanol adsorbed Rh_6 and Rh_4Ru_2 clusters is verified by performing a simulation at 300 K on the complexes. For each simulation, the cluster is equilibrated for a time period of 10 ps followed by a simulation time of 40 ps. The

temperature of the cluster is maintained using Berendsen's thermostat (τ = 0.5 ps) in an NVT ensemble. The nuclear positions are updated using the velocity verlet algorithm with a time step of 1 fs. I hold the total angular momentum of the cluster to zero thereby suppressing the cluster rotation.

5.3 Results and Discussion

I begin with a discussion on the geometry of optimized structure of Rh_6 cluster as shown in **Fig. 5.1**. The structure has Rh–Rh bond distances of 2.55 Å for the adjacent atoms. The calculated binding energy/atom of this Rh_6 cluster is -2.76 eV/atom. The bond distances and binding energy of this cluster are in agreement with previously reported values for Rh_6 cluster using different functional.[56-58, 84, 93-95] In order to have a Rh–Ru bimetallic cluster in 2:1 ratio having a heterogeneous environment, two diagonally opposite Rh atoms in octahedral Rh_6 are replaced by Ru atoms as shown in **Fig. 5.1**. This type of heterogeneous environment has already been shown to be important for effective activation and dissociation of C–H and O–H bonds in methanol.[42, 43, 96, 97] The fully optimized geometry of Rh_4Ru_2 cluster (see **Fig. 5.1**) is found to retain the octahedral conformation with a little distortion in the inter-atomic bond lengths with respect to its parent Rh_6 cluster. The Rh–Rh bond distances increase to 2.58 Å and bonded Rh–Ru bond distances are found to lie between 2.52 to 2.53 Å. My calculated binding energy/atom for bimetallic cluster is -2.90 eV/atom, which is significantly greater as compared to its mono-metallic counterpart. A comparative Mulliken charge analysis reveals that all the atoms in Rh_6 are neutral. On doping, Rh atoms in Rh_4Ru_2 gain approximately 0.03 electrons each from Ru atoms (see **Table 5.1**). This small amount of charge separation in Rh_4Ru_2 is suggestive of its higher potential towards methanol activation as compared to Rh_6. Most of the monometallic or bimetallic clusters, in spite of their excellent catalytic

properties, do not have practical applications due to their thermodynamic instability. Hence, before analyzing the catalytic property of bimetallic clusters, I have studied the thermodynamic behaviour of both the clusters by performing finite temperature BOMD simulations from 200 K to 700 K with an interval of 100 K. The simulations revealed that both the clusters retain their octahedral conformations up to at least 700 K.

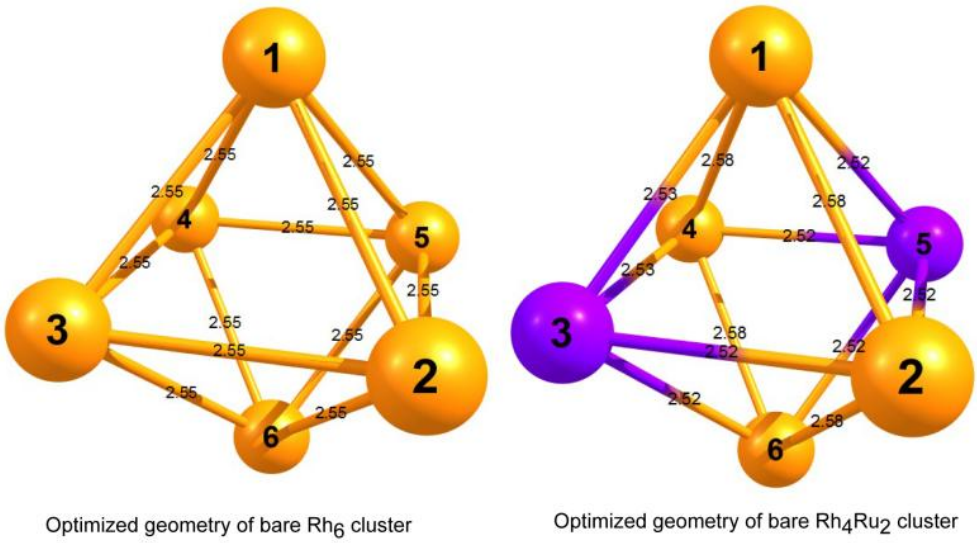

Figure 5.1 Structural parameters in Rh_6, Rh_4Ru_2 clusters (golden coloured atom: Rh; purple coloured atom: Ru); all bond distances are given in Å.

Table 5.1 Charge analysis data for the Rh4Ru2 cluster.

Rh_4Ru_2 (e)		
1	**Rh**	**~ - 0.03**
2	**Rh**	**~ -0.03**
3	**Ru**	**~ 0.07**
4	**Rh**	**~ -0.03**
5	**Ru**	**~ 0.07**
6	**Rh**	**~ -0.03**

5.3.1 Structural and Electronic Properties of Methanol Adsorbed Rh_6 and Rh_4Ru_2 Clusters

All sites are chemically equivalent in the Rh_6 cluster. On the other hand, it is

difficult to predict the center (either Rh or Ru) that is more favourable for adsorption of methanol molecule in Rh_4Ru_2 cluster. Though the charge analysis of Rh_4Ru_2 indicates that Ru center is a more favourable site (as it has small amount of positive charge) for methanol adsorption through oxygen atom, the following two orientations have been optimized, viz., a) orientation-I where methanol is adsorbed on the Ru center through the oxygen atom and b) orientation-II where methanol is adsorbed on the Rh center through the oxygen atom. Orientation-I is found to be energetically more stable by 5.7 kcal/mol with respect to the orientation-II (see **Fig. 5.2**). Differences in thermodynamic stabilities can be attributed to the greater charge separation between Ru and O atoms in orientation-I, leading to greater electrostatic interactions as compared to those in orientation-II (see **Table 5.2**).

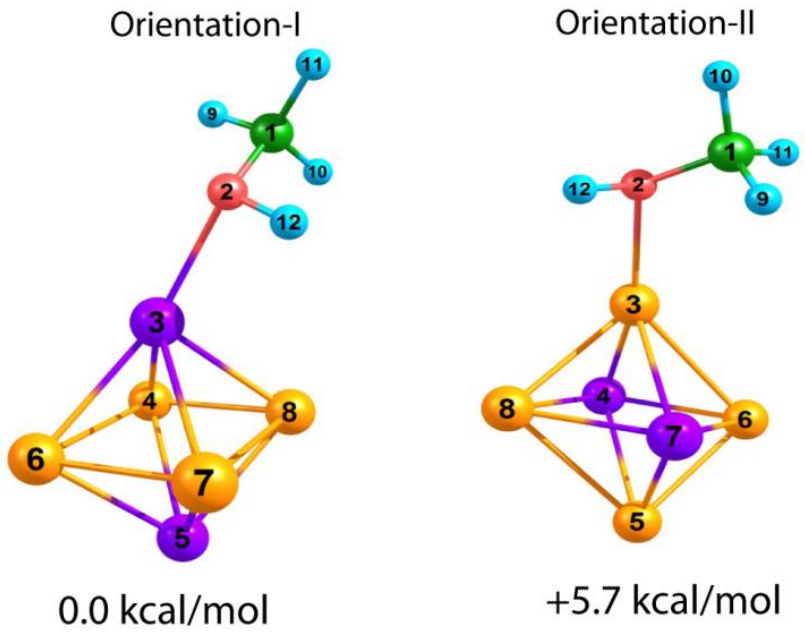

Figure 5.2 Relative energies of Rh_4Ru_2–$(MeOH)_{orient\text{-}I}$ and Rh_4Ru_2–$(MeOH)_{orient\text{-}II}$ complexes.

Table 5.2 Charge analysis data for the methanol adsorbed clusters.

Rh_6-MeOH (e)			**Rh_4Ru_2-MeOH Orient-I (e)**			**Rh_4Ru_2-MeOH Orient-II (e)**		
1	**C**	**0.219**	**1**	**C**	**0.228**	**1**	**C**	**0.218**
2	**O**	**-0.081**	**2**	**O**	**-0.088**	**2**	**O**	**-0.088**
3	**Rh**	**-0.010**	**3**	**Ru**	**0.143**	**3**	**Rh**	**-0.032**
4	**Rh**	**-0.032**	**4**	**Rh**	**-0.094**	**4**	**Ru**	**0.037**
5	**Rh**	**-0.023**	**5**	**Ru**	**0.080**	**5**	**Rh**	**-0.041**
6	**Rh**	**-0.020**	**6**	**Rh**	**-0.066**	**6**	**Rh**	**-0.035**
7	**Rh**	**-0.003**	**7**	**Rh**	**-0.111**	**7**	**Ru**	**0.014**
8	**Rh**	**-0.049**	**8**	**Rh**	**-0.091**	**8**	**Rh**	**-0.073**

Upon adsorption of methanol (MeOH) on Rh_6 and Rh_4Ru_2 clusters (orientation-I as well as orientation-II) (**Fig. 5. 3**), C–O bond length elongates by 0.2 Å (the C–O bond length is 1.43 Å in free methanol molecule). The C–H and O–H bond lengths in the adsorbed methanol are found to be similar as in free methanol. However, differences in bond lengths are observed for the M–O (M = Rh/Ru) bonds (Ru–$O_{orient\text{-}I}$ bond length= 2.27 Å; Rh–$O_{orient\text{-}II}$ bond length=2.29 Å; Rh–O bond length = 2.33 Å). Thus, Metal-Oxygen bond distance is slightly elongated in monometallic cluster as compared to the bimetallic Rh_4Ru_2 clusters. Interestingly, significant elongation in two of the Rh–Rh bond lengths (2.96 Å) is observed in case of the Rh_4Ru_2-$MeOH_{orient\text{-}II}$, leading to a slightly distorted octahedral structure (see **Fig. 5. 3 c**).

It is pertinent to take a close look at the thermodynamics of these methanol–adsorbed complexes and hence free energy of formation ($G_{formation}$) is calculated. Corresponding thermodynamic stability is evaluated by the following method:

$$G_{formation} = G_{complex} - (G_{cluster} + G_{MeOH}) \tag{5.9}$$

where, $G_{complex}$, $G_{cluster}$ and G_{MeOH} are the absolute free energies for the cluster–MeOH complex, cluster and a single methanol molecule respectively. $G_{formation}$ (free energy of formation) of the Rh_6–(MeOH) complex is found to be -0.62 kcal/mol, while $G'_{formation\text{-}orient\text{-}I}$ and $G'_{formation\text{-}orient\text{-}II}$ (free energy of formation of the Rh_4Ru_2–(MeOH)

complex of orient-I and orient-II respectively) are found to be -17.9 kcal/mol and -12.2 kcal/mol thereby suggesting greater thermodynamic stability of bimetallic-MeOH complexes as compared to the Rh_6–MeOH complex. It is very important to mention here that adsorption of methanol results in significant charge separations in both orientations of the Rh_4Ru_2–(MeOH) complex as compared to the charge separation in Rh_6–(MeOH) complex (see **Table 5.2**).

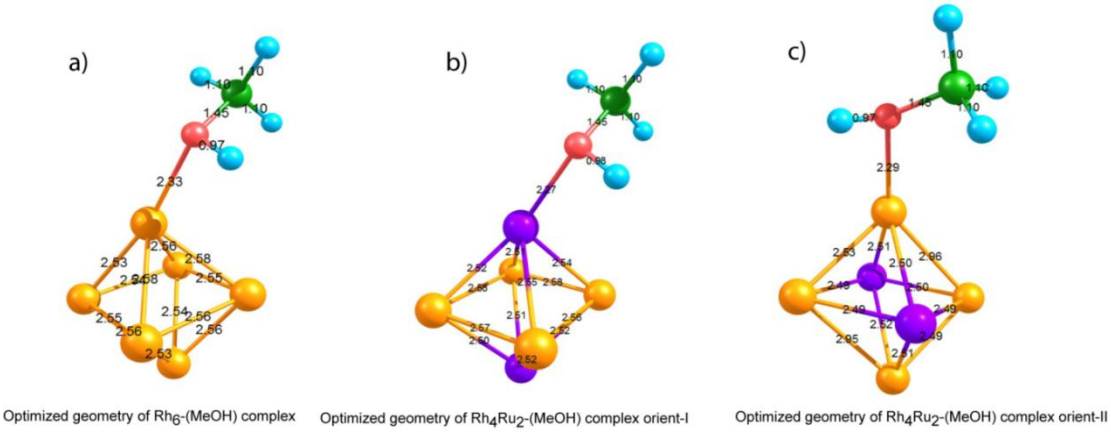

Figure 5.3 Optimized geometry for methanol adsorbed (a) Rh_6, (b) Rh_4Ru_2 in orientation-I and (c) Rh_4Ru_2 in orientation-II clusters. (golden: Rhodium; purple : Ruthenium; green: Carbon; red: Oxygen; sky blue : Hydrogen).

The difference in the values of $G_{formation}$ and $G'_{formation}$ can be further correlated following the analysis of frontier orbitals of both the complexes. HOMO of both Rh_4Ru_2–(MeOH) complexes show bonding character whereas the Rh_6–(MeOH) complex has non-bonding interactions (see **Fig. 5.4**). BOMD simulations at 300 K on both the Rh_4Ru_2–(MeOH) complexes demonstrate that the complexes do not undergo significant structural transformations and the molecule remains adsorbed on the cluster at this temperature. BOMD simulation at 300 K on Rh_6–(MeOH) complex also reveals the complex to be stable with methanol molecule undergoing rapid movements. This is easily demonstrated in the variations of Rh–O bond length as a function of time in Rh_6–(MeOH) complex (see **Fig. 5.5**). On the other hand, Ru–O bond length in orientation-I and Rh–O bond length in orientation-II of Rh_4Ru_2–

(MeOH) complexes equilibrate towards the end of the simulation (see **Fig. 5.6 and Fig. 5.7**). All the above mentioned facts contribute together to the higher values of $G'_{formation}$. Finally, all the methanol adsorbed complexes show negative free energy of formation and are thus thermally stable. Next, I will evaluate the efficiency of individual complexes towards methanol dissociation kinetics in the following section.

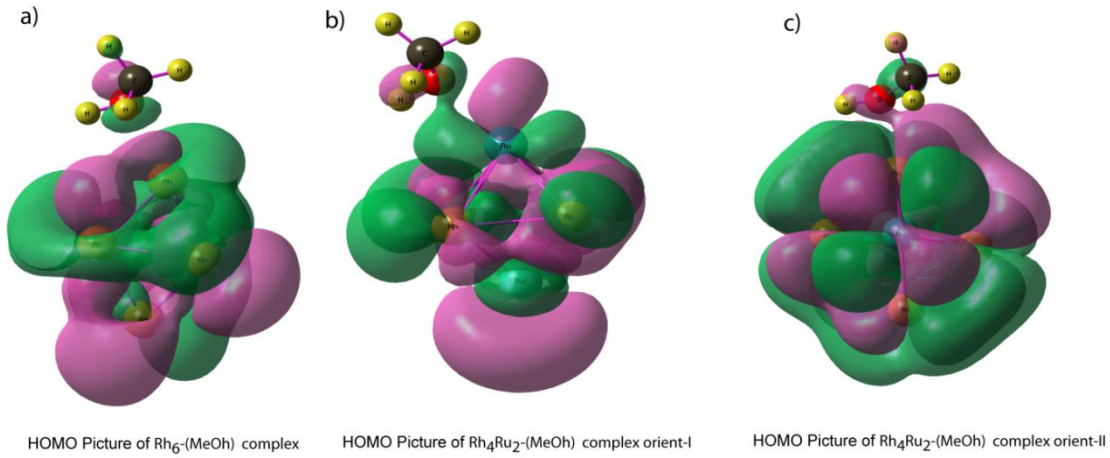

Figure 5.4 HOMO of methanol adsorbed (a) Rh_6, (b) Rh_4Ru_2 in orientation-I and (c) Rh_4Ru_2 in orientation-II Clusters.

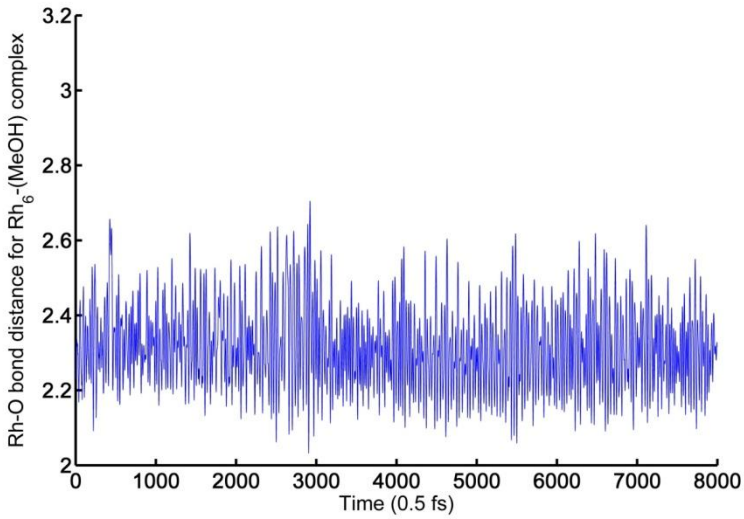

Figure 5.5 Rh–O bond distances versus time for Rh_6 cluster.

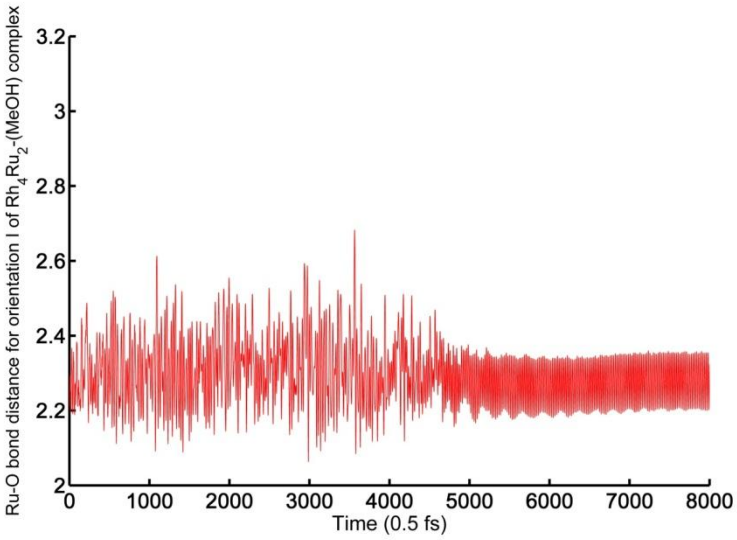

Figure 5.6 Ru–O bond distances versus time for the orientation-I of the Rh_4Ru_2 cluster.

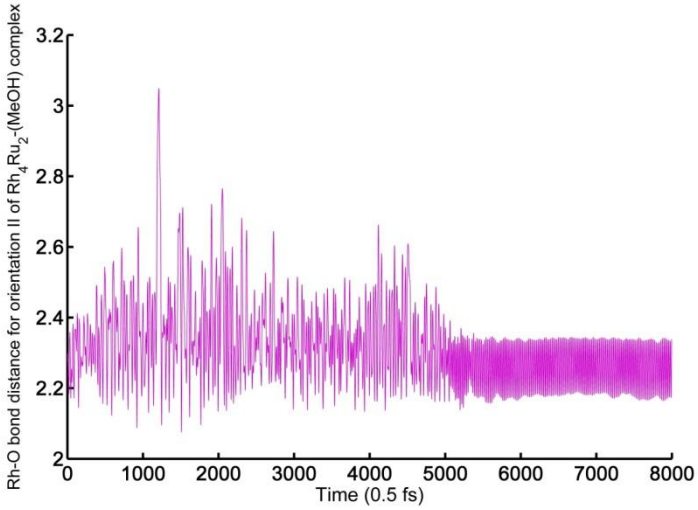

Figure 5.7 Rh–O bond distances versus time for the orientation-II of the Rh_4Ru_2 cluster.

5.3.2 Methanol dissociation on Rh_6 and Rh_4Ru_2 Clusters

My present study focuses on the catalytic activities of these clusters towards the dissociation of C–H and O–H bonds of single methanol molecule. Corresponding barriers for both the clusters are calculated and are used as indicators of catalytic activity throughout the remaining chapter.

Dissociation of O–H bond of methanol

Transition state corresponding to the O–H bond dissociation of methanol in presence of Rh_6 catalyst involves the breaking of the O–H bond and transfer of

hydrogen atom to any one of the consecutive Rh atoms. The barrier for the same is obtained to be 13.9 kcal/mol (ΔG) (see **Fig. 5.8 a**). The transition states corresponding to O–H bond dissociation in Rh_4Ru_2 clusters are shown in **Fig. 5.8 b** and **Fig. 5.8 c**. It is clear that both the orientations require less energy to dissociate the O–H bond in methanol. The reason behind lower O–H dissociation barrier in Rh_4Ru_2 is due to the fact that this reaction requires smaller stretching of the O–H bond as compared to that in Rh_6 species. The bond between the oxygen and hydrogen atoms (corresponding to the transition state geometry) is stretched to a greater extent in case of Rh_6 as compared to the bimetallic cases. The O–H distance is 1.57 Å in the transition state corresponding to the Rh_6 cluster as compared to 1.35 Å and 1.48 Å in the transition states involving Rh_4Ru_2 cluster in orientation-I and orientation-II, respectively (O–H bond distance in free methanol molecule is 0.99 Å). Incorporation of a second metal atom in the Rh_6 cluster significantly increases the charge separation between the atoms in the bare cluster (**Table 5.1)** and as well as in complexes (**Table 5.2**), leading to a more reactive cluster. HOMOs corresponding to the transition states of Rh_4Ru_2 cluster in both orientations (see **Fig. 5.9**) also account for the lower O–H dissociation barrier. In the bimetallic cases, the "*s*" orbital of the concerned hydrogen overlaps with the "*d*" orbital of the metal atom and thus provides some degree of stabilization to this particular transition state. Such an overlap is absent in the case of Rh_6 cluster. Finally, for the sake of completeness, I also calculated the activation barrier for methanol on Ru_6 cluster (a prism conformation which has the lowest energy among other conformations) which was found to be 17.5 kcal/mol (see **Fig. 5.10a**). Thus, Rh–Ru bimetallic clusters lower the activation barrier for methanol as compared to both the mono-metallic parent clusters.

Dissociation of C–H bond of methanol:

Transition states corresponding to the C–H bond dissociation are calculated for both the orientations of the bimetallic cluster and the Rh_6 cluster. The activation barrier for methanol on Ru_6 cluster is found to be 13.4 kcal/mol (see **Fig. 5.10b**) Transition state corresponding to the Rh_6 cluster has moderate barrier height of 13.6 kcal/mol (shown in **Fig. 5.11a**). However, reduction in the barrier heights (by 1.7 kcal/mol and by 2.7 kcal/mol for orientations I and II, respectively) is observed in case Rh_4Ru_2 cluster (see **Fig. 5.11b and 5.11c**). Furthermore, the product corresponding to the Rh_6 cluster is found to be endothermic (+3.5 kcal/mol) with respect to the reactant, whereas the products corresponding to the Rh_4Ru_2 clusters are exothermic in nature. The difference in energy between these pathways can also be explained from the point of view of C–H bond stretch in the corresponding transition state structures which is found to be 1.53 Å in Rh_6 as compared to 1.44 Å in orientation-I and 1.48 Å in orientation-II of Rh_4Ru_2 clusters.

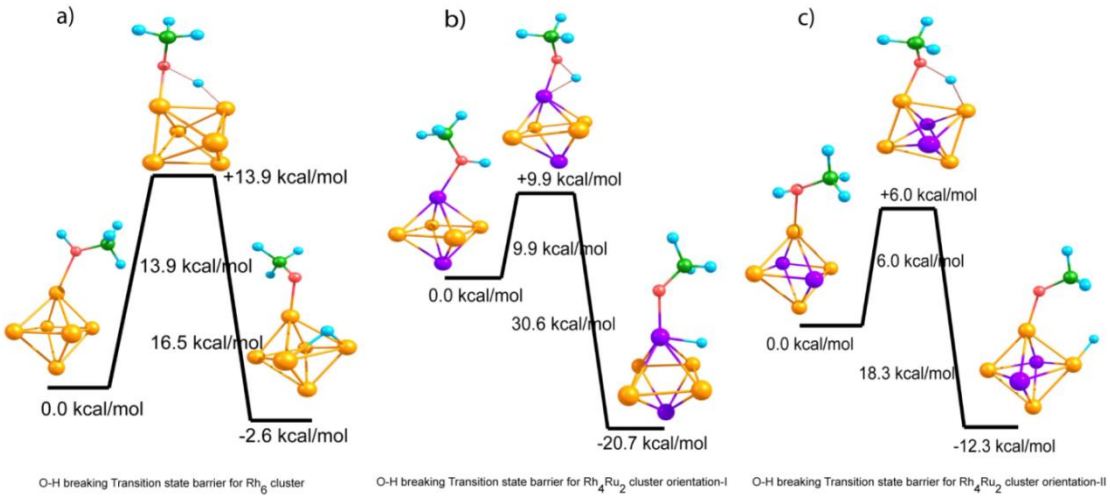

Figure 5.8 Transition barrier for O–H bond dissociation in methanol adsorbed (a) Rh_6, (b) Rh_4Ru_2 in orientation-I and (c) Rh_4Ru_2 in orientation-II clusters. (golden: Rhodium; purple: Ruthenium; green: Carbon; red: Oxygen; sky blue : Hydrogen).

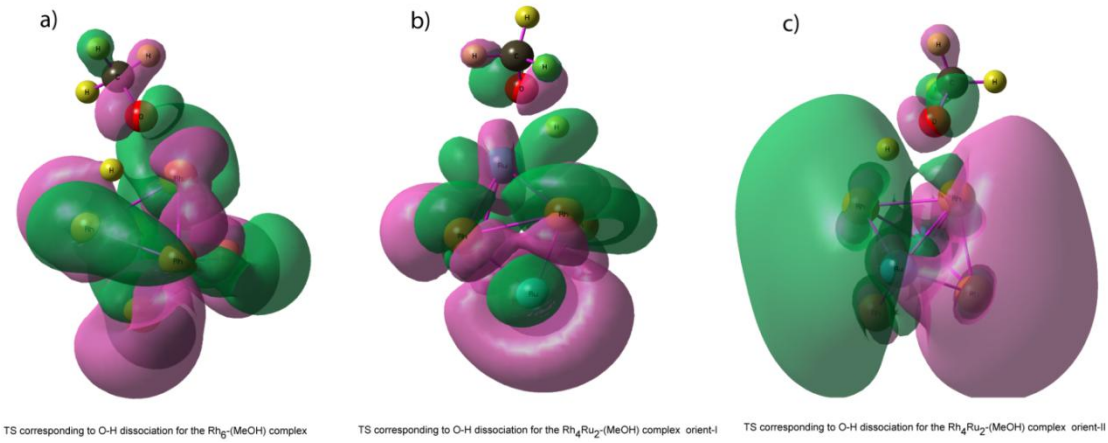

Figure 5.9 HOMO orbitals for O–H Bond activated (a) methanol–Rh_6, (b) methanol–Rh_4Ru_2 in orientation-I and (c) methanol–Rh_4Ru_2 in orientation-II Clusters.

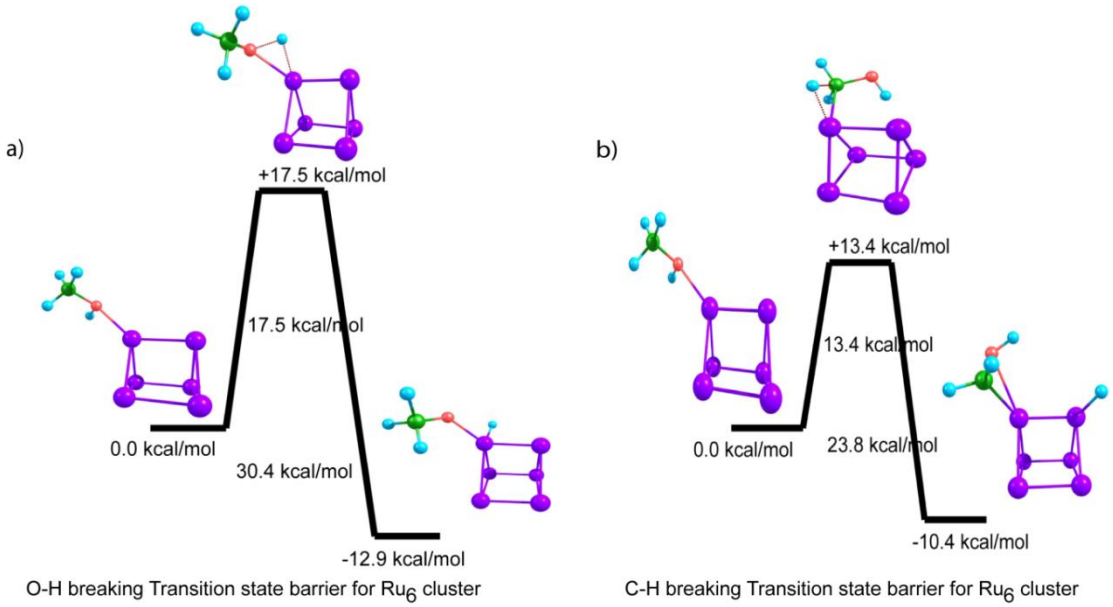

Figure 5.10 Transition barrier for O–H and C–H bonds dissociation in methanol adsorbed Ru_6 cluster. (purple: Ruthenium; green: Carbon; red: Oxygen; sky blue : Hydrogen).

Unlike the O–H dissociation process, it is clear from the frontier orbital pictures (see **Fig. 5.12a** and **Fig. 5.12b**) of this particular transition state that the dissociated hydrogen atom lacks proper stabilizing interaction with the adjacent Rh atom in Rh_6 cluster and orientation-I of Rh_4Ru_2 cluster. On the other hand, in case of orientation-II, the dissociated hydrogen gets slight stabilization due to the overlap of the corresponding metal and hydrogen orbitals (**Fig. 5.12c**). It is to be noted here that

HOMO picture of transition state structure involving Rh_6 cluster suggests more of an anti-bonding character, whereas non-bonding(orientation-I)/bonding(orientation-II) interactions are observed for Rh_4Ru_2 cases, which accounts for the slightly elevated barrier height in case of Rh_6 as compared to Rh_4Ru_2.

As orientation-I is the lowest energy conformation of the Rh_4Ru_2–(MeOH) complex (see **Fig. 5.2**), the total barrier height of the corresponding O–H and C–H activation for orientation-II (see **Fig. 5.8c** and **Fig. 5.11c**) are 11.7 kcal/mol and 16.6 kcal/mol (ΔG) respectively, following the addition of the stabilisation energy of 5.7 kcal/mol (see **Fig. 5.2**) to the calculated barrier heights (**Fig. 5.8c** and **Fig. 5.11c**). Therefore, from **Fig. 5.8** and **5.11** , it is clear that the transition states corresponding to both O–H and C–H activation will be more favourable for the orientation-I of the Rh_4Ru_2–(MeOH) complex.

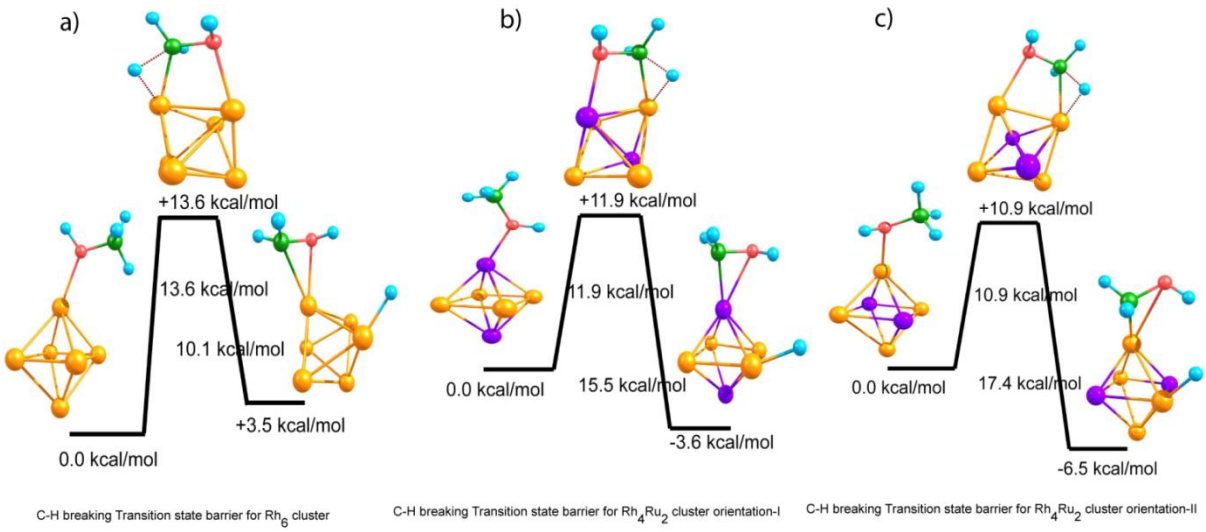

Figure 5.11. Transition barrier for C–H Bond dissociation in methanol adsorbed (a) Rh_6, (b) Rh_4Ru_2 in orientation-I and (c) Rh_4Ru_2 in orientation-II clusters. (golden: Rhodium; purple: Ruthenium; green: Carbon; red: Oxygen; sky blue : Hydrogen).

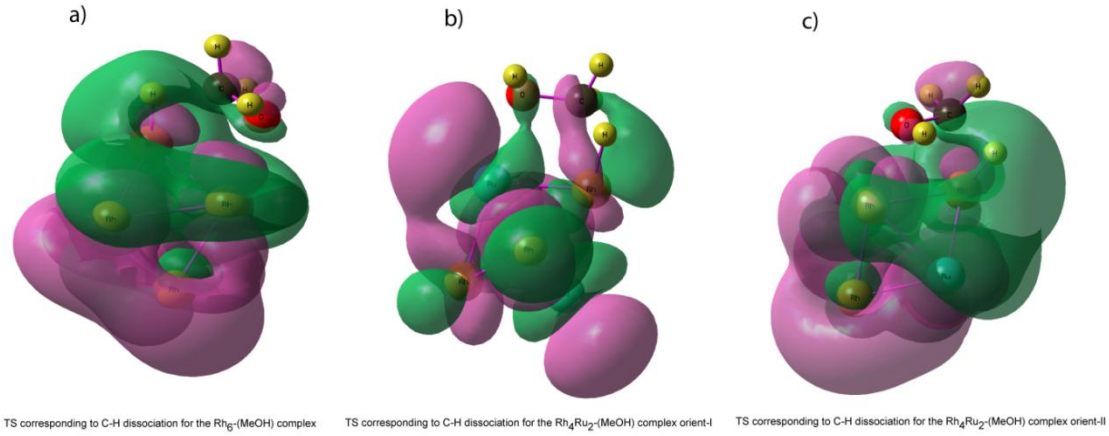

Figure 5.12 HOMO orbitals for C–H bond activated (a) methanol–Rh_6, (b) methanol–Rh_4Ru_2 in orientation-I and (c) methanol–Rh_4Ru_2 in orientation-II Clusters.

In short, in my calculations I have considered two competitive pathways (O–H breaking and C–H breaking) for the commencement of methanol dissociation in presence of rhodium and rhodium-ruthenium clusters. My investigation reveals that the initiation of methanol dissociation is kinetically more favoured to occur via the O–H breaking pathway in presence of both the clusters. The solution regarding the choice of a better catalyst can be inferred from both thermodynamic and kinetic point of view. The overall activation barrier for O–H dissociation is lower for orientation-I of Rh_4Ru_2 cluster as compared to the Rh_6 cluster. Since the energy difference between both the orientations of methanol adsorbed Rh_4Ru_2 complexes is not very high, formation of a small amount Rh_4Ru_2– $(MeOH)_{orient\text{-}II}$ is highly probable along with the Rh_4Ru_2–$(MeOH)_{orient\text{-}I}$, resulting in even lower O–H activation barrier (6.0 kcal/mol ; see **Fig. 5.8c**). Negative $G_{reaction}$ values (shown in **Fig. 5.8**) for all the cases also indicate that all the reactions are exothermic in nature, however the products are found to be more stable ($G_{reaction}$= -20.7 kcal/mol and -12.3 kcal/mol for orient-I and orient-II respectively) in both the Rh_4Ru_2 cases. My computational investigation thus reveals that both the clusters favour the O–H dissociation path but Rh_4Ru_2 cluster is catalytically more active towards initiation of methanol dissociation.

5.4 Conclusions

The present chapter investigates the potential of bimetallic Rh_4Ru_2 and pure Rh_6 clusters towards methanol activation and explores that both the clusters are well suited towards the same using DFT methodology. It has been shown that ruthenium doping enhances the reactivity of the parent cluster by creating a heterogeneous environment. In other words, Rh_4Ru_2 is found to possess higher catalytic activity towards the initiation of methanol dehydrogenation. My study indicates that dehydrogenation of methanol occurs through the O–H bond scission. It is important to note here that the calculated bond dissociation barriers are lower than some previously reported metal clusters (Co_4, Pd_4, Cu_3 etc.) and catalytic surfaces (Cu(111), Pd(111), Ir(111) etc.) as well.[30, 33-35] Thus, catalytic activity of this bimetallic catalyst can be further explored towards activation of other small molecules such as CO, HCOOH, NH_3BH_3 etc. and such studies are presently under consideration.

5.5 References

[1] B. Blank, S. Michlik, R. Kempe *Advanced Synthesis & Catalysis*. **2009**, 351, 2903-2911.
[2] R. Grigg, T. R. B. Mitchell, S. Sutthivaiyakit, N. Tongpenyai *Tetrahedron Letters*. **1981**, 22, 4107-4110.
[3] J. Moran, A. Preetz, R. A. Mesch, M. J. Krische *Nat Chem*. **2011**, 3, 287-290.
[4] J. Vancoillie, J. Demuynck, L. Sileghem, M. Van De Ginste, S. Verhelst *International Journal of Hydrogen Energy*. **2012**, 37, 9914-9924.
[5] Y. Pan, L. Ye, B.-J. Ni, Z. Yuan *Water Research*. **2012**, 46, 4832-4840.
[6] Y. Pan, B.-J. Ni, P. L. Bond, L. Ye, Z. Yuan *Water Research*. **2013**, 47, 3273-3281.
[7] P. Timmermans, A. Van Haute *Water Research*. **1983**, 17, 1249-1255.
[8] G. Lettinga *Antonie van Leeuwenhoek*. **1995**, 67, 3-28.
[9] G. Claus, H. Kutzner *Appl Microbiol Biotechnol*. **1985**, 22, 378-381.
[10] L. Foglar, F. Briški *Process Biochemistry*. **2003**, 39, 95-103.
[11] M. Li, K. Duraiswamy, M. Knobbe *Chemical Engineering Science*. **2012**, 67, 26-33.
[12] R. Pérez-Hernández, A. Gutiérrez-Martínez, M. E. Espinosa-Pesqueira, M. L. Estanislao, J. Palacios *Catalysis Today*.
[13] N. Yi, R. Si, H. Saltsburg, M. Flytzani-Stephanopoulos *Applied Catalysis B: Environmental*. **2010**, 95, 87-92.
[14] G. L. Chiarello, M. H. Aguirre, E. Selli *Journal of Catalysis*. **2010**, 273, 182-190.

[15] S. Sharma, B. G. Pollet *Journal of Power Sources*. **2012**, 208, 96-119.
[16] K. Motokura, D. Nishimura, K. Mori, T. Mizugaki, K. Ebitani, K. Kaneda *Journal of the American Chemical Society*. **2004**, 126, 5662-5663.
[17] B. A. Arndtsen, R. G. Bergman, T. A. Mobley, T. H. Peterson *Accounts of Chemical Research*. **1995**, 28, 154-162.
[18] O. Blum, D. Stöckigt, D. Schröder, H. Schwarz *Angewandte Chemie International Edition in English*. **1992**, 31, 603-604.
[19] J. S. Owen, J. A. Labinger, J. E. Bercaw *Journal of the American Chemical Society*. **2006**, 128, 2005-2016.
[20] G. Deo, I. E. Wachs *Journal of Catalysis*. **1994**, 146, 323-334.
[21] F. Schager, K. Seevogel, K.-R. Pörschke, M. Kessler, C. Krüger *Journal of the American Chemical Society*. **1996**, 118, 13075-13076.
[22] S. J. Blanksby, G. B. Ellison *Accounts of Chemical Research*. **2003**, 36, 255-263.
[23] X. Sun, X. Sun, C. Geng, H. Zhao, J. Li *The Journal of Physical Chemistry A*. **2014**, 118, 7146-7158.
[24] W. A. Donald, C. J. McKenzie, R. A. J. O'Hair *Angewandte Chemie International Edition*. **2011**, 50, 8379-8383.
[25] C. J. Zhang, P. Hu *The Journal of Chemical Physics*. **2001**, 115, 7182-7186.
[26] W. T. Lee, F. Thomas, R. I. Masel *Surface Science*. **1998**, 418, 479-483.
[27] D. Wang, E. R. Farquhar, A. Stubna, E. Münck, L. Que *Nat Chem*. **2009**, 1, 145-150.
[28] V. n. M. Sánchez, J. A. Cojulun, D. n. A. Scherlis *The Journal of Physical Chemistry C*. **2010**, 114, 11522-11526.
[29] S. K. Desai, M. Neurock, K. Kourtakis *The Journal of Physical Chemistry B*. **2002**, 106, 2559-2568.
[30] X.-K. Gu, W.-X. Li *The Journal of Physical Chemistry C*. **2010**, 114, 21539-21547.
[31] S. Lin, J. Ma, L. Zhou, C. Huang, D. Xie, H. Guo *The Journal of Physical Chemistry C*. **2013**, 117, 451-459.
[32] D. Mei, L. Xu, G. Henkelman *The Journal of Physical Chemistry C*. **2009**, 113, 4522-4537.
[33] H. Wang, C.-z. He, L.-y. Huai, J.-y. Liu *The Journal of Physical Chemistry C*. **2013**, 117, 4574-4584.
[34] F. Mehmood, J. Greeley, L. A. Curtiss *The Journal of Physical Chemistry C*. **2009**, 113, 21789-21796.
[35] F. Mehmood, J. Greeley, P. Zapol, L. A. Curtiss *The Journal of Physical Chemistry B*. **2010**, 114, 14458-14466.
[36] Y. Xie, F. Dong, S. Heinbuch, J. J. Rocca, E. R. Bernstein *The Journal of Chemical Physics*. **2009**, 130, -.
[37] A. C. Reber, P. J. Roach, W. H. Woodward, S. N. Khanna, A. W. Castleman *The Journal of Physical Chemistry A*. **2012**, 116, 8085-8091.
[38] S. Feyel, D. Schröder, H. Schwarz *The Journal of Physical Chemistry A*. **2009**, 113, 5625-5632.
[39] S. A. Tenney, B. A. Cagg, M. S. Levine, W. He, K. Manandhar, D. A. Chen *Surface Science*. **2012**, 606, 1233-1243.
[40] K. Bobuatong, S. Karanjit, R. Fukuda, M. Ehara, H. Sakurai *Physical Chemistry Chemical Physics*. **2012**, 14, 3103-3111.
[41] M. Ichihashi, T. Hanmura, R. T. Yadav, T. Kondow *The Journal of Physical Chemistry A*. **2000**, 104, 11885-11890.
[42] S. A. Tenney, S. I. Shah, H. Yan, B. A. Cagg, M. S. Levine, T. S. Rahman, D. A.

Chen *The Journal of Physical Chemistry C*. **2013**, 117, 26998-27006.
[43] S. Zhao, H. Tang, Y. Ren, A. Xu, J. Wang *Computational and Theoretical Chemistry*. **2014**, 1037, 14-21.
[44] S. H. Oh, J. E. Carpenter *Journal of Catalysis*. **1986**, 98, 178-190.
[45] A. Bouriazos, K. Mouratidis, N. Psaroudakis, G. Papadogianakis *Catal Lett*. **2008**, 121, 158-164.
[46] B. Engler, E. Koberstein*, P. Schubert *Applied Catalysis*. **1989**, 48, 71-92.
[47] P. R. d. l. Piscina, N. Homs *Chemical Society Reviews*. **2008**, 37, 2459-2467.
[48] D. Cao, A. Wieckowski, J. Inukai, N. Alonso-Vante *Journal of The Electrochemical Society*. **2006**, 153, A869-A874.
[49] G. N. Vayssilov, G. P. Petrova, E. A. I. Shor, V. A. Nasluzov, A. M. Shor, P. S. Petkov, N. Rosch *Physical Chemistry Chemical Physics*. **2012**, 14, 5879-5890.
[50] E. A. Ivanova Shor, V. A. Nasluzov, A. M. Shor, G. N. Vayssilov, N. Rösch *The Journal of Physical Chemistry C*. **2007**, 111, 12340-12351.
[51] A. M. Argo, B. C. Gates *The Journal of Physical Chemistry B*. **2003**, 107, 5519-5528.
[52] S. Shetty, R. A. van Santen, P. A. Stevens, S. Raman *Journal of Molecular Catalysis A: Chemical*. **2010**, 330, 73-87.
[53] V. Kiran, T. Ravikumar, N. T. Kalyanasundaram, S. Krishnamurty, A. K. Shukla, S. Sampath *Journal of The Electrochemical Society*. **2010**, 157, B1201-B1208.
[54] P. Serna, D. Yardimci, J. D. Kistler, B. C. Gates *Physical Chemistry Chemical Physics*. **2014**, 16, 1262-1270.
[55] S. M. Hamilton, W. S. Hopkins, D. J. Harding, T. R. Walsh, M. Haertelt, C. Kerpal, P. Gruene, G. Meijer, A. Fielicke, S. R. Mackenzie *The Journal of Physical Chemistry A*. **2011**, 115, 2489-2497.
[56] M. B. Torres, F. Aguilera-Granja, L. C. Balbás, A. Vega *The Journal of Physical Chemistry A*. **2011**, 115, 8350-8360.
[57] C. Barreteau, D. Spanjaard, M. C. Desjonquères *Physical Review B*. **1998**, 58, 9721-9731.
[58] Y. Jinlong, F. Toigo, W. Kelin *Physical Review B*. **1994**, 50, 7915-7924.
[59] B. V. Reddy, S. K. Nayak, S. N. Khanna, B. K. Rao, P. Jena *Physical Review B*. **1999**, 59, 5214-5222.
[60] L. Zhi-Qiang, Y. Jing-Zhi, K. Ohno, Y. Kawazoe *Journal of Physics: Condensed Matter*. **1995**, 7, 47.
[61] A. U. Volkan Ortalan1, Bruce C. Gates, Nigel D. Browning *Nat Nano*. **2010**, 5, 843-847.
[62] K. Bergamaski, E. R. Gonzalez, F. C. Nart *Electrochimica Acta*. **2008**, 53, 4396-4406.
[63] J. P. I. de Souza, S. L. Queiroz, K. Bergamaski, E. R. Gonzalez, F. C. Nart *The Journal of Physical Chemistry B*. **2002**, 106, 9825-9830.
[64] T. E. Shubina, M. T. M. Koper *Electrochimica Acta*. **2002**, 47, 3621-3628.
[65] B. D. McNicol, D. A. J. Rand, K. R. Williams *Journal of Power Sources*. **1999**, 83, 15-31.
[66] S. Sen Gupta, J. Datta *Journal of Electroanalytical Chemistry*. **2006**, 594, 65-72.
[67] F. Tao, M. E. Grass, Y. Zhang, D. R. Butcher, F. Aksoy, S. Aloni, V. Altoe, S. Alayoglu, J. R. Renzas, C.-K. Tsung, Z. Zhu, Z. Liu, M. Salmeron, G. A. Somorjai *Journal of the American Chemical Society*. **2010**, 132, 8697-8703.
[68] Z.-Y. K. Tzi-Yi Wu, Jiin-Jiang Jow,Chung-Wen Kuo,Cheng-Jang Tsai,Pin-Rong Chen,Ho-Rei Chen *International Journal of Electrochemical Science*. **2012**, 7, 8076-

8090.
[69] M. Li, W. P. Zhou, N. S. Marinkovic, K. Sasaki, R. R. Adzic *Electrochimica Acta*. **2013**, 104, 454-461.
[70] F. Hahn, B. Beden, C. Lamy *Journal of Electroanalytical Chemistry and Interfacial Electrochemistry*. **1986**, 204, 315-327.
[71] M. Watanabe, S. Motoo *Journal of Electroanalytical Chemistry and Interfacial Electrochemistry*. **1975**, 60, 267-273.
[72] J. W. Guo, T. S. Zhao, J. Prabhuram, R. Chen, C. W. Wong *Electrochimica Acta*. **2005**, 51, 754-763.
[73] M. S. Löffler, H. Natter, R. Hempelmann, K. Wippermann *Electrochimica Acta*. **2003**, 48, 3047-3051.
[74] K. A. Friedrich, K. P. Geyzers, U. Linke, U. Stimming, J. Stumper *Journal of Electroanalytical Chemistry*. **1996**, 402, 123-128.
[75] N. Toshima, Y. Wang *Langmuir*. **1994**, 10, 4574-4580.
[76] X. Liu, D. Tian, C. Meng *Computational and Theoretical Chemistry*. **2012**, 999, 246-250.
[77] N. Sahiner, O. Ozay, N. Aktas, E. Inger, J. He *International Journal of Hydrogen Energy*. **2011**, 36, 15250-15258.
[78] Q. Wu, W. L. Eriksen, L. D. L. Duchstein, J. M. Christensen, C. D. Damsgaard, J. B. Wagner, B. Temel, J.-D. Grunwaldt, A. D. Jensen *Catalysis Science & Technology*. **2014**, 4, 378-386.
[79] N. Rösch, G. Petrova, P. Petkov, A. Genest, S. Krüger, H. Aleksandrov, G. Vayssilov *Topics in Catalysis*. **2011**, 54, 363-377.
[80] D. S. Mainardi, P. B. Balbuena *The Journal of Physical Chemistry A*. **2003**, 107, 10370-10380.
[81] M. J. T. Frisch, G. W.;Schlegel, H. B.;Scuseria, G. E.;, M. A. C. Robb, J. R.; Scalmani, G.; Barone, V.; Mennucci,, G. A. N. B.; Petersson, H.; Caricato, M.; Li, X.; Hratchian, H., A. F. B. P.; Izmaylov, J.; Zheng, G.; Sonnenberg, J. L.; Hada, M.;, M. T. Ehara, K.; Fukuda, R.; Hasegawa, J.; Ishida, M.; Nakajima,, Y. K. T.; Honda, O.; Nakai, H.; Vreven, T.; Montgomery, J. A., Jr.;, P. E. O. Peralta, F.; Bearpark, M.; Heyd, J. J.; Brothers, E.;, K. N. S. Kudin, V. N.; Kobayashi, R.; Normand, J.;, K. R. Raghavachari, A.; Burant, J. C.; Iyengar, S. S.; Tomasi,, M. R. J.; Cossi, N.; Millam, N. J.; Klene, M.; Knox, J. E.; Cross, J., V. A. B.; Bakken, C.; Jaramillo, J.; Gomperts, R.; Stratmann, R., O. A. E.; Yazyev, A. J.; Cammi, R.; Pomelli, C.; Ochterski, J. W.;, R. L. M. Martin, K.; Zakrzewski, V. G.; Voth, G. A.; Salvador,, J. J. D. P.; Dannenberg, S.; Daniels, A. D.; Farkas, Ö.; Ortiz, J., J. F. V.; Cioslowski, D. J. *Gaussian, Inc, Wallingford CT*. **2009**.
[82] A. K. Srivastava, N. Misra *Computational and Theoretical Chemistry*. **2014**, 1047, 1-5.
[83] D. J. Harding, S. R. Mackenzie, T. R. Walsh *Chemical Physics Letters*. **2009**, 469, 31-34.
[84] J. L. F. Da Silva, M. J. Piotrowski, F. Aguilera-Granja *Physical Review B*. **2012**, 86, 125430.
[85] R. Camacho-Mendoza, E. Aquino-Torres, J. Cruz-Borbolla, J. Alvarado-Rodríguez, O. Olvera-Neria, J. Narayanan, T. Pandiyan *Struct Chem*. **2014**, 25, 115-126.
[86] H.-Q. Wang, H.-F. Li *RSC Advances*. **2014**, 4, 29782-29793.
[87] B. Chan, W.-L. Yim *Journal of Chemical Theory and Computation*. **2013**, 9, 1964-1970.
[88] T. Yumura, T. Nanba, H. Torigoe, Y. Kuroda, H. Kobayashi *Inorganic*

Chemistry. **2011**, 50, 6533-6542.
[89] H.-W. Yang, W.-C. Lu, L.-Z. Zhao, W. Qin, W.-H. Yang, X.-Y. Xue *The Journal of Physical Chemistry A*. **2013**, 117, 2672-2677.
[90] J. W. Ochterski *Gaussian Inc, Pittsburgh, PA*. **2000**, 1-17.
[91] D. A. McQuarrie, J. D. Simon, Molecular thermodynamics, University Science Books Sausalito, CA, **1999**.
[92] G. Geudtner, P. Calaminici, J. Carmona-Espíndola, J. M. del Campo, V. D. Domínguez-Soria, R. F. Moreno, G. U. Gamboa, A. Goursot, A. M. Köster, J. U. Reveles, T. Mineva, J. M. Vásquez-Pérez, A. Vela, B. Zúñinga-Gutierrez, D. R. Salahub *Wiley Interdisciplinary Reviews: Computational Molecular Science*. **2012**, 2, 548-555.
[93] F. Aguilera-Granja, L. C. Balbás, A. Vega *The Journal of Physical Chemistry A*. **2009**, 113, 13483-13491.
[94] M. Beltrán, F. Buendía Zamudio, V. Chauhan, P. Sen, H. Wang, Y. Ko, K. Bowen *Eur. Phys. J. D*. **2013**, 67, 1-8.
[95] C.-H. Chien, E. Blaisten-Barojas, M. R. Pederson *Physical Review A*. **1998**, 58, 2196-2202.
[96] F. Mehmood, R. B. Rankin, J. Greeley, L. A. Curtiss *Physical Chemistry Chemical Physics*. **2012**, 14, 8644-8652.
[97] T. Frelink, W. Visscher, J. A. R. van Veen *Surface Science*. **1995**, 335, 353-360.

Chapter 6: Summary

Metal hydrides and the complex hydride complexes have attracted reasonable attention for their suitable applications in the area of solid state hydrogen storage problem. Among them, ammonia borane and the corresponding amine borane complexes gained substantial popularity as the potential candidates for solid state hydrogen storage materials due to their high hydrogen content. Due to the strong binding nature of the B–H and N–H bonds, the dehydrogenation cycle needs a catalytic support to ease the process. In this thesis, I have particularly worked on the problems related to the dehydrogenation of ammonia borane via Iridium pincer catalyst Ir(POCOP)(H_2) ([POCOP = η^3-1,3(OP^tBu_2)$_2C_6H_3$];[1] one of the most efficient catalysts. One of the major problem associated with this catalyst is that it forms an insoluble cyclic pentamer of the amino borane species [$(NH_2BH_2)_5$]. On the other hand, all other catalysts are able to form soluble polyborazylene species from which ammonia borane regeneration is a facile process. I have considered the complete mechanistic pathways towards $(NH_2BH_2)_5$ formation from amino borane; NH_2BH_2 (the immediate side product of the dehydrogenation reaction) with the intervention of the Ir(POCOP)(H_2) catalyst. Moreover, I have tried and tested different reaction pathways for ammonia borane dehydrogenation by Ir(POCOP)(H_2) catalyst along with the possibility of metal–carbon(*sp2*) cooperativity playing a major role. It is relevant to mention here that the tridentate nature of Ir(POCOP)(H_2) causes steric hindrances throughout the metal–carbon activation pathway. In this regard, we have designed a bidentate analogue of the mentioned Ir-Pincer catalyst to reduce the steric strain of the catalyst along the reaction pathway. Hence, our model catalyst is examined for a number of various reactions via the incorporation of the metal–carbon(*sp2*) cooperativity. Not only that, one non–metal bidendate catalyst (a similar analogue of the same was already synthesized), an already synthesized bidentate Ta-

based catalyst, a tridendate catalyst (with one of the terminal arm holding a phenyl group) were also taken into consideration to study their dehydrogenation barrier through metal (or non–metal)–carbon activation pathway.

Methanol is one of the most versatile compounds having several applications in areas such as: a) in organic synthesis; b) in wastewater denitrification; c) in steam reforming, d) in transportation fuel, e) in polymer industries and most importantly d) in fuel cell. A vital step in almost every applications of methanol requires the activation of its strong O–H and C–H bonds and thus these applications require the interference of a catalyst to ease up the whole procedure. In this regard, Rh–Pt binary clusters are the most popular catalysts towards alcohol oxidation in direct alcohol fuel cells. Generally, Rh is the reason behind the inhibition of the CO poisoning effects in these clusters. On the other hand, the rate of methanol oxidation reactions are known to get increased in case of Ru doped Pt clusters. Hence, I have explored the unique combination of Rh–Ru binary clusters to have best of both sides. In my study, I have compared the catalytic activities of the Rh_6 (octahedral; one of the well studied nano-cluster of rhodium) and Rh_4Ru_2 (octahedral) clusters towards the activation of the methanol molecule.

Summary of the results

I. Quantum mechanical calculations[2] using MP2/BP-86 methods reveal that Ir(POCOP)(H_2) is actively involved in converting NH_2BH_2 (the immediate product of ammonia borane dehydrogenation) into the experimentally observed cyclic pentameric species $(NH_2BH_2)_5$.[1, 3] The work thus unfolds the dual role of the catalyst: a) first catalyzing the reaction, and then b) being involved in oligomerisation. As $(NH_2BH_2)_5$ is an undesired side product, some modifications have been suggested such as: a) by increasing the steric bulk on the ancillary phosphorus of the iridium

catalyst, b) by using amine borane instead of ammonia borane, c) by performing the reaction at higher temperature and d) by replacing THF with a more polar solvent.

II. Quantum mechanical calculations[4] using B3LYP/BP-86 methods explore and identify the possibility of metal (or non-metal)−ipso C(*sp2*) cooperativity (discussed for the first time) for achieving important chemical transformations such as dehydrogenation of AB and formic acid and activation of aromatic N–H bond.

III. Quantum mechanical calculations[5] using PBE-PBE functional suggest that ruthenium doping enhances the reactivity (higher catalytic activity towards the initiation of methanol dehydrogenation) of the parent Rh_6 cluster by creating a heterogeneous environment. It has been confirmed by both thermodynamic and kinetic study that Ru doping increases the charge separation throughout the cluster and therefore, decreases both the O–H and C–H activation barriers as compared to the Rh_6 cluster. Our study reveals that dehydrogenation of methanol initiates through the O–H bond scission and our calculated barriers are lower than some previously reported data.[6-9]

6.5 References

[1] M. C. Denney, V. Pons, T. J. Hebden, D. M. Heinekey, K. I. Goldberg *Journal of the American Chemical Society*. **2006**, 128, 12048-12049.
[2] K. Ghatak, K. Vanka *Computational and Theoretical Chemistry*. **2012**, 992, 18-29.
[3] K. W. Böddeker, S. G. Shore, R. K. Bunting *Journal of the American Chemical Society*. **1966**, 88, 4396-4401.
[4] K. Ghatak, M. Mane, K. Vanka *ACS Catalysis*. **2013**, 3, 920-927.
[5] K. Ghatak, T. Sengupta, S. Krishnamurty, S. Pal *Theor Chem Acc*. **2014**, 134, 1-11.
[6] X.-K. Gu, W.-X. Li *The Journal of Physical Chemistry C*. **2010**, 114, 21539-21547.
[7] H. Wang, C.-z. He, L.-y. Huai, J.-y. Liu *The Journal of Physical Chemistry C*. **2013**, 117, 4574-4584.

[8] F. Mehmood, J. Greeley, P. Zapol, L. A. Curtiss *The Journal of Physical Chemistry B*. **2010**, 114, 14458-14466.
[9] F. Mehmood, J. Greeley, L. A. Curtiss *The Journal of Physical Chemistry C*. **2009**, 113, 21789-21796.